Doctoral Dissertations

Student Theses and Dissertations

Summer 2015

Energy management in electric vehicles: Development and validation of an optimal driving strategy

Warren Santiago Vaz

Recommended Citation

ENERGY MANAGEMENT IN ELECTRIC VEHICLES:

DEVELOPMENT AND VALIDATION OF AN OPTIMAL DRIVING STRATEGY

by

WARREN SANTIAGO VAZ

A DISSERTATION

Presented to the Faculty of the Graduate School of the

MISSOURI UNIVERSITY OF SCIENCE AND TECHNOLOGY

In Partial Fulfillment of the Requirements for the Degree

DOCTOR OF PHILOSOPHY

in

MECHANICAL ENGINEERING

2015

Approved by

Umit O. Koylu, Advisor
John W. Sheffield
Robert G. Landers
Arup K. Nandi
Mehdi Ferdowsi

PUBLICATION DISSERTATION OPTION

This dissertation has been prepared in the form of four papers for publication. Pages 4-40 have been published in the *International Journal of Electric and Hybrid Vehicles*. Pages 41-85 have been published in the *Journal of Power Sources*. Pages 86-130 have been submitted to *IEEE Transactions on Vehicular Technology*. Pages 131-159 have been accepted to the *9th International Conference on Sustainable Energy (ASME 2015)*. The first three have been prepared in the format for publication in the corresponding journals. The last one has been formatted for the corresponding conference. The remainder of this dissertation follows the standard dissertation format.

ABSTRACT

Electric vehicles (EVs) are a promising alternative energy mode of transportation for the future. However, due to the limited range and relatively long charging time, it is important to use the stored battery energy in the most optimal manner possible. Existing research has focused on improvements to the hardware or improvements to the energy management strategy (EMS). However, EV drivers may adopt a driving strategy that causes the EMS to operate the EV hardware in inefficient regimes just to fulfil the driver demand. The present study develops an optimal driving strategy to help an EV driver choose a driving strategy that uses the stored battery energy in the most optimal manner. First, a strategy to inform the driver about his/her current driving situation is developed. Then, two separate multi-objective strategies, one to choose an optimal trip speed and another to choose an optimal acceleration strategy, are presented. Finally, validation of the optimal driving strategy is presented for a fleet-style electric bus. The results indicated that adopting the proposed approach could reduce the electric bus' energy consumption from about 1 kWh/mile to 0.6-0.7 kWh/mile. Optimization results for a fixed route around the Missouri S&T campus indicated that the energy consumption of the electric bus could be reduced by about 5.6% for a 13.9% increase in the trip time. The main advantage of the proposed strategy is that it reduces the energy consumption while minimally increasing the trip time. Other advantages are that it allows the driver flexibility in choosing trip parameters and it is fairly easy to implement without significant changes to existing EV designs.

ACKNOWLEDGMENTS

It is only fitting that I start by thanking my advisor, Dr. Koylu, for helping me to become a better researcher and for his guidance and support. I wish to express my gratitude to Dr. Sheffield for his belief in my abilities and for sharing his enormous perspective and vision with me. I cannot omit acknowledging the contributions of Dr. Nandi as his singular ideas were instrumental in helping me cross the finish line. I also thank Dr. Landers for his guidance and expertise and Dr. Ferdowsi for his time and cooperation. Without my advisory committee, this work would not have been possible. Additionally, I also wish to thank Dr. S. N. Balakrishnan for helping me become a better instructor.

I thank all my instructors not only in the department but also at Missouri S&T. Studying at this institution has been nothing short of a privilege. I cannot overstate the value of my friends in Rolla. My friend and roommate, Greg, must be specially mentioned for everything he did for me. I must also thank all the people at the Newman Center, especially Sr. Renita and George. I also thank my sister and my brother for putting up with me. Together, my family and friends made my time in Rolla and the United States a real blessing.

Finally, and most importantly, I thank my parents. I am incalculably grateful to them for always believing in me, for setting my feet on the path of knowledge, and for always being there for me. I may never know the full extent of the sacrifices they made for my sake but I can honor their actions by dedicating this work to them.

TABLE OF CONTENTS

APPENDICES

LIST OF ILLUSTRATIONS

PAPER III

PAPER IV

SECTION

LIST OF TABLES

1. INTRODUCTION

Electric vehicles (EVs) first gained prominence towards the end of the 19th century when they outsold vehicles with external combustion engines fueled by coal and internal combustion (IC) engines fueled by diesel or gasoline [1]. With improvements in IC engines, the expansion of roads, and the reduction of the price of gasoline, EVs were not able to keep up with IC engines. The main problems that caused their decline were the limited range afforded by a single charge and the considerable length of time to charge a battery. With the rising price of gasoline precipitating a demand for vehicles that are more efficient and more environmentally friendly than conventional IC engines, EVs are starting to make a comeback. Electric vehicles (EVs) are free of the widespread emissions suffered by IC engine vehicles, in addition to being more energy efficient [2]. They are especially effective in reducing urban pollution [3]. Government regulations like Corporate Average Fuel Economy (CAFE) standards and funding initiatives are also helping drive the EV market. EVs have seen tremendous improvements in range over the last two decades. Charging times have been reduced as well. Finally, the growth of charging infrastructure is slowly catching up to the growth in the number of EVs. Market data indicate that EV sales in the US increased from around 1000 in 2008 to 10,064 in 2011 and 14251 in 2012 and are projected to reach over 400,000 in the US and 3.8 million worldwide by 2020. While there were only a couple of EV models available before 2010, there were around fifteen available in 2012 [4, 5, 6]. With EV sales projected to grow, several challenges relating to different stages in the life cycle of EVs still need to be overcome. Of these, perhaps the most important one is the energy management and range extension. Despite the recent technology progress, the biggest

challenge unique to EVs is the limited range on a single battery charge. Even if charging

stations were more plentiful than they are, it takes a lot longer (several hours) to charge

an EV than it takes to refuel an IC engine vehicle (several minutes). Therefore, it is

essential to use the stored battery energy in the most optimal manner possible by

minimizing the wasted energy. Optimal use of the battery energy results in maximizing

the range of the EV.

Existing research efforts on EVs can broadly be divided into two categories. The

first category is improvements to the hardware of the vehicle. The second category is

improvements to the energy management strategy (EMS) of the vehicle. The need for an

EMS came about when researchers realized that it was simply not enough to improve the

hardware of the EV; it was also important to use the stored energy of the battery in the

most optimal manner. The goal of the EMS is to properly manage the energy of the EV

while fulfilling the driver's demand.

A driving strategy refers to the combination of acceleration and speed values

chosen by the driver to traverse a given distance. Typically, a driver does not plan a trip

based on acceleration and speed values but simply follows the flow of traffic, which

means the chosen driving strategy may be suboptimal. This means that, no matter how

much the hardware and the EMS are improved, the EV will not perform to the best extent

possible because the driver's demands cause the EMS to waste energy by operating the

hardware in a suboptimal regime. Therefore, it is essential to adopt a driving strategy that

optimally operates the EV hardware and allows the EMS to properly manage the stored

energy. This is termed optimal driving or adopting an optimal driving strategy. In this

dissertation, a third category of EV research is proposed and developed: improvements to the driving strategy adopted by the driver.

The layout of the dissertation is as follows. The first paper develops a strategy to inform an EV driver about the current driving situation by classifying the driving behavior as aggressive or defensive and the driving cycle as highway or urban. The second paper proposes a multi-objective strategy to choose a trip speed by maximizing the electric motor efficiency and minimizing the power consumption. The driver is presented with several options so that he/she can use the results to choose a speed based on a trade-off between maximum range and minimum trip time. The third paper proposes a multi-objective strategy to choose the appropriate acceleration strategy to attain the optimal trip speed. The fourth paper focuses on validating the proposed approach using the operational data of an electric bus. Finally, Section 2 combines the constant speed and the optimal acceleration strategies to optimize a demonstrative trip traveled by the bus. Section 3 summarizes the research and highlights the most important conclusions along with discussing some ideas for future work.

PAPER

I Neural Network Strategy for Driving Behavior and Driving Cycle Classification

Warren Vaz*, Robert G. Landers, and Umit O. Koylu

Department of Mechanical & Aerospace Engineering,

Missouri University of Science and Technology,

400 W. 13th Street, Rolla, MO 65409, USA

E-mail: wsvvf9@mst.edu

E-mail: landersr@mst.edu

E-mail: koyluu@mst.edu

*Corresponding author

Abstract

The driving behavior and the driving cycle type affect the range of an electric vehicle. Previous studies have devised methods to *identify* driving cycle type in order to formulate an energy management strategy. This approach does not take driving behavior into account and fails to account for differences in predefined driving cycles and real-time driving. A novel strategy that *classifies* driving behavior as aggressive or defensive and driving cycles as highway or urban using accelerator and brake positions is proposed. A method to simulate aggressive and defensive driving behavior was developed and implemented. An electric vehicle (EV) was simulated and made to follow 11 driving cycles aggressively and defensively and the accelerator and brake positions of the simulated EV were recorded. Five statistical parameters were computed for the recorded data: average, covariance, standard deviation, total, and variance. A neural network was

trained to identify patterns in the recorded data in order to classify the driving behavior as aggressive or defensive and the driving cycle as highway or urban. The neural network successfully differentiated between aggressive and defensive driving behavior and highway and urban driving cycles in all 11 training cases. Furthermore, the simulated EV followed four additional driving cycles not used to train the neural network. The neural network was able to properly classify the driving behavior and the driving cycle type for the four new driving cycles as well. The proposed method of classifying driving behavior and driving cycles overcomes the limitations posed by identifying driving cycles. It provides real-time information about the driving behavior and the driving cycle and is not limited to any particular driving cycle or group or driving cycles.

Keywords: driving behavior classification, driving cycle classification, electric vehicle, neural network, pattern recognition, supervised training

1 Introduction

The range of an electric vehicle (EV) is influenced by both the driving behavior of the driver and the driving cycle. It is important to take both into account when designing an energy management strategy for an EV. Information about the driving behavior and the driving cycle could be used to remove differences in fuel efficiency due to differences in driving behavior and to make appropriate changes to the energy management strategy based on the driving cycle type resulting in greater EV range, more accurate range prediction, and reduced vehicle component wear. It could help a driver regulate driving habits and also be used by car insurance companies, some of which already offer

discounts to drivers who have completed a defensive driving course. The information obtained by the driving behavior classification algorithm proposed in this study could be used to aid in the decisions made by car insurance companies while setting insurance rates and offering discounts.

In general, EVs have better efficiency in the city where the average speed is lower and the electric motor operates in a more efficient regime providing greater amounts of regenerative energy than on the highway where the average speed and the drag force to overcome are higher and the electric motor operates in a more inefficient regime with almost no regenerative energy. Existing methods (Constantinescu et al., 2010; He et al., 2012; Jeon et al., 2002; Park et al., 2009; Ryu et al., 2010; Xu et al., 2012) involve *identifying* the driving cycle based on driving data and using a predefined control strategy or optimization scheme specific to the identified driving cycle to improve performance. Ryu et al. (2010) developed an identification strategy (referred to as a "stochastic fuzzy controller") in which the average power and the standard deviation of the power were used to differentiate between two particular cycles. These methods either assume the vehicle is driven according to a particular driving cycle or incorporate a way to identify what driving cycle the vehicle is following, or most closely following, before implementing the appropriate energy management strategy. However, it is virtually impossible to find a typical driver driving exactly according to a predefined driving cycle. Driving cycles fail to capture the influence of unique trip details such as road signs, traffic lights, or other vehicles. Driving characteristics such as acceleration, average speed, braking, maximum speed, etc. vary from one trip to another even if the same

driver drives the same route. Besides being cycle-dependent, existing methods often rely on precise measurements of a number of vehicle parameters in real time. To obtain the necessary data, a variety of measurement tools such as accelerometers, position sensors, temperature sensors, etc. is needed, adding complexity and cost to the identification method and increasing the possibility of errors due to faulty measurements and failed sensors. An efficient method to *classify* driving cycles in real time in order to account for changes in the driving cycle type based on real-world conditions is needed. This would overcome the limitations posed by assuming the vehicle is driven according to a particular driving cycle or by identifying a particular driving cycle from a limited number of preselected driving cycles.

The aggressiveness of acceleration and braking, in general, has a greater impact on the fuel economy of vehicles with internal combustion (IC) engines than the average speed (Cheng et al., 2010; Fiat, 2010). Knowles et al. (2010) conducted a study on the effect of driving behavior on EV performance and concluded that the journey speed was a more important factor than the number of junctions (starts/stops). Furthermore, previous research indicates that modifications to driving behavior could increase fuel economy in IC engines (Fiat, 2010; Van Mierlo et al., 2004). However, it is unclear whether or not these conclusions can be extended to EVs. Bingham et al. (2012) conducted a study on EVs that concluded that more energy could be saved by decreasing the amount of acceleration and deceleration. Research on driving behavior classification is lacking. Constantinescu et al. (2010) applied data mining techniques to real-time vehicle tracking data in order to classify drivers based on aggressiveness. However, this classification was

not done in real time. Similar to the fact that the driving cycle may change due to real-world conditions, the driving behavior of a particular driver may also change between trips or even during a trip due to unforeseen circumstances (e.g., weather-related emergencies). Therefore, a method to classify driving behavior as aggressive or defensive based on real-time driving data is needed. This study develops a novel, real-time method to *classify* driving behavior as aggressive or defensive and driving cycle type as highway or urban. There are only a few examples of previous studies with a similar goal. Kolmanovsky et al. (2002) used a dynamic programming approach to reduce the dependence of the control strategy on any driving cycle. However, this resulted in a control strategy developed to perform best in an *average sense* against a "drive cycle generator". Langari and Won (2005) developed an intelligent energy management system that could *identify* the driving environment, the driving style, and the vehicle operating mode. The strategy developed centered on parallel hybrid vehicles.

2 Driving Cycle and Driving Behavior

2.1 Driving Cycle

In this study, driving cycles have been broadly divided into two categories based on the speed: highway and urban. Highway cycles are characterized by high speeds (greater than 60 kmh^{-1}) and very little, if any, instances of stopping. Urban cycles are characterized by low speeds (less than 60 kmh^{-1}) and significant instances of stopping. For example, the highway fuel economy test cycle has an average speed of 77.7 kmh^{-1} and 6 s of stopping time out of 765 s (at the beginning and end) whereas the urban dynamometer driving schedule has an average speed of 31.5 kmh^{-1} and 259 s of stopping time out of 1369 s.

Certain driving cycles have sections that have the characteristics of highway driving cycles and sections that have the characteristics of urban driving cycles. These are categorized as hybrid driving cycles.

2.2 Driving Behavior

There are different ways to classify driving behavior. Broadly speaking, drivers can be classified as aggressive or defensive. Classification can be more specific to account for certain tendencies by grouping drivers as aggressive, attentive, calm, defensive, passive, polite, reckless, etc. Aggressive drivers tend to engage in harsh or sudden acceleration and braking and generally drive over posted speed limits. They tend to change lanes frequently, follow vehicles closely, overtake vehicles, and bend or break traffic regulations. Defensive drivers tend to engage in gentle or smooth acceleration and braking, and generally drive at or below posted speed limits. They try to avoid using the brake as much as possible preferring to let the engine, the gradient, or coasting slow the vehicle down. They anticipate changes in speed, do not change lanes frequently, follow vehicles at a safe distance, yield to other vehicles whenever possible, and follow traffic regulations. There is not a universal definition or set of rules to classify drivers as aggressive or defensive because of the complexity involved. Different studies have generated their own ways of describing driving behavior. Constantinescu et al. (2010) generated several increasing levels of aggressive driving based on the acceleration, braking, and speed of various drivers. De Vlieger et al. (2000) had a similar approach to classifying drivers as aggressive, calm, or normal based on the average acceleration for different city driving cycles. The acceleration values for city driving are 0.45-0.65 ms^{-2}

for calm driving, 0.65-0.80 ms^{-2} for normal driving, and 0.85 to 1.10 ms^{-2} for aggressive driving. The accelerations for highway driving range from 0.08 ms^{-2} to 0.20 ms^{-2}. Ericsson (2001) described up to 62 parameters that may be extracted from a given driving cycle. These parameters (such as deceleration factor, speed oscillation factor, and stop factor) may be used to describe driving behavior. Berry (2010) proposed a way to evaluate the aggressiveness of a driver based on the energy consumed per unit distance. These "aggressiveness factors", computed based on the work done by vehicles with IC engines, were extended to driving cycles such that aggressiveness factors for various driving cycles could be computed. However, it is unclear how this would relate to other powertrains. A set of metrics to distinguish between aggressive and defensive driving behavior are presented in Section 3.

2.3 Neural Networks

Neural networks have been successfully used in classification, identification, and pattern recognition in applications such as roadway type detection (Won and Langari, 2005) and traffic congestion prediction (Park et al., 2009). In this study, multi-layer feed-forward neural networks were used. The neural networks were trained using the Levenberg-Marquardt (1944) backpropagation algorithm. The neural networks have multiple layers with non-linear transfer functions, except for the output layer, which has a linear transfer function allowing the neural networks to produce outputs within any range.

3 Model

In this study, an EV was simulated in MATLAB/Simulink with a driving cycle as its

primary input. The secondary input was the choice between an aggressive or defensive

driving algorithm. The simulation was run with eleven different driving cycles as inputs.

The simulation was programmed to stop at the end of a driving cycle or when the state of

charge of the battery dropped below 10%. Figure 1 shows the MATLAB/Simulink

program with the associated inputs and outputs.

3.1 Controller/Motor Model

The model's inputs are the driving cycle and the real speed and the outputs are the battery

current, the electric motor torque, and the brake force. Table 1 shows the electric motor

parameters used in this study.

3.1.1 Driving Behavior Simulation

The speed error, which is the difference between the driving cycle and the real (vehicle)

speed, was computed. It was used to obtain accelerator and brake positions to simulate

the commands of a driver driving the EV. Using accelerator and brake positions allows

unique trip details to be taken into account. It was assumed that the accelerator and brake

could take on any value between 0 and 1, with 0 being fully released and 1 being fully

pressed. In addition to the steering wheel, the main control inputs of an EV are the

accelerator position and the brake position. For a single-speed transmission, no other

input is necessary to drive an EV. For a multi-speed transmission, the gear number or the

gear ratio would be an additional input. These accelerator and brake positions were then used to recalculate the speed error to feed to the electric motor drive.

The simulation was run in two modes: aggressive and defensive. The aggressive driving mode was programmed to maintain a steady-state speed error whose absolute value was less than 1.6 kmh^{-1}. The accelerator was fully pressed when the speed error was greater than 8 kmh^{-1} to allow for maximum acceleration. The brake was used to ensure the EV remained as close to the speed error as possible rather than letting the EV coast to decrease speed. The defensive driving mode was programmed to follow the driving cycle without setting any speed error limits. The accelerator was pressed when a positive speed error was encountered and released when a negative speed error was encountered. The accelerator was programmed to be pressed and released gradually allowing gentler acceleration and deceleration than generated by the aggressive driving algorithm. The brake was only used when the EV was more than 11.2 kmh^{-1} faster than the driving cycle or when the EV needed to be brought to a stop. In all other instances, the EV was controlled with the accelerator allowing for coasting and cruising. Figure 2 shows a plot of a 30-second driving cycle (speed reference) with the simulation set to follow it in the aggressive mode. The EV follows the driving cycle closely, the maximum steady-state speed error being less than 1.6 kmh^{-1}. The accelerator and brake positions are shown in the same plot. It should be noted that the accelerator and the brake are never depressed simultaneously. This plot clarifies the relationship between the acceleration, deceleration, real speed, and accelerator and brake positions.

A plot was generated with the simulation set to follow the same 30-second driving cycle in the defensive mode. The result is shown in Figure 3. The differences between aggressive and defensive driving behavior become clear when comparing Figures 2 and 3: defensive driving features gradual pedal presses and therefore gentler acceleration and deceleration than aggressive driving; the aggressive driving simulation switches between the accelerator and the brake five times whereas the the defensive driving simulation does so only twice; the maximum speed error in aggressive driving is 12.6 kmh^{-1} whereas it is 57.8 kmh^{-1} in defensive driving; there is very little coasting in aggressive driving whereas defensive driving has almost three seconds of coasting from 11 s to 13 s and from 16 s to almost 19 s. The brake is pressed nine times in the aggressive driving simulation versus only twice in the defensive driving simulation. However, the error computed by subtracting the real speed from the speed reference is larger for defensive driving. Figure 3 also illustrates the differences between the accelerator and brake positions for highway and urban driving. The first 10-11 s of the driving cycle can be classified as highway driving with relatively high speed and no braking. The accelerator position is 0.55 during the flat portion of the speed reference and the brake position is 0. The remainder of the plot can be classified as urban driving with relatively low speed and some braking. The accelerator position is consequently lower (0.33) during the flat portion of the speed reference and the brake position changes between 0 and 0.2.

3.1.2 Driving Behavior Metrics

The EV accelerations and velocities while following the 11 driving cycles aggressively and defensively were recorded. The average acceleration, the maximum acceleration, the

maximum deceleration, and the standard deviation of the acceleration were calculated.

Only the net positive acceleration was considered while calculating the average

acceleration since the net positive acceleration is equal to the net negative acceleration.

The results for the 15 driving cycles used in this study are shown in Figure 4. As

expected, the aggressive driving mode has higher values for all calculated metrics than

the defensive driving mode, especially the average acceleration and the maximum

deceleration. These values do not always fall within the ranges prescribed in the literature

but are sufficiently different so as to allow one to clearly distinguish one type of driving

behavior from the other. This definition ignores some of the legal and safety aspects of

driving behavior and focuses more on fuel efficiency.

3.2 Vehicle Model

The vehicle model used to simulate the vehicle dynamics was the one used by Gantt et al.

(2011). The relevant vehicle parameters for this study are shown in Table 2. These

parameters are typical values for EVs found in the literature (Gantt et al., 2011; Xu et al.,

2011). The model's inputs are the electric motor torque and the brake force and the

outputs are the real speed and the distance covered.

3.3 Battery

Chen and Rincon-Mora (2006) developed a lithium-ion battery model capable of

capturing the battery's essential current-voltage characteristics. This model was used to

simulate the lithium-ion battery in the EV model used in the present study. Table 3 shows

the battery parameters. The model's input is the battery current, I_P, and the model's outputs are the battery voltage, V_P, and the state of charge, *SOC*.

4 Neural Network Approach

The accelerator and brake positions are related to the acceleration, deceleration, and speed of an EV. From Figures 2 and 3, it is evident that driving an EV according to a driving cycle either aggressively or defensively would produce a unique combination of accelerator and brake positions. This study develops a method to classify driving behavior as aggressive or defensive and the driving cycle type as highway or urban using neural networks. There are several studies involving EVs, fuel cell EVs, and hybrid EVs that aim to improve efficiency and/or performance by using neural networks for pattern recognition. He et al. (2012) used a learning vector quantization neural network to identify driving patterns with an aim to reduce the sampling time needed by driving pattern recognition algorithms. Certain representative features of driving cycles such as the averages and maximums of the acceleration, deceleration, and speed and the percentage of idle time were used in the neural network training. Park et al. (2009) used neural networks to predict the road type and traffic congestion. Fourteen features to predict road types were selected including the averages and maximums of the acceleration and deceleration and the standard deviation of the acceleration. Jeon et al. (2002) developed a control strategy for parallel hybrid electric vehicles centered around identifying which representative driving cycle is closest to the current vehicle trip. Twenty-four characteristic parameters of driving cycles were used including average speed and averages and standard deviations of acceleration and deceleration.

Table 4 shows a list of the driving cycles used for training the neural networks in this study. Four different driving cycles, as shown in Table 5, were also used for testing the neural networks. These driving cycles were chosen to form a diverse group of conditions. Some were highway driving cycles, some were urban driving cycles, and some had features of both highway and urban driving cycles. It should be emphasized that the method developed here does not depend on the driving cycles used for training or testing.

Driving data were collected during uniformly sized sample windows. The sample window size during which accelerator and brake positions were recorded was 120 s. Previous methods (He et al., 2012; Jeon et al., 2002; Langari and Won, 2005; Won and Langari, 2005) used a sample window size of around 120-180 s. In all cases, the first 120 s of data were processed and fed to the neural network. The purpose of the EV simulation was to obtain a series of accelerator and brake positions. For each simulation run, an accelerator matrix was constructed with time in the first column and accelerator position in the second column, and a brake matrix was constructed with time in the first column and brake position in the second column. Once the EV's accelerator and the brake positions during a 120-s sample window were obtained, five statistical parameters were computed for the accelerator and the brake positions: average, covariance, standard deviation, total, and variance. A column vector containing ten elements (five statistical parameters for the accelerator position and five statistical parameters for the brake position) was created to correspond to each matrix of accelerator and brake positions. This 10-element column vector was used as an input to the neural network. This

procedure was repeated for all 11 driving cycles. For each driving cycle, two column

vectors were generated: one for aggressive driving and the other for defensive driving. A

total of 22 inputs were obtained to train the neural network. The statistical parameters

computed for all 15 driving cycles used for training and testing are listed in Table 6.

A feed-forward, backpropagation neural network was implemented in MATLAB. The

number of layers and the number of neurons within the particular layers were varied as

will be discussed in Section 5. It must be noted that the number of neurons in any

particular layer that is not the output layer is selected by the user. The number of neurons

in the output layer depends on the output vector. The performance function was the Mean

Square Error (MSE) function, which is

$$MSE = \frac{1}{N}\sum_1^N (T_i - A_i)^2 \qquad (1)$$

where A is a vector of neural network outputs, T is a vector of desired outputs, also called

targets, and N is the total number of training cases. The driving behavior, whether

aggressive or defensive, was selected before running the simulation. Supervised training

was chosen to train the neural network since the desired output, which in this case was

the classification of driving behavior as aggressive or defensive, for each set of input

matrices was known. In other words, the neural network was fed training data in order to

train it to map a set of inputs to particular outputs (or targets). Then, when presented with

new data, it would classify the data using the rules developed during training. In other

words, new data similar to the training data would generate the same outputs as the

training data. This principle was used to create one neural network to classify driving behavior as aggressive or defensive, regardless of the driving cycle, and a second neural network to classify driving cycles as highway or urban, regardless of the driving behavior, by simply changing the targets used for training.

5 Results and Discussion

The EV model was simulated, both aggressively and defensively, for the 11 driving cycles in Table 4. The accelerator positions (**A**) and the brake positions (**B**) were recorded and the five statistical parameters previously mentioned were computed. The input matrix used to train the neural network had 10 rows, which contained the five statistical parameters for the **A** values followed by the five statistical parameters for the **B** values. The input matrix had 22 columns with 11 aggressive driving cycles in the first 11 columns followed by 11 defensive driving cycles in the next 11 columns. The desired output matrix, also called the target matrix, was a 2x22 matrix. The first row had a "1" for aggressive driving and a "0" for defensive driving. The second row had a "1" for defensive driving and a "0" for aggressive driving. Therefore, the first 11 entries in the first column were ones followed by 11 zeroes and the first 11 entries in the second column were zeroes followed by 11 ones. In some cases, the neural network did not produce exactly one or zero. Therefore, any number greater than 0.5 was taken as a "1" and any number less than 0.5 was taken as a "0". In each case, after training the neural network with inputs and targets, the neural network was simulated with the same inputs to see if it would produce the targets. In Section 5.3, the results of testing with fresh data (i.e., data not used in training) will be discussed.

5.1 Driving Behavior

The 10x22 input matrix with **A** and **B** values was used to train the neural network. The number of layers was varied from one to four and the number of neurons in the hidden layers was varied from five to twenty, which affected the number of classification errors. Table 7 shows the best case with no classification errors and the lowest MSE, which was when the neural network had 4 layers and 20 neurons in each hidden layer. When presented with the 10x22 input matrix, the aggressive and defensive driving data were correctly classified as aggressive and defensive respectively. For every driving cycle, aggressive driving had a higher average, standard deviation, total, and variance for the accelerator and brake positions. The absolute value of the covariance between the accelerator and brake positions was higher for aggressive driving. The MSE value was 7.01×10^{-2}. Additionally, a 5x22 input matrix with only **B** values was used to train the neural network. The number of layers was varied from one to four and the number of neurons in the hidden layers was varied from five to twenty. Even when presented with only brake data, the neural network correctly classified driving data as aggressive or defensive. The MSE value was 3.39×10^{-5} for a neural network with 4 layers and 11 neurons in each hidden layer, which is lower than the MSE value of 7.01×10^{-2} when using both the accelerator and brake information in the neural network. The neural network performs the task of classification with less error using only brake positions rather than accelerator and brake positions implying that using only the brake positions may be sufficient to distinguish between aggressive and defensive driving. The accelerator and brake are used by both aggressive and defensive drivers, but aggressive

drivers use the brake more frequently than defensive drivers. Defensive drivers tend to use the brake only in unexpected situations or when coming to a complete stop while aggressive drivers use the brake whenever they need to slow down.

5.2 Driving Cycle

After the neural network was successfully used to classify driving behavior, the driving cycles were used to train a second neural network to distinguish between highway and urban driving cycles. The input matrix was modified to exclude the five driving cycles marked with an asterisk in Table 4. The resulting input was a 10x12 matrix containing six driving cycles driven both aggressively and defensively. The six driving cycles were chosen based on the fact that the first 120 s of these cycles can clearly be classified as highway or urban. It is important to select some driving cycles that are highway cycles and some that are urban cycles in order to properly train the neural network. Based on this prior knowledge of the classification of the six driving cycles, a target matrix was created. The first row had a "1" for highway driving cycles and a "0" for urban driving cycles. The second row had a "1" for urban driving cycles and a "0" for highway driving cycles. The number of layers was varied from one to four and the number of neurons in the hidden layers was varied from five to twenty. Table 8 shows the best case, which was when the neural network had 4 layers and 5 neurons in each hidden layer. When given the 10x12 input matrix, the highway and urban driving cycles were correctly classified. Highway driving cycles have higher speeds than urban driving cycles, so the average and the total are higher for the accelerator positions. For the brake positions, highway driving cycles driven aggressively have averages and totals that are higher than or almost equal to

urban driving cycles driven aggressively. With defensive driving, however, highway driving cycles have similar or lower values than urban driving cycles. The standard deviation and the variance follow similar trends. The covariance between the accelerator positions and the brake positions tends to be higher for the highway driving cycles than it is for the urban driving cycles. The neural network is able to classify the driving cycle training data according to the target matrix regardless of whether the data represents aggressive driving or defensive driving. The MSE value was 9.12×10^{-5}.

Additionally, a 5x12 input matrix with only **A** values was used to train the neural network. The number of layers was varied from one to four and the number of neurons in the hidden layers was varied from five to twenty. When presented with only accelerator data, the neural network correctly classified driving cycles as highway or urban regardless of the driving behavior. The MSE value was 7.64×10^{-5} for a neural network with 4 layers and 10 neurons in each hidden layer, which is slightly lower than the MSE value 9.12×10^{-5} when using both the accelerator and brake information in the neural network. As comparison, the MSE value obtained by Langari and Won (2005) when identifying driving cycle segments was 1.62×10^{-2}. The neural network performs the task of classification with less error using only accelerator positions rather than accelerator and brake positions. For driving cycle type, the accelerator positions were a better indicator of whether a cycle was highway or urban than the brake positions. Highway driving cycles have higher speeds than urban driving cycles, so the accelerator positions have higher values during a fixed sample window.

5.3 Testing

After training both neural networks, one to classify driving behavior and the other to

classify driving cycle, they were fed with four new driving cycles that were not used for

training. These driving cycles are listed in Table 5. Table 9 shows the response of the

neural network with 4 layers and 20 neurons in each hidden layer using **A** and **B** values.

The same results were obtained when using the neural network with 4 layers and 11

neurons in each hidden layer using only **B** values. No misclassification was encountered.

The MSE values were 7.91×10^{-3} and 3.53×0^{-3} respectively when using **A** and **B** values

and when using **B** value. It may be noted that the performance of the neural network

using only **B** values is, once again, better than the neural network when using **A** and **B**

values as indicated by a lower MSE value.

Along with testing the ability to distinguish driving behavior, the ability to distinguish

driving cycle type was also tested. The first 120 s of the four driving cycles are shown in

Figure 5. As seen in the figure, the first three driving cycles (MODEM HyZem Road,

OSCAR F.V5-15D15-40, and OSCAR G1.V5-15D40-70) have low speeds (<60 kmh^{-1}),

typical for urban driving cycles. The last driving cycle (TRL Motorway) has high speeds,

typical for highway driving cycles. Table 10 shows the response of the neural network

with 4 layers and 5 neurons in each hidden layer using **A** and **B** values. The same results

were obtained when using the neural network with 4 layers and 10 neurons in each

hidden layer using only **A** values. Again, no misclassification was encountered. The

neural network results matched the driving cycle type that was predicted by visual

inspection of Figure 5. The MSE values were 1.02×10^{-2} and 7.72×10^{-4} respectively. It

may be noted that the performance of the neural network using only **A** values is, once again, better than the neural network using **A** and **B** values as indicated by a lower MSE value.

There were 15 driving cycles used in this study. Six of those driving cycles were used to train a neural network to classify driving cycles as highway or urban. Of the remaining nine driving cycles, the driving cycle type was not clear in every case. Some parts of these remaining driving cycles had features of highway driving cycles and other parts had features of urban driving cycles. It must be remembered that only the first 120 s of the driving cycles were used for this classification. Figure 6 shows an example of how the proposed strategy would classify a full driving cycle. The driving cycle was divided into seven 120-s sample windows. The first and the last sample windows are clearly urban driving and therefore classified as such. The second, third, and fifth windows have features of highway driving and were classified as such. The fourth and sixth windows could be classified as either, and the neural network interprets these windows as highway driving. A reason for the classification being highway rather than urban is that the fourth and sixth windows have speeds reaching over 60 kmh^{-1}, which would result in higher accelerator positions leading to a classification as highway rather than urban. The driving behavior did not affect the classification of the driving cycle type.

6 Summary, Conclusions, and Future Work

A neural network-based strategy to classify driving behavior and driving cycle for EVs was developed. This strategy is an improvement and generalization over previous

methods that identify specific driving cycles rather than classifying driving behavior and driving cycle type. A method to simulate aggressive and defensive driving behavior for a wide variety of driving cycles was developed and implemented in MATLAB/Simulink. The accelerator and brake positions of a simulated EV following a given driving cycle aggressively or defensively during a 120-s sample window were obtained. Five statistical parameters (average, covariance, standard deviation, total, and variance) were calculated for the accelerator and brake positions. These calculated parameters contained information about the trip and were used as inputs to train a neural network with 11 driving cycles driven both aggressively and defensively. The neural network with 4 layers and 20 neurons in each hidden layer was found to accurately distinguish between aggressive and defensive driving when using the accelerator and brake positions. The same results were obtained when only the brake positions were used to train a neural network with 4 layers and 11 neurons in each hidden layer. Furthermore, when presented with fresh data comprising four driving cycles not used in training, the neural network was also able to correctly classify the driving data as aggressive or defensive. The effect of using two neural networks for classification, one that accepts accelerator and brake positions and one that accepts only brake positions, needs to be explored.

Six of the 11 driving cycles were then selected based on the fact that they could be clearly classified as highway or urban, and the corresponding statistical parameters for both aggressive and defensive driving were used to train another neural network. The neural network with 4 layers and 5 neurons in each hidden layer was found to accurately classify driving cycles as highway or urban, regardless of driving behavior. The same

results were obtained when only the accelerator positions were used to train a neural network with 4 layers and 10 neurons in each hidden layer. When presented with fresh data comprising nine driving cycles not used in training, the neural network was able to correctly classify the driving cycles as highway or urban. When classifying an entire 843-second driving cycle by breaking it up into 120-s sample windows, the neural network correctly classified the sections of the driving cycle. It was found that the classification did not depend on whether the driving cycle was driven aggressively or defensively. The effect of using two neural networks for classification, one that accepts accelerator and brake positions and one that accepts only accelerator positions, also needs to be explored.

It must be emphasized that the strategy developed in this study differs from previous studies because it is independent of any particular driving cycle and provides real-time information about the driving behavior *and* the driving cycle. Future work includes experimental verification of the strategy. The classification needs to be more granular. Future studies need to take into consideration other inputs such as gear number for multi-speed transmissions and the steering wheel position to more accurately classify driving behavior. The effect of the interaction of statistical parameters with each other has to be studied. The effect of the sample window size on the classification and its location relative to driving data also needs to be considered. For example, this study has not explored whether or not the classification shown in Figure 6 would change if the sample window size was decreased or increased or if the beginning of the sample window did not coincide exactly with the beginning of the driving cycle but was offset by some time.

References

Andre, M. (2004) 'Real-world driving cycles for measuring car pollutant emissions – Part A: The ARTEMIS European driving cycles', *Report INRETS-LTE 0411*.

Barlow, T.J., Latham, S., McCrae, I.S., Boulter, P.G. (2009) 'A reference book of driving cycles for use in the measurement of road vehicle emissions', TRL Limited, PPR354.

Berry, M.I., (2010) 'The effects of driving style and vehicle performance on the real-world fuel consumption of US light-duty vehicles', Masters Thesis, Massachusetts Institute of Technology, available at http://web.mit.edu/sloan-autolab/research/beforeh2/files/IreneBerry_Thesis_February2010.pdf (accessed on 2 July 2013).

Bingham, C., Walsh, C., Carroll, S. (2012) 'Impact of driving characteristics on electric vehicle energy consumption and range', *IET Intell. Transp. Syst.*, Vol. 6, No. 1, pp. 29-35.

Chen, M., Rincon-Mora, G. (2006) 'Accurate Electrical Battery Model Capable of Predicting Runtime and I-V Performance', *IEEE Transactions on Energy Conversion*, Vol. 21, No. 2, pp. 504-511.

Cheng, C., McGordon, A., Poxon, J., Jones, R., Jennings, P. (2010) 'A model to investigate the effects of driver behaviour on hybrid vehicle control', *25th World Battery, Hybrid, and Fuel Cell Electric Vehicle Symposium and Exhibition*, EVS-25, 5–9 November, Shenzhen, China.

Constantinescu, Z., Marinoiu, C., Vladoiu, M. (2010) 'Driving Style Analysis Using Data Mining Techniques', *Int. J. of Computers, Communications & Control*, Vol. 5, No. 5, pp. 654-663.

De Vlieger, I., De Keukeleere, D., Kretzschmar, J. (2000) 'Environmental effects of driving behaviors and congestion related to passenger cars', *Atmosph. Environ.*, Vol. 34, pp. 4649-4655.

Ericsson, E. (2001) 'Independent driving pattern factors and their influence on fuel use and exhaust emission factors', *Transportation Res. Part D*, Vol. 6, pp. 325–341.

Fiat Eco: Drive (2010) 'Eco-driving uncovered: the benefits and challenges of eco-driving based on the first study using real journey data', available at http://www.lowcvp.org.uk/assets/reports/Fiat_Eco-Driving%20Uncovered.pdf (accessed on 2 July 2013).

French National Institute for Transport and Safety Research (INRETS), 'All ARTEMIS Cycles', available at http://www.inrets.fr/ur/lte/publi-autresactions/fichesresultats/ficheartemis/road3/method31/All_Cycles_in_Artemis_BD_009200.xls (accessed on 1 July 2013).

Gantt, L.R., Alley, R.J., Nelson, D.J. (2011) 'Battery Sizing as a Function of Powertrain Component Efficiencies for Various Drive Cycles', *Proceedings of the ASME 2011 International Design Engineering Technical Conferences & Computers and Information in Engineering Conference (IDETC/CIE 2011)*, August 28-31, Washington, DC.

He, H., Sun, C., Zhang, X. (2012) 'A method for identification of driving patterns in hybrid electric vehicles based on LVQ neural network', *Energies*, Vol. 5, pp. 3363-3380.

Jeon, S., Jo, S., Park, Y., Lee. J. (2002) 'Multi-Mode Driving Control of a Parallel Hybrid Electric Vehicle Using Driving Pattern Recognition', *ASME Journal of Dynamic Systems, Measurement, and Control*, Vol. 124, pp. 141-149.

Knowles, M., Scott, H., Baglee, D. (2012) 'The effect of driving style on electric vehicle performance, economy, and perception', *Int. J. of Electric and Hybrid Vehicles*, Vol. 4, No. 3, pp. 228-247.

Kolmanovsky, I., Severguina, I., Lygoe, B. (2002) 'Optimization of Powertrain Operating Policy for Feasibility Assessment and Calibration: Stochastic Dynamic Programming Approach', *Proceedings of the American Control Conference*, May 8-10, Anchorage, AK.

Langari, R., Won, J. (2005) 'Intelligent Energy Management Agent for a Parallel Hybrid Vehicle – Part 1: System Architecture and Design of the Driving Situation Identification Process', *IEEE Transactions on Vehicular Technology*, Vol. 54, No. 3, pp. 925-934.

Levenberg, K. (1944) 'A Method for the Solution of Certain Non-Linear Problems in Least Squares', *Quarterly of Applied Mathematics*, Vol. 2, pp. 164-168.

Park, J., Chen, Z., Kiliaris, L., Ming, K., Masrur. M., Phillips, A., Murphey, Y. (2009) 'Intelligent vehicle power control based on machine learning of optimal control parameters and prediction of road type and traffic congestion', *IEEE Transactions on Vehicular Technology*, Vol. 58, No. 9, pp. 4741-4756.

Ryu, J., Park, Y., Sunwoo, W. (2010) 'Electric powertrain modeling a fuel cell hybrid electric vehicle and development of a power distribution algorithm based on driving mode recognition', *J. Power Sources*, Vol. 195, pp. 5735-5748.

Xu, G., Li, W., Xu, K., Song, Z. (2011) 'An Intelligent Regenerative Braking Strategy for Electric Vehicles', *Energies*, Vol. 4, pp. 1461-1477.

United States Environmental Protection Agency (2013) 'Dynamometer Drive Schedules', available at http://www.epa.gov/nvfel/testing/dynamometer.htm (accessed on 1 July 2013).

Van Mierlo, J., Maggetto, G., Van De Burgwal, E., Gense, R. (2004) 'Driving style and traffic measures – influence on vehicle emissions and fuel consumption', *Proceedings of Institute of Mechanical Engineers Part D: Journal of Automobile Engineering*, Vol. 218, No. 1, pp. 43-50.

Won, J., Langari, R. (2005) 'Intelligent Energy Management Agent for a Parallel Hybrid Vehicle – Part 2: Torque Distribution, Charge Sustenance, and Performance Results', *IEEE Transactions on Vehicular Technology*, Vol. 54, No. 3, pp. 935-953.

List of Tables

Table 1 Electric Motor Parameters.

Peak Current (A)	256
Peak Rotational Speed, ω_{max} (rpm)	9300
Power, P_M (kW)	80
Torque (Nm)	280
Type	AC induction
Voltage, V_M (V)	375

Table 2 EV Model Parameters.

Air Density, ρ_{air} (kgm^{-3})	1.225
Asphalt Friction Coefficient, μ_a	0.9
Battery Capacity (kWh)	30
Drag Coefficient, C_D	0.35
Frontal Area, A_f (m^2)	2.5
Grade, θ (°)	0
Inertial Correction Factor, δ	1.04
Mass, m (kg)	1350
Overall Gear Ratio, r	7.9:1
Range (km)	100-192
Rolling Friction Coefficient, μ	0.014
Tire Radius, R (m)	0.3429
Transmission	Single-speed

Table 3 Lithium-Ion Battery Parameters.

Capacity (A·h)	80
Number of cells in parallel, N_P	1
Number of cells in series, N_S	96
Type	Lithium-Ion
Voltage, V_P (V)	~375

Table 4 Driving Cycles Used for Training (Andre, 2004; United States Environmental

Protection Agency, 2013).

Driving Cycle Number	Name	Duration (s)	Length (km)	Type
1	ARTEMIS Highway Cycle*	1068	29.5	Highway
2	ARTEMIS Urban Cycle	993	4.9	Urban
3	Elementary Urban Cycle	195	1.0	Urban
4	Extra-Urban Driving Cycle	400	7.0	Highway
5	Highway Fuel Economy Driving Schedule	765	16.5	Highway
6	LA92 Dynamometer Driving Schedule*	1435	15.8	Hybrid
7	New European Driving Cycle*	1220	11.0	Hybrid
8	New York City Cycle	598	1.9	Urban
9	SC03 Supplemental FTP Driving Schedule*	600	5.8	Urban
10	Urban Dynamometer Driving Schedule*	1369	12.0	Urban
11	US06 Supplemental FTP Driving Schedule	600	12.9	Highway

Table 5 Driving Cycles Used for Testing (Andre, 2004; Barlow et al., 2009; French

National Institute for Transport and Safety Research (INRETS), 2013).

Driving Cycle Number	Name	Duration (s)	Length (km)	Type
12	MODEM HyZem Road Driving Cycle	843	7.0	Hybrid
13	OSCAR F.V5-15D15-40 Driving Cycle	423	1.0	Urban
14	OSCAR G1.V5-15D40-70 Driving Cycle	455	1.0	Urban
15	TRL Motorway Driving Cycle	643	10.9	Highway

Driv-ing Cycle	Aggressive									
	Accelerator Position					Brake Position				
	Average	Covariance	Standard Deviation	Total	Variance	Average	Covariance	Standard Deviation	Total	Variance
1	0.229	8.190E-04	0.189	274.600	3.560E-02	0.038	8.190E-04	0.139	45.950	1.930E-02
2	0.157	4.010E-04	0.144	188.990	2.080E-02	0.017	4.010E-04	0.094	20.430	8.800E-03
3	0.152	1.977E-03	0.105	182.660	1.110E-02	0.022	1.977E-03	0.107	26.030	1.140E-02
4	0.385	6.260E-03	0.211	462.530	4.450E-02	0.048	6.260E-03	0.149	57.290	2.210E-02
5	0.429	7.544E-03	0.228	514.730	5.180E-02	0.053	7.544E-03	0.156	63.420	2.420E-02
6	0.136	-1.010E-03	0.120	163.590	1.430E-02	0.025	-1.010E-03	0.116	30.120	1.340E-02
7	0.152	1.890E-03	0.091	182.270	8.200E-03	0.017	1.890E-03	0.093	19.920	8.600E-03
8	0.103	-1.004E-03	0.095	123.080	9.100E-03	0.015	-1.004E-03	0.099	17.760	9.800E-03
9	0.160	8.330E-04	0.148	191.770	2.180E-02	0.027	8.330E-04	0.116	32.190	1.340E-02
10	0.211	3.858E-03	0.174	253.190	3.010E-02	0.027	3.858E-03	0.115	32.730	1.320E-02
11	0.284	-2.620E-03	0.307	340.970	9.430E-02	0.030	-2.620E-03	0.122	35.780	1.480E-02
12	0.198	8.470E-04	0.164	238.030	2.690E-02	0.026	8.470E-04	0.116	31.140	1.340E-02
13	0.132	-2.120E-04	0.117	158.150	1.360E-02	0.024	-2.120E-04	0.115	28.550	1.320E-02
14	0.150	-9.759E-03	0.103	180.410	1.070E-02	0.025	-9.759E-03	0.117	30.420	1.370E-02
15	0.494	4.485E-03	0.308	593.570	9.480E-02	0.020	4.485E-03	0.098	23.520	9.600E-03

Table 6 Statistical Parameters Used in Neural Network Training.

	Defensive									
	Accelerator Position					Brake Position				
	Average	Covariance	Standard Deviation	Total	Variance	Average	Covariance	Standard Deviation	Total	Variance
1	0.156	-1.870E-03	0.148	187.350	2.190E-02	0.012	-1.870E-03	0.052	14.400	2.700E-03
2	0.078	-7.327E-04	0.114	93.950	1.290E-02	0.009	-7.327E-04	0.047	11.250	2.200E-03
3	0.064	-8.012E-04	0.089	76.780	7.900E-03	0.013	-8.012E-04	0.057	15.050	3.200E-03
4	0.292	-6.078E-05	0.200	350.670	3.980E-02	0.000	-6.078E-05	0.004	0.250	0.000E+00
5	0.342	0.000E+00	0.189	411.220	3.570E-02	0.000	0.000E+00	0.000	0.000	0.000E+00
6	0.055	-9.366E-04	0.089	65.900	8.000E-03	0.017	-9.366E-04	0.066	20.500	4.400E-03
7	0.054	-2.233E-04	0.083	64.420	6.900E-03	0.004	-2.233E-04	0.037	5.000	1.400E-03
8	0.025	-1.400E-04	0.050	30.500	2.500E-03	0.005	-1.400E-04	0.041	6.500	1.700E-03
9	0.091	-7.720E-04	0.113	109.760	1.270E-02	0.009	-7.720E-04	0.036	10.150	1.300E-03
10	0.138	-3.678E-04	0.135	165.790	1.830E-02	0.003	-3.678E-04	0.021	3.200	4.000E-04
11	0.213	-4.649E-03	0.258	255.960	6.670E-02	0.022	-4.649E-03	0.068	26.200	4.600E-03
12	0.118	-4.710E-04	0.132	141.900	1.730E-02	0.004	-4.710E-04	0.028	5.000	8.000E-04
13	0.046	-7.695E-04	0.085	54.680	7.200E-03	0.017	-7.695E-04	0.064	20.300	4.100E-03
14	0.049	-5.308E-04	0.070	58.670	4.900E-03	0.011	-5.308E-04	0.060	13.050	3.600E-03
15	0.400	0.000E+00	0.268	480.230	7.180E-02	0.000	0.000E+00	0.000	0.000	0.000E+00

Table 6 Statistical Parameters Used in Neural Network Training (cont.).

Table 7 Driving Behavior Classification Results using **A** and **B** Values with 4 Layers and

20 Neurons per Hidden Layer.

	Aggressive Driving				Defensive Driving			
Driving Cycle	Target Classification		Neural Network Classification		Driving Cycle	Target Classification		Neural Network Classification	
	First Row	Second Row	First Row	Second Row		First Row	Second Row	First Row	Second Row
1	1	0	1.004	0.001	1	0	1	0.008	0.994
2	1	0	1.004	0.054	2	0	1	0.014	0.979
3	1	0	1.004	0.005	3	0	1	0.019	0.983
4	1	0	0.984	-0.002	4	0	1	-0.012	1.125
5	1	0	1.002	-0.001	5	0	1	0.007	0.995
6	1	0	0.994	0.009	6	0	1	0.002	1.015
7	1	0	1.005	0.005	7	0	1	0.018	0.988
8	1	0	0.987	0.014	8	0	1	-0.029	1.020
9	1	0	1.002	0.005	9	0	1	0.014	0.989
10	1	0	0.839	-0.002	10	0	1	0.009	0.997
11	1	0	1.004	0.002	11	0	1	-0.098	0.932

Table 8 Driving Cycle Classification Results using **A** and **B** Values with 4 Layers and 5 Neurons per Hidden Layer ("1" in the first row represents highway, "0" in the first row represents urban, "1" in the second row represents urban, "0" in the first row represents highway).

	Aggressive Driving				Defensive Driving				
Driving Cycle	Target Classification		Neural Network Classification		Driving Cycle	Target Classification		Neural Network Classification	
	First Row	Second Row	First Row	Second Row		First Row	Second Row	First Row	Second Row
2	0	1	0.002	1.002	2	0	1	0.004	1.005
3	0	1	0.012	0.998	3	0	1	0.005	1.006
4	1	0	0.996	0.005	4	1	0	0.999	0.001
5	1	0	0.996	0.005	5	1	0	1.180	-0.185
8	0	1	0.005	1.005	8	0	0	0.062	0.959
11	1	0	0.999	0.001	11	1	1	1.039	-0.034

Table 9 Driving Behavior Testing Results (**A** and **B** values, Neural Network with 4 Layers and 20 Neurons per Hidden Layer).

	Aggressive Driving				Defensive Driving				
Driving Cycle	Expected Classification		Neural Network Classification		Driving Cycle	Expected Classification		Neural Network Classification	
	First Row	Second Row	First Row	Second Row		First Row	Second Row	First Row	Second Row
12	1	0	0.976	-0.031	12	0	1	0.010	1.006
13	1	0	1.067	-0.027	13	0	1	0.370	0.714
14	1	0	1.077	-0.065	14	0	1	0.129	0.870
15	1	0	0.782	0.432	15	0	1	0.479	0.923

Table 10 Driving Cycle Testing Results using **A** and **B** Values with 4 Layers and 5

Neurons per Hidden Layer.

Driving Cycle	Aggressive Driving		Classification Result	Defensive Driving		Classification Result
	Neural Network Classification			Neural Network Classification		
	First Row	Second Row		First Row	Second Row	
12	0.086	0.908	Urban	0.039	0.964	Urban
13	0.001	1.007	Urban	-0.007	1.017	Urban
14	0.007	1.000	Urban	0.023	0.991	Urban
15	0.768	0.256	Highway	0.747	0.202	Highway

List of Figures

Figure 1 MATLAB/Simulink Electric Vehicle Simulation Block Diagram.
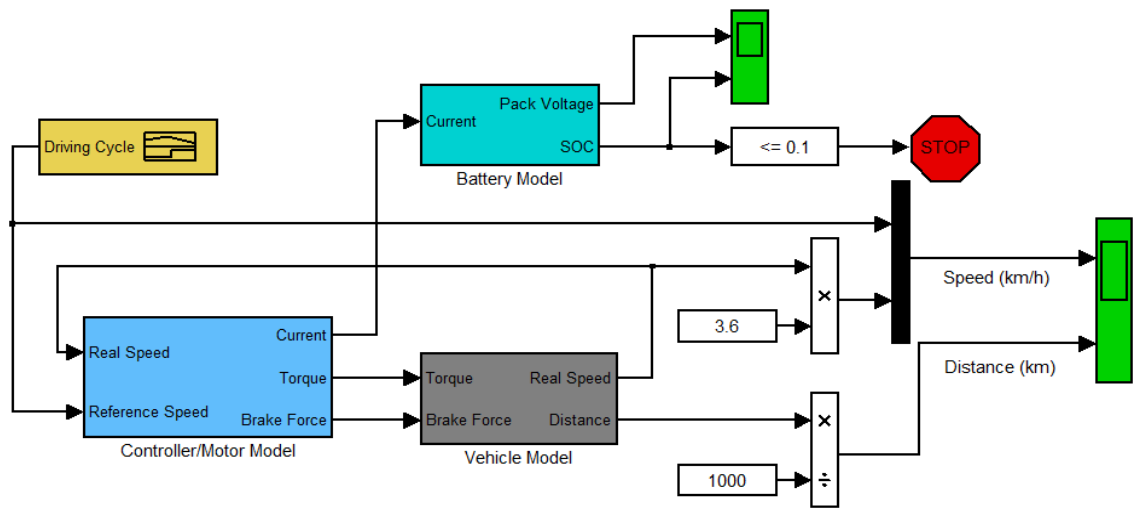
Figure 2 Accelerator Position, Brake Position, and Real Speed for 30-second Example

Driving Cycle (Aggressive Driving).
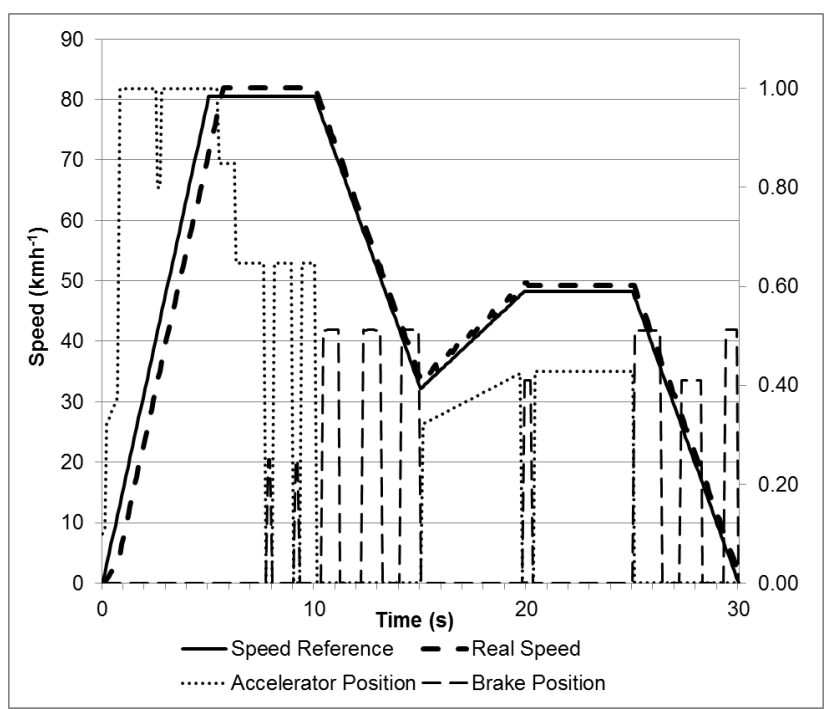
Figure 3 Accelerator Position, Brake Position, and Real Speed for 30-second Example

Driving Cycle (Defensive Driving).
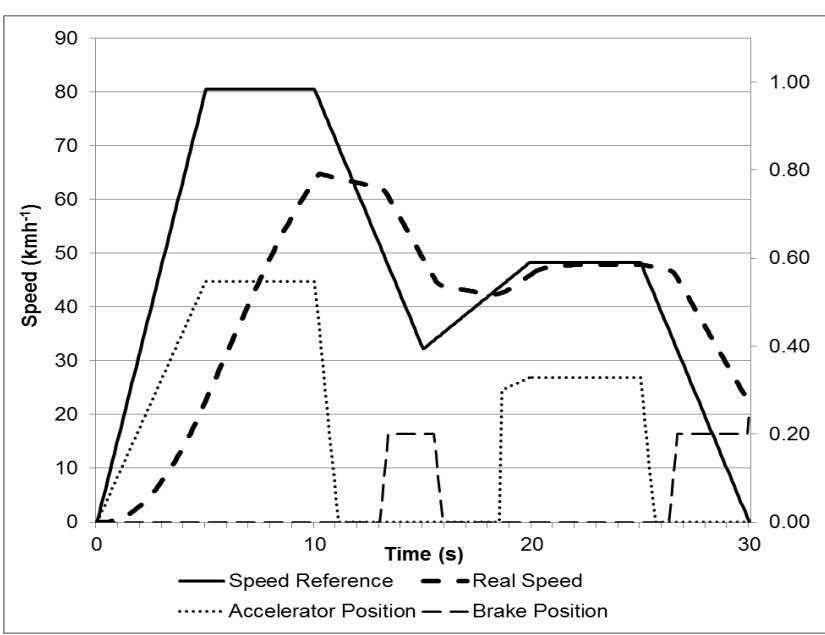
Figure 4 Maximum Acceleration, Maximum Deceleration, Standard Deviation of

Acceleration, and Average Acceleration for 15 Driving Cycles.
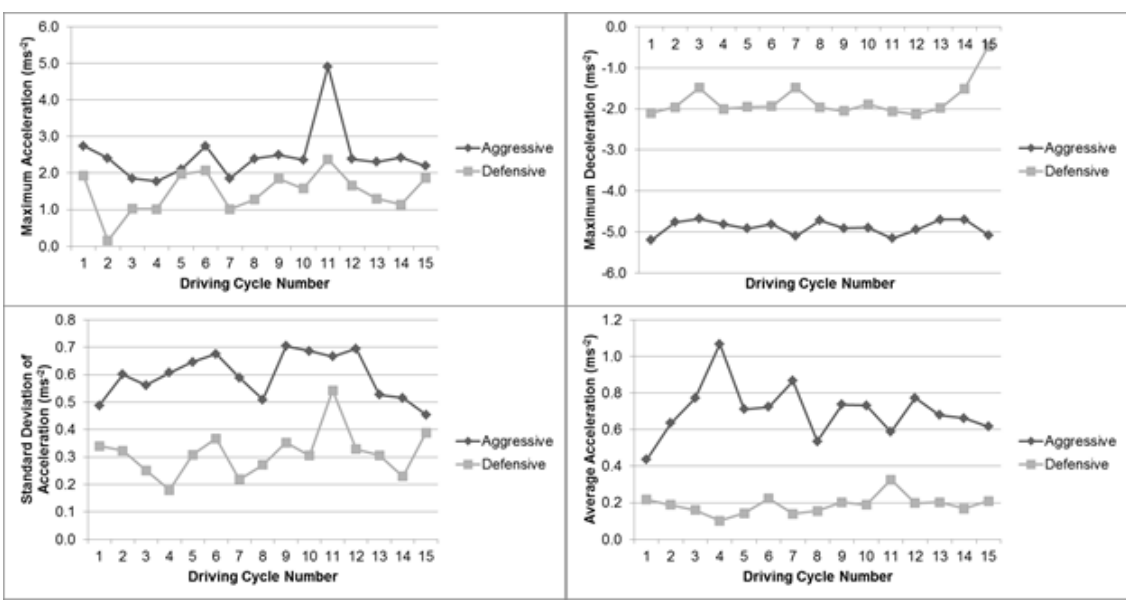
Figure 5 First 120 s of Four Driving Cycles Used for Testing the Neural Network

Driving Cycle Classification Algorithm.
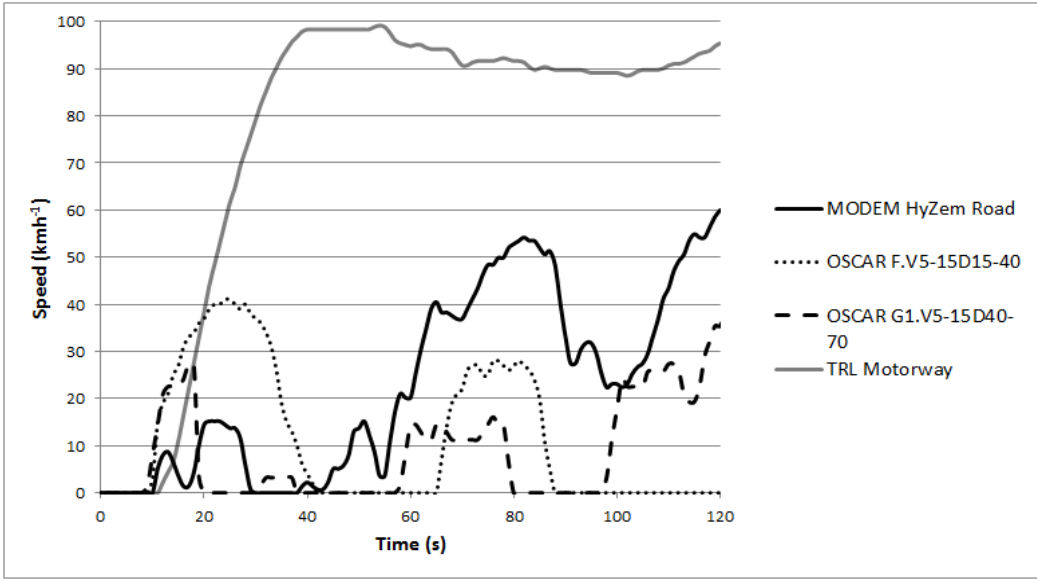
Figure 6 Driving Cycle Classification for Sections of MODEM HyZem Road Driving

Cycle.
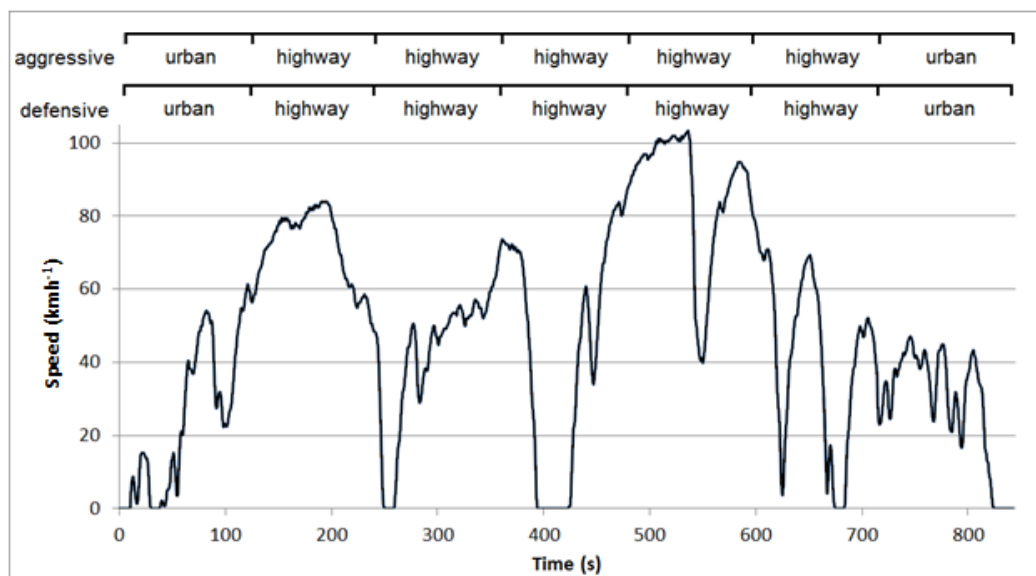
II Electric Vehicle Range Prediction for Constant Speed Trip using Multi-Objective Optimization

Warren Vaz[1], Arup K. Nandi[2], Robert G. Landers[3], Umit O. Koylu[4]

Department of Mechanical & Aerospace Engineering, Missouri University of Science

and Technology, Rolla, Missouri, USA

E-mail[1] (corresponding author): wsvvf9@mst.edu; E-mail[2]:

nandi@cmeri.res.in/nandia@mst.edu; E-mail[3]: landersr@mst.edu; E-mail[4]:

koyluu@mst.edu

ABSTRACT

Due to the limited range and long charging time for electric vehicles, proper utilization of

the stored battery energy is crucial. Current methods for electric vehicle range estimation

do not help the driver to formulate a driving strategy based on trip parameters (e.g., trip

speed) related to power savings. This can be done by predicting the driving range based

on optimal trip parameters prior to the trip enabling the driver to formulate a suitable

driving strategy. This study proposes a novel strategy that presents a number of optimal

trip speeds to the driver, along with the total trip time corresponding to a predicted range.

The optimal speeds were obtained by solving a multi-objective optimization problem that

maximized electric motor efficiency and minimized power consumption. Two approaches

to calculate the objective functions were considered: using constant battery voltage and

using battery voltage as a function of the state-of-charge. Pareto-optimal fronts were

obtained and a plot of the predicted range and trip times for optimal speeds was created.

It was found that the shape of the fronts was not affected by the approach; however, the range was overestimated when a constant battery voltage was used.

Keywords: Electric vehicle, driving strategy, range prediction, multi-objective optimization, genetic algorithm

List of Symbols

a	Acceleration (ms^{-2})
A_f	Frontal area (m^2)
β	Fraction of v_{ref} used as a stopping criterion
Cap	Battery capacity (A·h)
C_D	Drag coefficient
$C_{Transient\_L}$	Battery long transient capacitance (MF)
$C_{Transient\_S}$	Battery short transient capacitance (MF)
e	Speed error (kmh^{-1})
F_D	Aerodynamic drag force (N)
F_r	Friction force (N)
F_t	Traction force (N)
g	Gravitational acceleration (ms^{-2})
G	Overall gear ratio
H	Electric motor efficiency
I_a	Armature current (A)
I_{cell}	Current flowing through an individual battery cell (A)
I_f	Field current (A)

I_P	Battery pack current (A)
K	Geometric constant $(\text{VA}^{-1} \cdot (\text{rads}^{-1})^{-1})$
K_P	Proportional gain
κ	Knee value
L_a	Armature inductance (H)
m	Vehicle mass (kg)
N_P	Number cells in parallel
N_S	Number cells in series
P	Power consumption (W)
R	Tire radius (m)
R_g	Range (km)
$R_{Transient\_L}$	Battery long transient resistance (mΩ)
$R_{Transient\_S}$	Battery short transient resistance (mΩ)
R_{Series}	Battery series resistance (mΩ)
R_a	Armature resistance (Ω)
SF	Switching function
SOC	State-of-charge
SOC_{init}	Initial state-of-charge
t	Time (s)
T^*	Time period during which v_{ref} can be maintain by the battery (min)
v	Real vehicle speed (kmh^{-1})
V_{C_L}	Battery long transient capacitor voltage (V)

V_{C_S}	Battery short transient capacitor voltage (V)
V_{cell}	Voltage of an individual battery cell (V)
v_{max}	Maximum speed (kmh^{-1})
v_{min}	Minimum speed (kmh^{-1})
V_{OC}	Open-circuit battery voltage (V)
V_P	Battery pack voltage (V)
v_{ref}	Reference speed (kmh^{-1})
V_T	Terminal voltage (V)
x	Distance (m)
μ	Rolling friction coefficient
ρ_{air}	Air density (kgm^{-3})
τ	Electric motor torque (Nm)
ω	Rotational speed (rads^{-1})
Θ	Time at which objective functions are calculated (s)

1. Introduction

Electric vehicles (EVs), like most vehicles, have a limited range. However, it takes much longer to recharge an EV than to refuel a conventional diesel or gasoline vehicle. Additionally, charging stations for EVs are not as plentiful as fueling stations for Internal Combustion (IC) engines. Therefore, efficient use of the stored energy in the EV is critical. It is very important to formulate a driving strategy (characterized by the specific values of acceleration, speed, etc.) that uses the stored energy in the most efficient way to obtain a desired range and trip time. It is also beneficial to predict the

driving range based on optimal parameters (acceleration, speed, etc.) that characterize a driving strategy prior to the trip.

Battery SOC methods generally focus on accurately determining the battery SOC (analogous to the fuel gage on a conventional vehicle) in order to obtain an estimate of how much usable energy is left. Since the distance that was covered while depleting the battery from 100% to the current SOC is known, the range available from the residual SOC can be approximately estimated. There are several studies on range estimation using battery SOC methods (Ceraolo and Pede, 2001; Hansen and Wang, 2005; Shen et al., 2005; Szumanowski and Chang, 2008; Smith et al., 2010; Sun et al., 2011; Alvarez Anton et al., 2013; Baronti et al., 2013; Du et al., 2013). This information, while important, is insufficient by itself because the battery's residual energy can be used in many different ways depending on how the driver executes the rest of the trip. It should be used optimally to fulfill the driver's objective; however, the driver does not have any driving strategies presented to properly utilize the residual energy of the battery. Additionally, road conditions may change during the trip as well, and the existing methods mostly fail to capture such variable effects as they are inherently averaging methods.

Energy-based methods of range estimation involve using current or recent trip and vehicle data to calculate the energy or power consumption. This data is then used to predict the vehicle range based on the remaining battery capacity or fuel. Chen et al. (2012) used an Artificial Neural Network (ANN) to predict the residual driving range and driving period for an IC engine vehicle. The input parameters were the fuel capacity (remaining fuel), engine speed, vehicle speed and weight, and road slope. The ANN was

able to predict the residual driving range with a maximum error of 2.2-4.0 km out of a

total range of about 12-85 km and the residual driving period with a maximum error of

14-25 s from the actual period of 40 minutes. This approach provides useful information

to the driver during the duration of the trip based on instantaneous driving parameters.

However, the driver does not know the expected range before starting the trip.

Additionally, no optimization of trip parameters was performed. A method for estimating

the energy consumption of EVs and plug-in hybrid EVs under real-world driving

conditions was presented by Shankar and Marco (2013). This method used an ANN

trained using trip and vehicle parameters such as average speed, average acceleration,

total distance travelled, total duration, etc. to predict the road category and traffic

congestion and, based on this classification, the EV energy consumption per unit distance

was predicted. Prediction results of this method varied in accuracy from 20-30% to 70-

80% of the measured energy consumption. The authors suggested that their proposed

method would enable users to better predict the range of EVs since the energy

consumption per unit distance and total available energy would be known. Once again,

the driver has no knowledge of the expected range given the conditions mentioned in this

paper to formulate a driving strategy. A similar study was also reported by Sadrpour et al.

(2013). Another strategy was proposed by Kim et al. (2013) to predict the immediate

future power requirement of an EV based on power consumption history, acceleration

and speed, and the road information from a pre-downloaded map. A drawback of this

reported strategy is that it is a passive method that only predicts the power requirement

based on the driver's actions. It does not tell the driver how to formulate a driving

strategy. In this study, the goal was to protect the battery; however, such information could also be used in range estimation.

Generally, the three parameters associated with a trip are the distance (range), the speed, and the trip time. Therefore, knowing the range is not always sufficient for a driver because the trip time is also important. Lipp and Boyd (2014) listed several applications where trip time minimization was either the primary goal or highly desirable. Zhang and Rice (2003) developed a method to predict the short-term travel time of freeway drivers using sensor data from the road. Moreover, the driving situation, i.e., acceleration, speed, etc., which depend on road conditions, is important as well. There are several studies (Cheng et al., 2010; Fiat Eco: Drive, 2010; Knowles et al., 2012; Van Mierlo et al., 2004; Bingham et al., 2012) to support the notion that driving parameters, such as the harshness of acceleration or braking, the average trip speed, the number of starts or stops, all influence the vehicle energy consumption and, consequently, the range. Moreover, in order to properly utilize the EV battery's stored energy, it is important to formulate a driving strategy that negotiates the predicted range in an optimal manner. To accomplish this, one must operate the EV in the most efficient regimes of its various components (battery, motor, etc.).

In this paper, a strategy is presented where a number of optimal speeds are presented to the driver along with the range and total trip time corresponding to those optimal speeds. Then the driver chooses a speed based on one or more higher-level decision-making criteria such as distance to destination, total trip time, etc. Knowing the range and total trip time for multiple optimal speeds prior to a trip gives the driver flexibility in choosing a speed that would give a better range while properly utilizing the

stored energy of the EV. This is especially useful in a situation where the driver wants to get to a charging station with a low battery charge. Thus, the primary motivation of this paper is to predict the range of an EV for optimal speeds based on solving the associated optimization problem.

2. Problem Definition

The range (distance) that can be traveled by an electric vehicle travelling at a constant speed is

$$R_g = v_{ref} \times T^*$$

(1)

where v_{ref} is the constant vehicle speed and T^* is the time during which v_{ref} can be feasibly maintained by the battery. However, in practice, there is a small difference between the real vehicle speed and v_{ref}. Thus, v_{ref} can be treated as the commanded or desired speed. The instantaneous speed error is

$$e = v_{ref} - v$$

(2)

In steady state, v_{ref} and v are very close. In order to maximize the range, the time, T^*, should be maximized. This time, T^*, depends on the energy stored in the battery and the power consumption. Since the battery energy is a constant, the lower the power consumption, the longer the time period (T^*) during which v_{ref} can be feasibly maintained by the battery. Consequently, to have a maximum value of T^*, the vehicle power consumption should be minimized. On the other hand, the electric motor, which produces the desired torque for the EV, has an efficiency that also depends on the speed, v_{ref}, and should be maximized. Therefore, it is important to find the optimal value of v_{ref} that minimizes power consumption as well as maximizes electric motor efficiency. The

dependence of power consumption and efficiency on v_{ref} is shown in Fig. 1. This figure

was developed using models described by Larminie and Lowry (2012). From Fig. 1, it is

seen that the objectives are conflicting in nature.

Therefore, range prediction of an EV based on a constant optimal speed is a

Multi-Objective Optimization Problem (MOOP) with conflicting objectives and may be

formulated as follows.

$$\min P = f_P\left(v(t)\right)\big|_{t=\Theta}$$
$$\max H = f_H\left(v(t)\right)\big|_{t=\Theta} \tag{3}$$

subject to

$$v_{\min} \le v_{ref} \le v_{\max}$$
$$P \ge 0 \tag{4}$$
$$0 \le H < 1$$

The power consumption to be minimized and the efficiency to be maximized were

measured at $t = \Theta$. The calculation of Θ will be discussed in Section 4. The real vehicle

speed (v) was the decision variable of the present optimization problem since it is one of

the prime controllable variables that affect both power consumption and efficiency. The

search range for the vehicle speed was taken to be from v_{min} (8 kmh^{-1}) to v_{max} (112 kmh^{-1}).

Drivers do not typically drive slower than 8 kmh^{-1} (very close to walking speed) and 112

kmh^{-1} is close to the top speed of EVs and the typical speed limit on US highways. There

are other reasons for using the vehicle speed as the decision variable: familiarity of

drivers with speed, rather than other parameters like electric motor rotational speed,

torque, etc., road signs generally use speed-related guides for drivers (e.g., speed limits),

and driving cycles, which are generated for simulation and testing purposes, are simply

speed traces. In addition, using speed instead of parameters like motor current or torque

as the decision variable allows easy interpretation of the optimization results. Finally, it allows easy decision-making for related trip objectives such as trip time.

Evolutionary Algorithms (EAs) were successfully applied to solve various single-objective optimization problems and MOOPs (Jain et al., 2009; Ribau et al., 2013; Desai et al., 2010; Dandurand et al., 2013; Shahi et al. 2011). Sometimes, EA-based hybrid methods are also used to solve vehicle problems (Baby Anitha and Duraiswamy, 2012; Niu et al., 2013). Meng et al. (2013) used extreme learning machines to obtain real-time Pareto-optimal solutions for an extended range EV based on objectives of IC engine efficiency, speed, and torque. In this paper, vehicle range estimation is solved using a Multi-Objective Genetic Algorithm (MOGA). In order to solve the MOOP, appropriate models of each objective were formulated according to the concepts used in both approaches. Then, based on these models, a set of Pareto-optimal solutions was generated. Finally, a set of preferred optimal (alternative) solutions of EV speed, v, was selected from the Pareto-optimal front based on Multi-Criteria Decision-Making (MCDM) techniques and using higher-level information of the decision maker (i.e., the driver).

3. EV Model to Calculate Efficiency and Power

In the present study, the following models of different EV components were used to calculate EV efficiency and power. The models used for the EV simulations, including most of the relevant parameters, are well described in the literature (Larminie and Lowry, 2012; Gantt et al., 2011; Xu et al., 2011).

3.1 Electric Motor Model

The relevant electric motor parameters are shown in Table 1. The model's inputs are V_P, v_{ref}, v, ω, and the model's outputs are I_P and τ. The speed error was given in Equation 2. A proportional controller was used for speed control. The switching function $(-1 < SF < 1)$ of the electric motor is

$$SF = K_P e \tag{5}$$

where $K_P = 1$ for this study. The parameters V_T, I_a, I_P, and τ are, respectively,

$$V_T = V_P SF \tag{6}$$

$$I_a = \frac{1}{L_a} \int_0^t \left(V_T - KI_f \omega - I_a R_a \right) dt \tag{7}$$

$$I_P = I_a |SF| \tag{8}$$

$$\tau = KI_a I_f \tag{9}$$

3.2 Battery Model

The battery model's input is I_P and the model's outputs are V_P and *SOC*. By assuming V_P to be a constant, the battery model is simplified to exclude SOC and voltage effects. The relevant battery parameters are shown in Table 2. The parameters I_{cell} and *SOC* are

$$I_{cell} = \frac{I_P}{N_P} \tag{10}$$

$$SOC = SOC_{init} - \int \frac{I_{cell}}{Cap} dt \tag{11}$$

3.3 Vehicle Model

The EV model's input is τ and the model's outputs are v, x, and ω. The parameters F_D, F_r, and F_t are, respectively,

$$F_D = \frac{1}{2}\rho_{air}A_f C_D v^2 \tag{12}$$

$$F_r = \mu mg \tag{13}$$

$$F_t = \frac{\tau G}{R} \tag{14}$$

Assuming the road has no gradient, neglecting the force due to the inertia of the rotating wheels, and having all the braking force come from the electric motor, the acceleration is

$$a = \frac{Ft - F_D - Fr}{m} = \frac{\frac{\tau G}{R} - \frac{1}{2}\rho_{air}A_f C_D v^2 - \mu mg}{m} \tag{15}$$

The parameters v, x, and ω are, respectively,

$$v = \int_0^\Theta a\,dt \tag{17}$$

$$x = \int_0^\Theta v\,dt \tag{16}$$

$$\omega = \frac{vG}{R} \tag{18}$$

The objective function for efficiency, H, is

$$f_H(v(t)) = \frac{\omega \times \tau}{I_P \times V_P} \tag{19}$$

The objective function for power, P, is

$$f_P(v(t)) = I_P \times V_P \tag{20}$$

4. Proposed Approaches for Range Prediction

Two approaches are proposed here to predict EV range along with optimal speed and trip time based on two different scenarios. Approach 1 is based on using constant battery

voltage. It allows one to study the relationship between the objectives and how they are affected by the decision variable without extraneous effects such as varying battery voltage. However, Approach 1 is an ideal case, which is not applicable in a real driving situation because the battery voltage decreases as SOC decreases. The more realistic EV driving scenario, i.e., battery voltage as a function of the state-of-charge, is adopted in Approach 2.

Fig. 2 represents a typical EV simulation as a function of time, assuming a zero road gradient and no stop signs, traffic congestion, etc. Drivers typically choose a vehicle speed by setting an accelerator pedal position or a cruise control setting. In Fig. 2, v_{ref} represents the commanded constant speed. The vehicle is initially at rest at time $t = 0$ with a fully charged battery ($SOC = 1$). Due to its acceleration and the controller type (proportional) used, initially speed transients are observed. After some time v reaches a steady-state value close to v_{ref}. The steady-state vehicle speed is always lower than v_{ref} because the speed error is used to drive the motor if a proportional controller is used. For the proportional controller used, the value of v is always within 98.3% of v_{ref}. The acceleration period is excluded from the calculation of T^*. The time, t_1, at which the vehicle speed reaches within 98.3% of v_{ref} is the starting time to measure T^*. As the simulation continues, SOC decreases with time, t. As a result, V_P starts to drop, resulting in a reduction of v.

At time t_2, the battery's voltage has decreased to a point that it can no longer maintain a constant speed. At time t_3, the battery has almost run out of energy (SOC is around 0.1, depending on the value of v_{ref}) and the speed decreases substantially such that v is no longer close to v_{ref}. The speed becomes too slow for accurate range prediction. At

this speed (called the termination criterion, βv_{ref}, which is some fraction of v_{ref}) the

vehicle speed simulation is stopped. It must be noted that fulfilment of the termination

criterion was only considered as valid after the steady-state speed was achieved ($a = 0$).

The value of T^* in Equation 1 can be calculated as the time interval between t_1 and the

termination criterion. Depending on the termination criteria, if t_3 is the time at which the

vehicle simulation is stopped, T^* becomes $t_3 - t_1$ and the value of Θ mentioned in Section

2 is the same as t_3. The values of v, P, and H are recorded at time t_3. Since v_{ref} and v are

very close (v is within 98.3% of v_{ref}), to predict the range v_{ref} is used.

Depending on the selection of the termination criterion, the value of T^* varies.

Furthermore, T^* also depends on various considerations of the EV model. The two

approaches described above to measure T^* (based on various considerations of the EV

model and the termination criterion) are described as follows.

4.1 Approach 1: Constant Battery Voltage

By considering a constant battery voltage throughout the entire vehicle

simulation, v reaches a constant value after the initial acceleration period. That means, by

assuming that V_P is constant, it is possible to have a constant speed until the battery

completely runs out of energy. For this scenario, Fig. 2 is modified as shown in Fig. 3.

Therefore, a single termination criterion is chosen: when *SOC* reaches a specified limit.

Normally, *SOC* is not allowed to reach zero to protect the battery. Therefore, the

termination criterion was taken to be $SOC = 0.01$. This occurs at t_4 in Fig. 3. The value of

$T^* = t_4 - t_1$ and $t_4 = \Theta$. It may be noted that the actual value of t_4 varies with v_{ref}.

4.2 Approach 2: Battery Voltage as a Function of SOC

In Approach 2, V_P is a function of *SOC*. As *SOC* decreases, so does V_P and the battery is not able to maintain v close to v_{ref} after a certain *SOC* value as shown in Fig. 2. This *SOC* value is different for different batteries and speeds. The battery model presented in Section 3.2 was modified to include the battery's dependency on *SOC*. The lithium-ion battery model presented by Chen and Rincon-Mora (2006) was used. The model is briefly described as follows (in addition to Equations 10 and 11)

$$V_P = N_S V_{cell} \tag{21}$$

$$\frac{d}{dt}\left(V_{C\_L}\right) = \frac{I_{cell}}{C_{Transient\_L}} - \frac{V_{C\_L}}{C_{Transient\_L} R_{Transient\_L}} \tag{22}$$

$$\frac{d}{dt}\left(V_{C\_S}\right) = \frac{I_{cell}}{C_{Transient\_S}} - \frac{V_{C\_S}}{C_{Transient\_S} R_{Transient\_S}} \tag{23}$$

$$V_{OC} = -1.031e^{(-35SOC)} + 3.685 \\ + 0.2156SOC - 0.1178SOC^2 + 0.3201SOC^3 \tag{24}$$

$$V_{cell} = V_{OC} - V_{C\_S} - V_{C\_L} - I_{cell} R_{Series} \tag{25}$$

The model constants are in Table 3. The first part of the trip (starting from rest to a steady-state speed) is similar to the trip shown in Fig. 2. However, as the *SOC* decreases, so do v and V_P. The motor drive draws a higher current from the battery to maintain a constant speed for as long as possible. Between times t_2 and t_3, v is close to v_{ref} but cannot be maintained at a constant value due to the deteriorating *SOC*. As t approaches t_3, the *SOC* and V_P decrease to the point where v can no longer be maintained close to v_{ref}. The vehicle speed drops until it is below some fraction, β, of v_{ref} at t_3. The value of T^* is now $(t_3 - t_1)$ and $t_3 = \Theta$. The value of T^* is different for different values of β. Additionally, during the MOOP, the instantaneous efficiency and power at the end of

the simulation are considered. Therefore, the termination criterion is critical. If it is too lax, the vehicle speed will differ significantly from the commanded speed, but would be preferentially chosen by MOGA since the power would be lowered as the vehicle loses speed. Thus, unlike in Approach 1, the simulation process in Approach 2 was stopped based on either one of the following two termination criteria, $SOC < 0.01$ or $v < \beta v_{ref}$, whichever was satisfied first.

For the EV model used in this study, it was observed that steady-state speed (v) was always within 98.3% of v_{ref}. This value was a result of the proportional speed controller and gain value used. Fig. 4 shows the steady-state speed (v) for three different reference speeds (v_{ref}). It can be seen that v is always within 98.3% of v_{ref}. The upper limit for β was found to be 98.4%. Beyond this, v is not guaranteed to reach a steady-state value within βv_{ref} for all values of v_{ref}. Keeping in mind the scenario described above for Approach 2, the termination criterion, β, was taken to be 98.3%. It is clear that it is important to pick the value of β carefully. If it is too low (significantly below 98.3%), the range will be overestimated since the simulation will continue for a longer time period at a speed that is not close to the reference speed. On the other hand, if it is too high (above 98.4%), the range will be underestimated since the simulation will be terminated prematurely whenever the vehicle speed first begins to drops as a result of decreasing battery voltage.

5. Multi-Objective Genetic Algorithm

Multi-Objective Genetic Algorithms are a class of tools based on Genetic Algorithms (GAs) to solve multi-objective optimization problems having conflicting objectives. A GA is an optimization technique that mimics the principle of natural

selection and natural genetics (Goldberg, 1989) to find the best solution, with respect to an objective function for an engineering problem. Genetic algorithms operate on a population of feasible solutions by applying the principle of "survival of the fittest" to successively produce better approximations in each generation (i.e., iteration of the algorithm). During each generation, a new set of solutions is created by the process of selecting individuals according to their level of fitness (i.e., value of their fitness functions) and breeding them together using operators (such as crossover and mutation) borrowed from natural genetics. This process leads to the evolution of populations of individuals that are better suited to their environment (i.e., they have better objective functions) than the individuals that they were created from, just as in natural adaptation. The working principle of a binary-coded GA is lucidly described by Nandi (2012).

Unlike a single-objective optimization problem where the objective is to find a single solution, the task of an optimizer in a MOOP is to obtain a set of solutions based on the concept of domination by comparing two solutions on the basis of whether or not one dominates the other solution or not. The plot of the objective functions for the non-dominated solutions is called a non-dominated front. If the non-dominated solutions are optimal in terms of the objectives, then the non-dominated front is called the Pareto-optimal front and the solutions lying on the Pareto-optimal front are called Pareto-optimal solutions. Thus, the primary goal in a multi-objective optimization problem is to obtain a set of solutions as close as possible to the true Pareto-optimal front in addition to being spread out as diversely as possible throughout the Pareto front. Optimization techniques based on GAs were found to be most suitable to solve such kind of multi-objective optimization problems because a GA is itself a population-based algorithm. In the present

work, one of the most popular non-dominated sorting GA, NSGA-II (Deb et. al., 2002) was adopted.

Fig. 5 describes the working procedure of a six bit binary-coded NSGA-II in order to solve the problem of predicting EV range based on optimal speeds obtained by the minimization of P and the maximization of H using v_{ref} as the decision variable. For a given set of GA parameters, such as population size = 6 (in order to obtain a maximum of 6 solutions), maximum number of generations = 10 (set as the termination criterion of the MOGA), chromosome length = 6 (6 bits are considered to encode the value of the decision variable, v_{ref}), tournament size = 2, mutation probability = 0.01, and crossover probability = 0.98, a maximum of six non-dominated solutions can be obtained after a complete run of the MOGA. For each speed, the EV simulation was run for a certain time period as determined by the termination criteria stated in Approaches 1 and 2 (described in Sections 4.1 and 4.2, respectively). The EV power and efficiency were recorded at the end of each time period. By plotting the values of power and efficiency corresponding to each speed, a non-dominated front (i.e., Pareto front) was obtained.

In order to verify the results, exhaustive searches of the objective functions were conducted. The vehicle speed was varied from 8-112 kmh^{-1} in increments of 1.6 kmh^{-1} and the corresponding H and P values were calculated and plotted, along with the GA results for comparison.

Although there are advantages to knowing the range of each objective for Pareto optimality and the shape of the Pareto-optimal front itself in a problem for adequate decision-making, the task of choosing a single preferred Pareto-optimal solution is important because the user finally adopts the preferred single solution for

implementation. Various MCDM techniques are available and may be adopted either

before the optimization (a priori approach), after the optimization (a posteriori approach),

or during the optimization process (progressive approach). In the present work, an "a

posteriori" approach was adopted where the selection of a set of preferred solutions was

made by analyzing the knee value (Branke et al., 2004) of each solution on the Pareto

front. Sometimes, the shape of the Pareto-optimal front is such that there may be

solutions where a small improvement in one objective will lead to a large deterioration in

other objectives, which makes moving in either direction unattractive. For a MOOP that

seeks to maximize f_1 and minimize f_2, a knee value of the ith solution is

$$\kappa_i = \frac{\dfrac{f_1^{(i-1)} - f_1^{(i)}}{f_2^{(i-1)} - f_2^{(i)}} + \dfrac{f_2^{(i+1)} - f_2^{(i)}}{f_1^{(i+1)} - f_1^{(i)}}}{2} \qquad (26)$$

A solution point having a higher knee value than that of others is said to be a

stronger knee point. Without any knowledge about the user's preferences, it may be

argued that the stronger knee point is the most likely to be interesting for the decision

maker, in this case, the driver.

6. Results and Discussion

Determining EV range is a multi-objective optimization problem (as described in

Section 2). In order to solve this problem, a MOGA (presented in Section 5) is adopted

here considering two different approaches (Approaches 1 and 2, presented in Section 4)

based on a typical EV model (discussed in Section 3). The results of solving the MOOP

for the two approaches are presented in this section.

The vehicle parameters adopted for the present study are shown in Table 4, and the relevant GA parameters used to solve the present problem are shown in Table 5. After running the MOGA, a non-dominated front with a maximum of 50 non-dominated solutions was obtained. An MCDM strategy was applied based on the knee concept (Branke et al., 2004) to identify the 20 best Pareto-optimal solutions out of the 50 non-dominated solutions. Corresponding to these 20 Pareto-optimal solutions, the range and trip time are presented to the driver for trip planning.

6.1 Approach 1: Constant Battery Voltage

In Approach 1, a constant battery voltage is assumed. While carrying out the multi-objective optimization, the calculation of power and efficiency are made at $SOC = 0.01$. According to Approach 1, this task may be performed by two ways: based on the steady-state forms of the EV model equations or using an EV model simulation that accounts for vehicle acceleration. The steady-state equations of the EV model are

$$
\begin{aligned}
&\left(\frac{1}{2}\rho_{air}A_f C_D\right)v^2 - \frac{KI_f G}{RR_a}\left(\frac{KI_f G}{R} + K_P V_P\right)v \\
&+ \mu mg - \frac{KI_f G K_P V_P v_{ref}}{RR_a} = 0
\end{aligned}
\tag{27}
$$

$$
I_P = \frac{\left(\frac{1}{2}\rho_{air}A_f C_D v^2 + \mu mg\right)}{\dfrac{KI_f G}{R}}\left(v_{ref} - v\right)
\tag{28}
$$

Table 6 presents calculated values of EV efficiency and power, as well as the corresponding time, using the simulation and steady-state methods (for $v_{ref} = 48$ kmh^{-1}). From Table 6, the efficiency and power resulting from both methods are the same. To compare the computational time, both methods were coded in MATLAB R2013a and run

on an Intel® Core™ i5-2400 computer (@ 3.1 GHz with 4 CPUs). The steady-state

method took 0.0071 s on average and the simulation method took 0.051 s on average.

However, it was found that the calculated values of T^* using the steady-state method

were 3.6 min higher than those obtained through the simulation method. As a result, the

steady-state method predicts a higher range than the range predicted by running the

simulation since the calculation of range is made based on Equation 1. This is due to the

fact that the steady-state method assumes the vehicle is moving at v_{ref} throughout the trip

without accounting for the initial acceleration period during which the vehicle speed is

less than v_{ref}. The simulation method, on the other hand, completely neglects the distance

covered by the vehicle during acceleration because Equation 1 is not applicable here to

calculate the range. A different technique to deal with the acceleration period is needed.

The authors are working on methods to incorporate the acceleration period into the

proposed strategy. This would also enable the driver to effectively address changing road

conditions, which were not considered in this study, that require a reduction of speed or a

complete stop.

Furthermore, it was found that the disparity between the two methods in

calculating the range increased as v_{ref} increases, as observed in Fig. 6. The disparity

between the two methods is because the steady-state range is predicted using the steady-

state current, which is much lower than the current during acceleration. Since the battery

capacity is fixed, for higher v_{ref} values, the effect of assuming the EV speed is v_{ref} during

the acceleration period is amplified. Another drawback of the steady-state approach is

that the equations become more complicated and difficult to solve when the battery

voltage is no longer assumed to be constant. Additionally, even though this study does

not consider them, acceleration and changing road conditions become harder to implement using this method. For these reasons, for the rest of the study, all calculations related to EV were carried out by running the EV simulation for different v_{ref} values.

Fig. 7 shows the results of the optimal solutions obtained using MOGA plotted along with those obtained by an exhaustive search method of all possible solutions from 8-112 kmh^{-1}. Both the exhaustive search and the MOGA are expected to give the same front because the problem deals with only one decision variable, the vehicle speed. Still, there are two differences observed in the fronts. As seen in the figure, MOGA does not pick solutions past a certain point in the search space, which is when H decreases while P increases, whereas the exhaustive search uniformly gives solutions throughout the search space, even if they are sub-optimal. The reason is that MOGA selects the optimal solutions based on the concept of non-domination suggesting that MOGAs have better optimization capability than the exhaustive search method. Additionally, the distribution of exhaustive search solutions is based on the granularity of the search whereas the distribution of the MOGA solutions is based on the concept of non-domination. The non-dominated GA solutions are distributed from efficiencies in the range 0.66-0.89 and powers in the range 600-7500 W.

Fig. 8 describes the Pareto fronts obtained using MOGA for different initial SOC values based on Approach 1. The shape of all of the Pareto fronts irrespective of the initial SOC is the same since there is only one decision variable. However, it can be seen that the set of solutions comprising each front is different for different fronts. Moreover, the distribution of solutions of the fronts where initial $SOC > 0.1$ was found to be the same as Fig. 7. However, when initial $SOC = 0.1$, solutions above 6200 W were not

picked. This is because as the initial *SOC* decreases and the commanded speed increases, by the time the vehicle is able to accelerate to the commanded speed, the battery is no longer able to maintain the speed. This is why the highest power picked was around 6200 W, corresponding to efficiency of 0.89. Fig. 9 shows the range for each point in Fig. 8. Fig. 10 shows the associated trip time. As expected, the range for a particular speed decreased as the initial *SOC* decreased. The trip time followed a similar trend as well. For a given initial *SOC*, as the speed increases, the corresponding trip time decreases. The range, however, first increases, and then decreases. This is the effect of the conflicting objectives. The initial increase in range for increasing constant speeds is due to the sharp increase in efficiency (Fig. 1). The subsequent decrease is due to the effect of power increasing as a function of v^2.

After analyzing the fronts (i.e., the plot of the non-dominated GA solutions), a knee zone is clearly visible in the middle of the front. Fig. 11 shows the Pareto front corresponding to the set of optimal speeds obtained using Approach 1 by maximizing motor efficiency and minimizing EV power using MOGA. In Fig. 11, normalized values of *H* and *P* were plotted. After running the MOGA with 50 initial solutions (population size) for 50 generations, 50 non-dominated solutions were found in the final population. This is expected: in Fig. 1, *H* and *P* are both monotonically increasing functions (up to a certain speed) with only one decision variable. Therefore, when any two random solutions in this speed zone are compared, they will be non-dominated with respect to each other. Out of the 50 non-dominated solutions, the top 20 solutions based upon the strength of their knee value as calculated in Equation 26 were selected and plotted along with the non-dominated solutions as shown in Fig. 11. They represent the best trade-off

between the two conflicting objectives: minimum loss in one objective per unit gain in the other.

Fig. 12 presents the ranges and trip times for different optimal speeds along with the knee values. In this case, the maximum range occurs at a vehicle speed of 19.2 kmh^{-1}, which is between the maximum efficiency (around 67.5 kmh^{-1}) and the minimum power (0 kmh^{-1}). It must be noted that the numbers presented were due to the EV model used in this study. It is expected that the maximum range would shift to a different speed if a different model is used, or if the EV model parameters are varied. Fig. 12 shows the knee solutions plotted along with the corresponding ranges and trip times for the respective speeds. This plot would be presented to the driver prior to the trip to help in decision-making to select a trip speed.

In the two-step optimization process, the driver selects an optimal solution from Fig. 11 and uses the corresponding v_{ref} to determine the associated range and time from Fig. 12. For example, the best knee solution in Fig. 11 corresponds to a speed of 32.5 kmh^{-1}. This corresponds to a range of 41.2 km and a trip time of 79.5 min as seen in Fig. 12. The selection of an optimal solution can be done from two perspectives. If a certain minimum range is desired, the driver can choose the optimal speed(s) that would guarantee this range. Based on the optimal speed, the driver can determine the associated trip time. On the other hand, if time is a constraint, then the driver would choose the optimal speed(s) that maximizes the range. For example, from Fig. 12, if the driver wants to travel at least 32 km, vehicle speeds between 15.2 and 50.9 kmh^{-1} are viable options. The trip times associated with these speeds are 176.7 and 38.0 min, respectively. The driver would choose the higher speed to reach the destination faster and the lower speed

to travel more efficiently (in the event of unforeseen circumstances). On the other hand, if the driver has at most 50 min for the trip, the driver can choose a vehicle speed between 43.9 kmh^{-1} and 70.0 kmh^{-1}. The ranges associated with these trip times are 35.7 and 24.8 km, respectively. The driver would choose the optimal speed based on the distance to the destination.

Approach 1 provides an idea of how to predict the EV range by selecting an optimal speed based on maximizing efficiency and minimizing power. However, as stated previously, Approach 1 is not applicable in a real driving situation because the battery voltage decreases as *SOC* decreases. With a decreasing battery voltage, *v* also gradually decreases regardless of v_{ref}. This means that the EV simulation termination criterion (as explained in Section 4) to calculate *T** cannot be based only on *SOC*. The effect of the gradually decreasing *v* should also be included in the termination criterion to obtain a realistic range.

6.2 Approach 2: Battery Voltage as a Function of SOC

Unlike Approach 1, the scenario considered in Approach 2 is more realistic. The modified battery model presented in Section 4.2 is used in Approach 2; however, the same vehicle parameters (presented in Table 4) and motor model are used in Approach 2. The termination criteria for the EV simulations are $SOC < 0.01$ or $v < \beta v_{ref}$.

Fig. 13 describes the Pareto fronts obtained using MOGA for different initial *SOC* values based on Approach 2 when $\beta = 98.3\%$. The shape of all of the Pareto fronts irrespective of the initial *SOC* obtained in Approach 2 is the same as Approach 1. Similarly, it can be seen that the set of solutions comprising each front is different for different fronts. Moreover, the distribution of solutions of the fronts where initial *SOC* >

0.1 was found to be the same as in Approach 1 (from efficiencies in the range of 0.66-0.89 and power in the range of 600-7500 W). Finally, when initial $SOC = 0.1$, the spread of solutions was significantly reduced (from efficiencies in the range of 0.70-0.86 and power in the range of 700-1950 W). This trend was also observed in Fig. 8c in Approach 1.

Figs. 14 and 15 show the range and the trip time, respectively, for different initial SOC values when $\beta = 98.3\%$. As expected, the range for a particular speed decreased as the initial SOC decreased. The trip time followed a similar trend as well. As mentioned in Section 6.1, Approach 1 is an ideal case: no other approach can have a higher range for a particular speed than Approach 1 (for initial $SOC = 1.0$). This postulate was verified by comparing Fig. 9 with Fig. 14. This is because in Approach 2 the battery voltage decreases as the SOC decreases, implying the total available battery energy is lower than assumed in Approach 1 with a constant battery voltage. One significant difference of Approach 2 relative to Approach 1 in the range and trip time trends was that for very low speeds, the range dropped sharply as did the trip time. This can be explained as follows. The steady-state speed error is a function of v_{ref}. For very low speeds, the steady-state speed error is very close to βv_{ref} as seen in Fig. 4. Due to this, even a slight decrease in steady-state v due to decreasing V_P results in one of the termination criteria being satisfied ($v < \beta v_{ref}$) and the simulation ending. Therefore, even though the SOC was significantly greater than 0.01, the simulation was terminated and the value of T^* was found to be lower than expected. This results in the range and trip time being significantly lower than expected. This does not happen in Approach 1 since V_P is constant throughout the simulation. Figs. 14 and 15 map the range and trip time,

respectively, to the initial battery *SOC*. Such a map can be used by the driver during the course of a trip when the initial *SOC* is not 1.

Approaches 1 and 2 are proposed in the present study to predict EV ranges made based on a constant trip speed. Constant speed-based results of range are characteristic of highway driving. For example, consider a driver who needs to travel from one city to another. The driver is presented with multiple ranges and selects the speed that guarantees completion of the trip before completely depleting the battery. Another consideration in choosing the speed may be trip time: the driver may be willing to sacrifice range in order to reach his/her destination within a certain time period. The driver would be able to make this decision with full knowledge about the penalty of the choice (in terms of loss of range or trip time). This information would assist the driver in trip planning. A demonstration of the impact of prior information was conducted by Jou (2001). It was concluded that having pre-trip information makes commuters more likely to change their original choice of departure time and route when they were presented with pre-trip information than when they were not.

The proposed strategy can immediately benefit the driver since adopting it does not require any changes to existing EVs. However, there are certain shortcomings to the proposed approaches. The commanded reference speed was used here to compute the range. In reality, the vehicle is moving at v, not v_{ref}. Therefore, the predicted range has an inherent error of about 1.7%. On the other hand, while the energy to accelerate the vehicle to v_{ref} was included in the range prediction, the distance covered during the initial acceleration period was not. The distance covered during acceleration is small, which

means the range predicted is slightly lower than the actual range. As mentioned

previously, the acceleration period will be considered separately.

7. Summary and Conclusions

Range prediction for EVs was cast as a multi-objective problem with conflicting

objectives. Two approaches were considered: one assuming constant battery voltage and

the other allowing battery voltage to be a function of *SOC*. Approach 1 provided a basis

for more realistic approaches by showing the shape of the Pareto fronts and by capping

the expected range for any given speed. Approach 2 showed Pareto fronts whose shapes

were the same as those obtained in Approach 1. The predicted range was lower since the

battery voltage was no longer assumed to be constant. A map of the EV range and trip

time for different initial *SOC* values was created, which would be useful to the driver in

two different cases: when starting a trip with a battery that is not fully charged and when

choosing a new speed once a trip has already started and the battery is partially depleted.

However, it did not affect which solutions were picked by the GA from the search range.

The strategy presented in this paper is aimed at assisting the driver in formulating

a driving strategy and for trip planning based on optimization of trip parameters. The

results obtained by solving the MOOP presented in this paper are subject to the model

parameters and assumptions stated in the previous sections. They provide insight into

vehicle design and optimization. Furthermore, trip planning is of general interest to the

transportation industry. Knowing the range and trip time for multiple optimal speeds

prior to a trip gives the driver flexibility in choosing a speed that would give a better

range while properly utilizing the stored EV energy. The final selection of the trip speed,

however, is decided by the driver. This type of trip planning could be used with existing

methods to incorporate GPS and traffic data in order to properly utilize the EV and to

improve the driving experience.

Acknowledgements

References

[1] Alvarez Anton, J.C., Garcia Nieto, P.J., Blanco Viejo, C., Vilan Vilan, J.A., 2013. Support vector machines used to estimate the battery state of charge. IEEE Transactions on Power Electronics 28 (12), 5919-5926.

[2] Baby Anitha, E., Duraiswamy, K., 2012. A heuristic moving vehicle location prediction technique via optimal paths selection with aid of genetic algorithm and feed forward back propagation neural network. Journal of Computer Science 8 (12), 2008-2016.

[3] Baronti, F., Zamboni, W., Femia, N., Saletti, R., Chow, M.-Y., 2013. Parameter identification of Li-Po batteries in electric vehicles: A comparative study. IEEE International Symposium on Industrial Electronics 6563887.

[4] Bingham, C., Walsh, C., Carroll, S., 2012. Impact of driving characteristics on electric vehicle energy consumption and range. IET Intelligent Transport Systems 6 (1), 29-35.

[5] Branke, J., Deb, K., Dierolf, H., Osswald, M., 2004. Finding knees in multi-objective optimization. Yao, X., et al. (eds.) PPSN 2004, LNCS 3242, Springer, Heidelberg, 722–731.

[6] Ceraolo, M. Pede, G., 2001. Techniques for estimating the residual range of an electric vehicle. IEEE Transactions on Vehicular Technology 50 (1), 109-115.

[7] Chen, M., Rincon-Mora, G.A., 2006. Accurate electrical battery model capable of predicting runtime and I-V performance. IEEE Transactions on Energy Conversion 21 (2), 504-511.

[8] Chen, Y.L., Huang, C.H., Kuo, Y.W., Wang, S.S., 2012. Artificial neural network for predictions of vehicle drivable range and period. 2012 IEEE International Conference on Vehicular Electronics and Safety, July 24-27, Istanbul, Turkey, 329-333.

[9] Cheng, C., McGordon, A., Poxon, J., Jones, R., Jennings, P., 2010. A model to investigate the effects of driver behaviour on hybrid vehicle control. 25th World Battery, Hybrid, and Fuel Cell Electric Vehicle Symposium and Exhibition, November 5-9, Shenzhen, China.

[10] Dandurand, B., Guarneri, P., Fadel, G., Wiecek, M.M., 2013. Equitable multi-objective optimization applied to the design of a hybrid electric vehicle battery. ASME Journal of Mechanical Design, 135 (4), 041004.

[11] Deb K., Pratap, A., Agarwal S., Meyarivan, T., 2002. A fast elitist non-dominated sorting genetic algorithm for multi-objective optimisation: NSGA-II. IEEE Transactions on Evolutionary Computation 6 (2), 182-197.

[12] Desai, C., Berthold, F., Williamson, S.S., 2010. Optimal drivetrain component sizing for a plug-in hybrid electric transit bus using multi-objective genetic algorithm. EPEC 2010 - IEEE Electrical Power and Energy Conference: "Sustainable Energy for an Intelligent Grid" 5697242.

[13] Du, L.L., Li, B., Zhang, H.D., 2013. Estimation on state of charge of power battery based on the grey neural network model. Applied Mechanics and Materials 427-429, 1158-1162.

[] Fiat Eco: Drive, 2010. Eco-driving uncovered: the benefits and challenges of eco-driving based on the first study using real journey data, available at http://www.lowcvp.org.uk/assets/reports/Fiat_Eco-Driving%20Uncovered.pdf.

[14] Gantt, L.R., Alley, R.J., Nelson, D.J., 2011. Battery sizing as a function of powertrain component efficiencies for various drive cycles. ASME International Design Engineering Technical Conferences & Computers and Information in Engineering Conference (IDETC/CIE 2011), August 28-31, Washington, DC.

[15] Goldberg, D.E., 1989. Genetic algorithms for search, optimization, and machine learning. Addison-Wesley, Reading, MA.

[16] Hansen, T., Wang, C.-J., 2005. Support vector based battery state of charge estimator. Journal of Power Sources 141 (2), 351-358.

[17] Jain, M., Desai, C., Williamson, S.S., 2009. Genetic algorithm based optimal powertrain component sizing and control strategy design for a fuel cell hybrid electric bus. 5th IEEE Vehicle Power and Propulsion Conference 5289740, 980-985.

[18] Jou, R.C., 2001. Modeling the impact of pre-trip information on commuter departure time and route choice. Transportation Research Part B: Methodological 35, 887-902.

[19] Kim, E., Lee, J., Shin, K.G., 2013. Real-time prediction of battery power requirements for electric vehicles. ACM/IEEE International Conference on Cyber-Physical Systems, April 8-11, Philadelphia, PA, USA, 11-20.

[20] Knowles, M., Scott, H., Baglee, D., 2012. The effect of driving style on electric vehicle performance, economy, and perception. International Journal of Hybrid Vehicles 4 (3), 228-247.

[21] Larminie, J., Lowry, J., 2012. Electric vehicle technology explained, 2nd Edition, John Wiley & Sons, Ltd., Chichester, West Sussex, UK.

[22] Lipp, T., Boyd, S., 2014. Minimum-time speed optimisation over a fixed path. International Journal of Control 87 (6), 1297-1311.

[23] Meng, B., Wang, Y., Yang, Y., 2013. Efficiency-optimization control of extended range electric vehicle using online sequential extreme learning machine. 2013 9th IEEE Vehicle Power and Propulsion Conference 6671680, 146-151.

[24] Nandi, A.K., 2012. GA-Fuzzy approaches: application to modeling of manufacturing process. Statistical and Computational Techniques in Manufacturing, Springer-Verlag, Berlin, Heidelberg, ISBN: 978-3-642-25858-9, DOI 10.1007/978-3-642-25859-6), 145-185.

[25] Niu, J., Pei, F., Zhou, S., Zhang, T., 2013. Multi-objective optimization study of energy management strategy for extended-range electric vehicle. Advanced Materials Research 694-697, 2704-2709.

[26] Ribau, J.P., Sousa, J.M.C., Silva, C., 2013. Multi-objective optimization of fuel cell hybrid vehicle powertrain design - Cost and energy. SAE Technical Papers 6.

[27] Sadrpour, A., Jin, J., Ulsoy, A.G., 2013. Mission energy prediction for unmanned ground vehicles using real-time measurements and prior knowledge. Journal of Field Robotics 30 (3), 399-414.

[28] Shahi, S.K., Wang, G.G., An, L., Bibeau, E., 2011. Optimal hybridization of battery, engine and motor for PHEV20, Proceedings of the ASME Design Engineering Technical Conference 5 (PARTS A AND B), 315-324.

[29] Shankar, R. Marco, J., 2013, Method for estimating the energy consumption of electric vehicles and plug-in hybrid electric vehicles under real-world driving conditions. IET Intelligent Transport Systems 7 (1), 138-150.

[30] Shen, W.X., Chau, K.T., Chan, C.C., Lo, E.W.C., 2005. Neural network-based residual capacity indicator for nickel-metal hydride batteries in electric vehicles. IEEE Transactions on Vehicular Technology 54 (5), 1705-1712.

[31] Smith, K.A., Rahn, C.D., Wang, C.-Y., 2010. Model-based electrochemical estimation and constraint management for pulse operation of lithium ion batteries. IEEE Transactions on Control Systems Technology 18 (3), 654-663.

[32] Sun, F., Hu, X., Zou, Y., Li, S., 2011. Adaptive unscented Kalman filtering for state of charge estimation of a lithium-ion battery for electric vehicles. Energy 36 (5), 3531-3540.

[33] Szumanowski, A., Chang, Y., 2008. Battery management system based on battery nonlinear dynamics modeling. IEEE Transactions on Vehicular Technology 57 (3), 1425-1432.

[34] Van Mierlo, J., Maggetto, G., Van De Burgwal, E., Gense, R., 2004. Driving style and traffic measures – influence on vehicle emissions and fuel consumption. Proceedings of Institute of Mechanical Engineers Part D: Journal of Automobile Engineering 218 (1), 43-50.

[35] Xu, G., Li, W., Xu, K., Song, Z., 2011. An intelligent regenerative braking strategy for electric vehicles. Energies 4, 1461-1477.

[36] Zhang, X., Rice, J.A., 2003. Short-term travel time prediction. Transportation Research Part C: Emerging Technologies 11 (3-4), 187-210.

List of Tables

Table 1 Electric motor parameters.

Armature inductance, L_a (H)	0.1
Armature resistance, R_a (Ω)	0.5
Field current, I_f (A)	1.0
Geometric constant, K (VA^{-1}·(rads^{-1})$^{-1}$)	1.5
Type	DC brushed

Table 2 Lithium-ion battery parameters.

Capacity, Cap (A·h)	8.0
Initial state-of-charge, SOC_{init}	1.0
Number of cells in parallel, N_P	1
Type	Lithium-Ion
Voltage, V_P (V)	394

Table 3 Chen and Rincon-Mora Lithium-ion battery parameters.

$C_{Transient\_L}$ (MF)	0.22375
$R_{Transient\_L}$ (mΩ)	0.9968
$C_{Transient\_S}$ (MF)	0.03518
$R_{Transient\_S}$ (mΩ)	0.9338
R_{Series} (mΩ)	1.4932

Table 4 Vehicle model parameters.

Air density, ρ_{air} (kgm^{-3})	1.225
Drag coefficient, C_D	0.35
Frontal area, A_f (m^2)	2.5
Gravitational acceleration, g (ms^{-2})	9.81
Mass, m (kg)	1350
Overall gear ratio, G	2.1
Rolling friction coefficient, μ	0.014
Tire radius, R (m)	0.3429
Transmission	Single-speed

Table 5 MOGA parameter values for simulations conducted in this paper.

Parameter	Value
Initial Population Size	50
Chromosome Length (Number of Bits)	20
Crossover Probability	0.98
Mutation Probability	0.01
Number of Generations	50

Table 6 Results of simulation and steady-state methods for $v_{ref} = 48$ kmh^{-1}.

Method	H	P	T* (min)
Simulation	0.89	4169	41.7
Steady-state method	0.89	4169	45.3

List of Figures
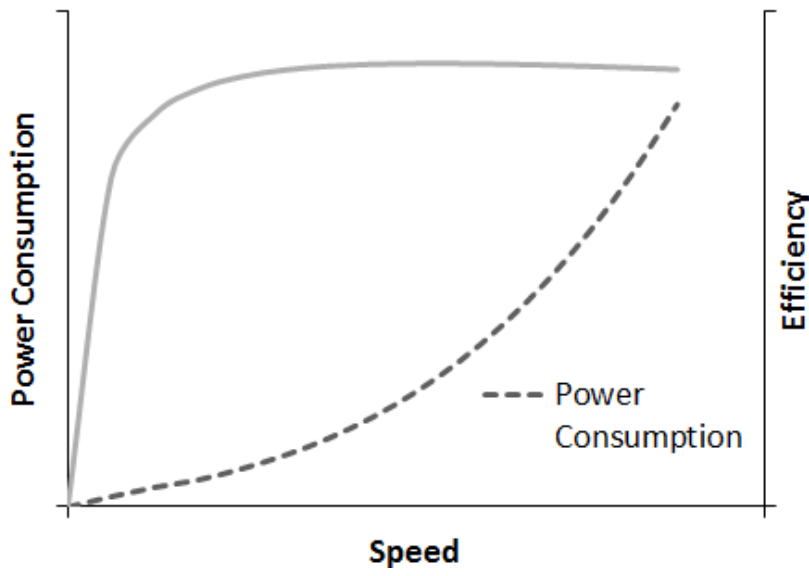
Fig. 1 Efficiency and power as a function of EV speed.
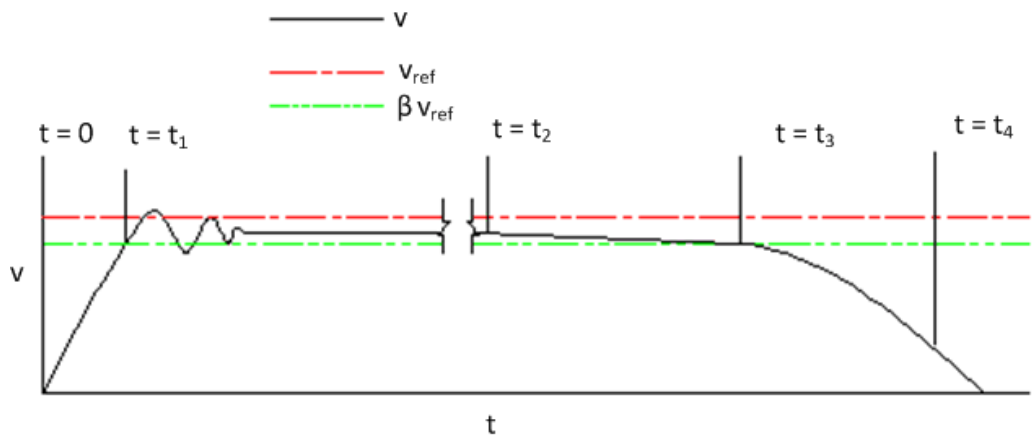
Fig. 2 Typical variation of EV speed as a function of time.
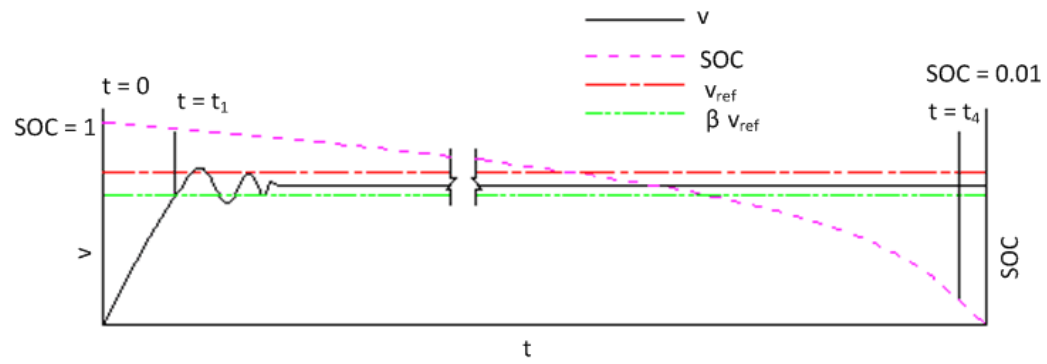
Fig. 3 Typical variation of EV speed as a function of time according to Approach 1.
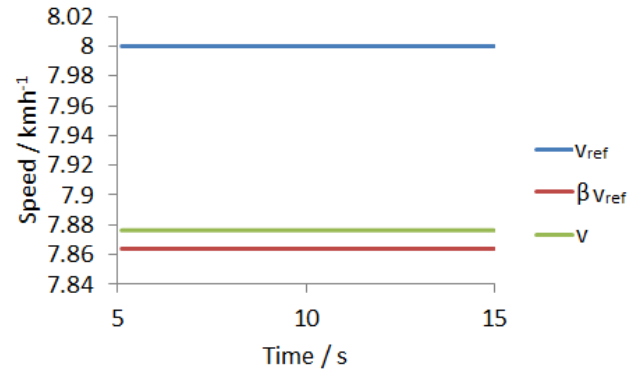
(a)
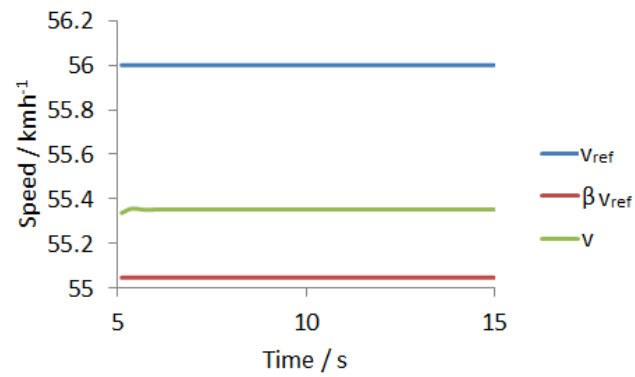
(b)
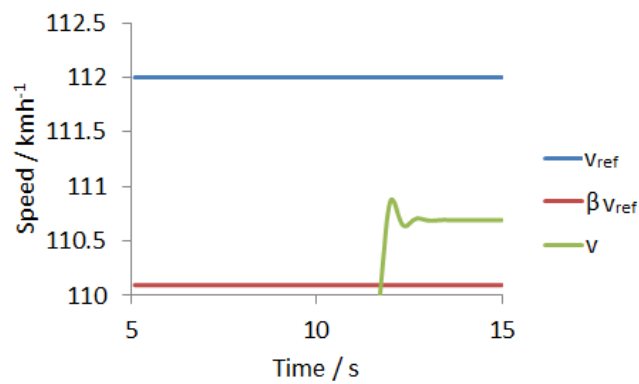
(c)

Fig. 4 Plot of reference speed (v_{ref}), termination criterion (βv_{ref}), and steady state-speed

(v) for different reference speeds: 8 kmh^{-1}, 56 kmh^{-1}, and 112 kmh^{-1}.
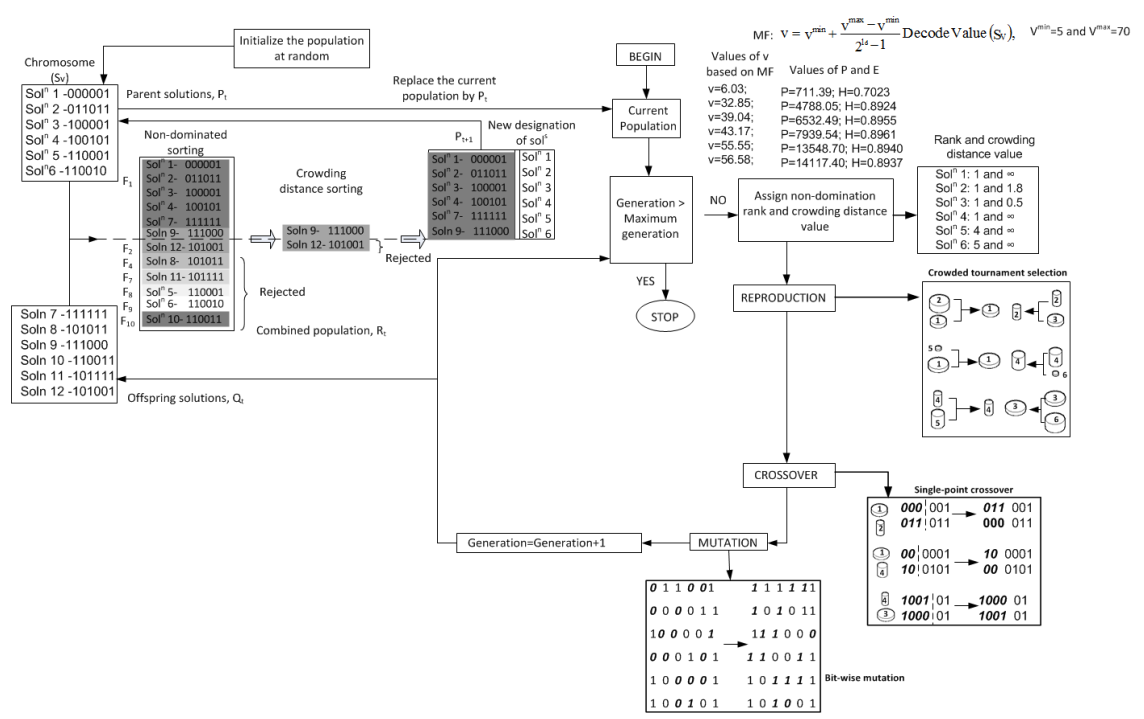
Fig. 5 Schematic representation of binary-coded NSGA-II for a two-objective problem

having one decision variable.
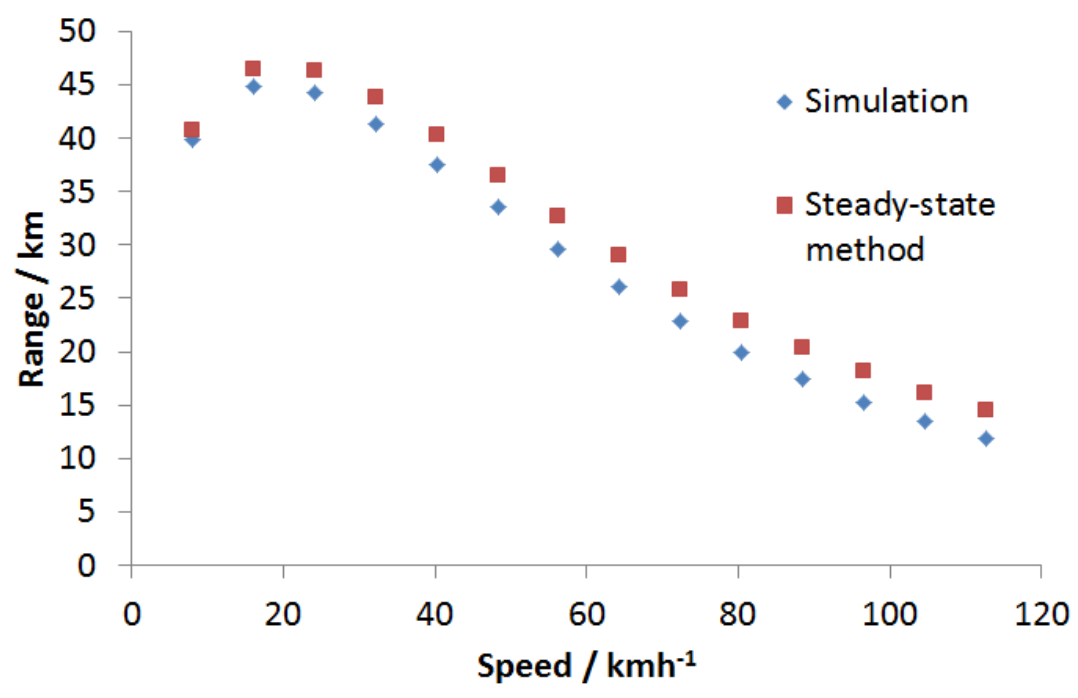
Fig. 6 Calculated range by simulation and steady-state methods.
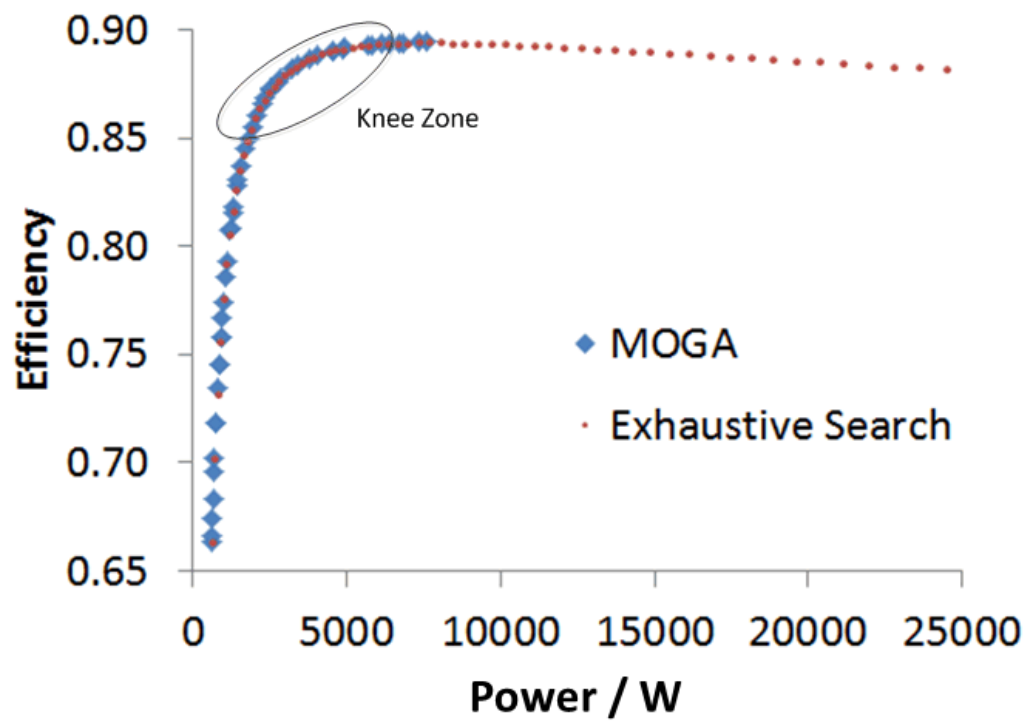
Fig. 7 Non-dominated solutions for exhaustive search and MOGA.
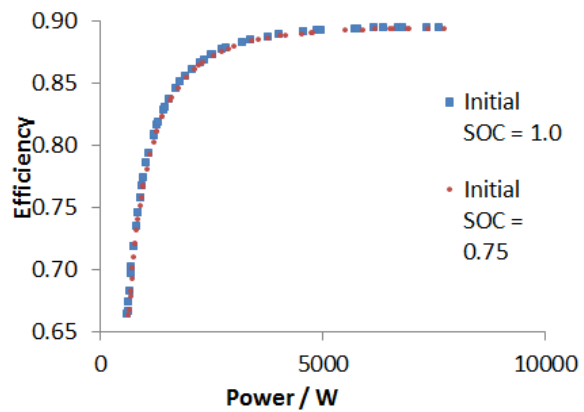
(a)
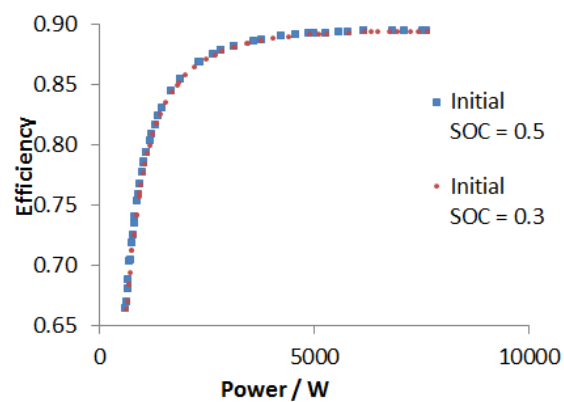
(b)
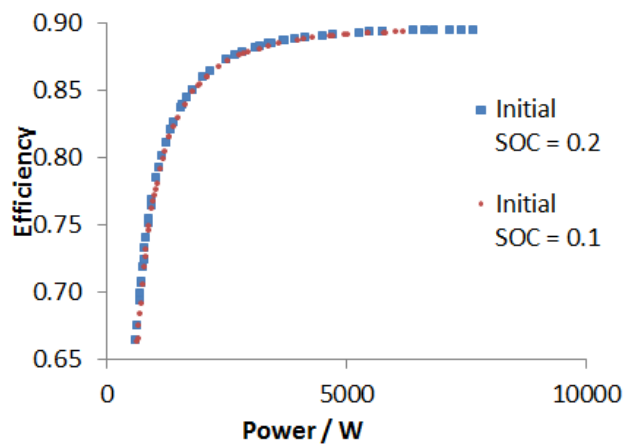
(c)

Fig. 8 Pareto fronts for different initial *SOC* values for Approach 1.
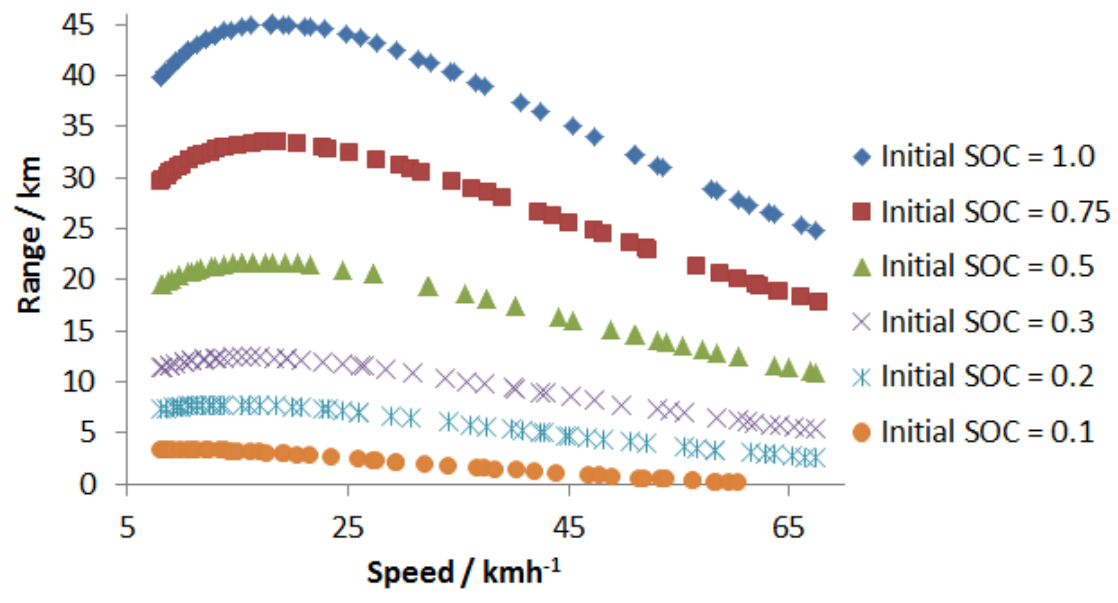
Fig. 9 Range versus speed for different initial *SOC* values for Approach 1.
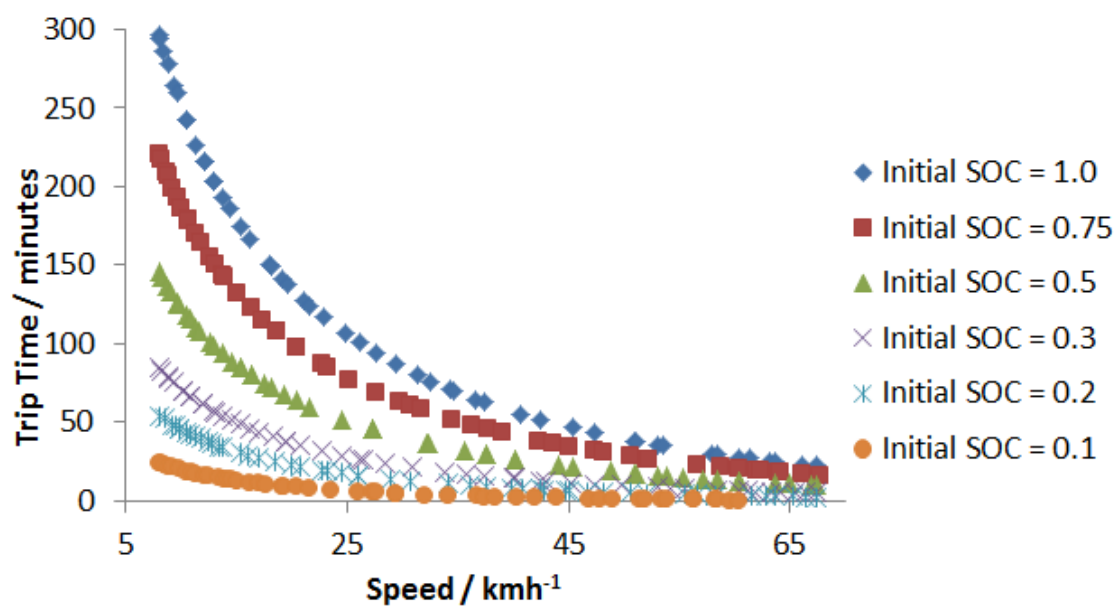
Fig. 10 Trip time versus speed for different initial *SOC* values for Approach 1.
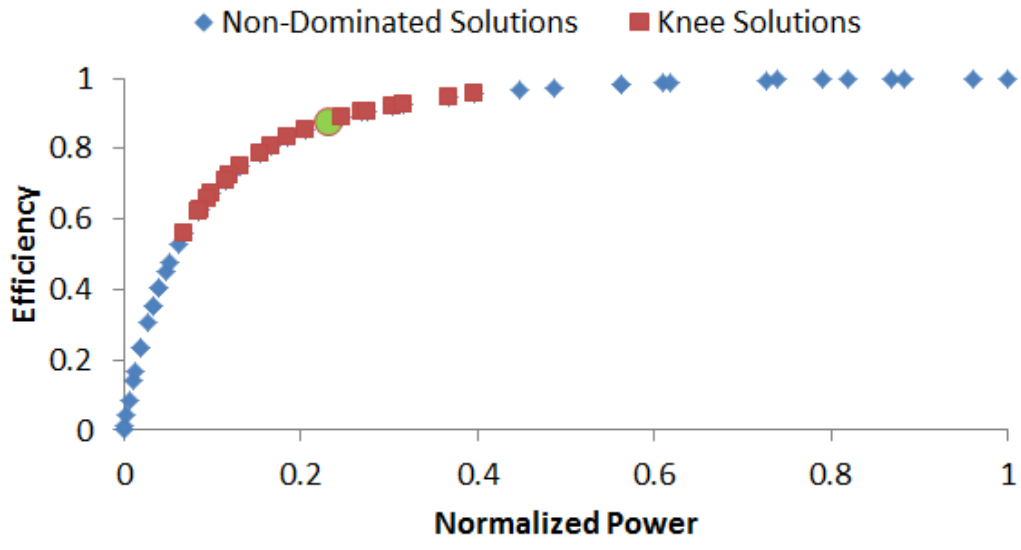
Fig. 11 Top twenty knee solutions presented on the normalized Pareto front.
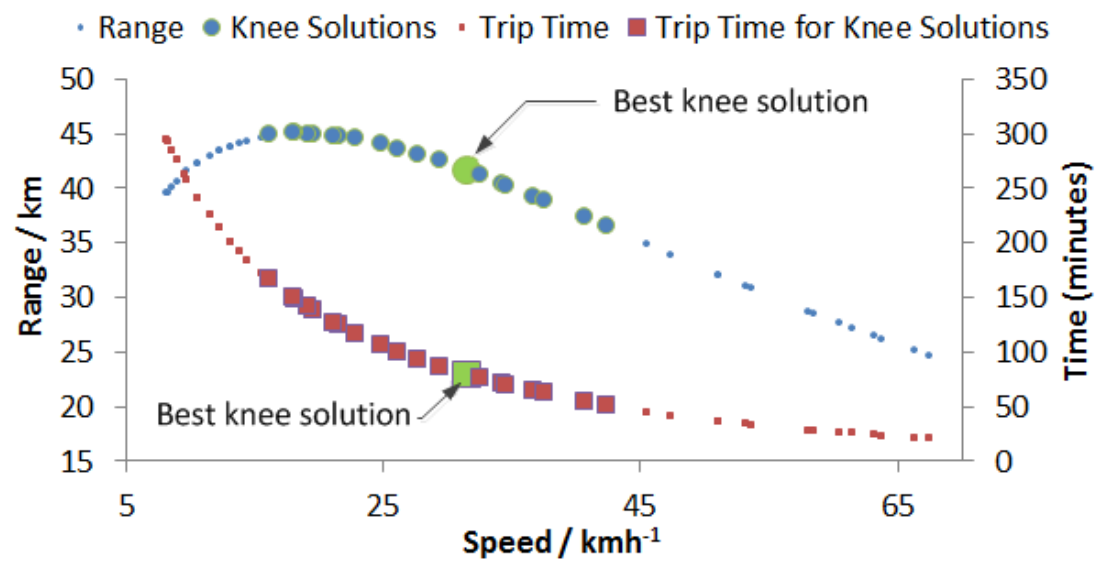
Fig. 12 Maximum range and trip time for knee solutions.
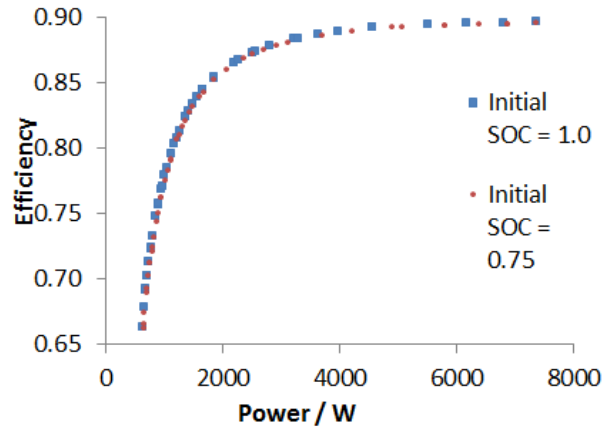
(a)
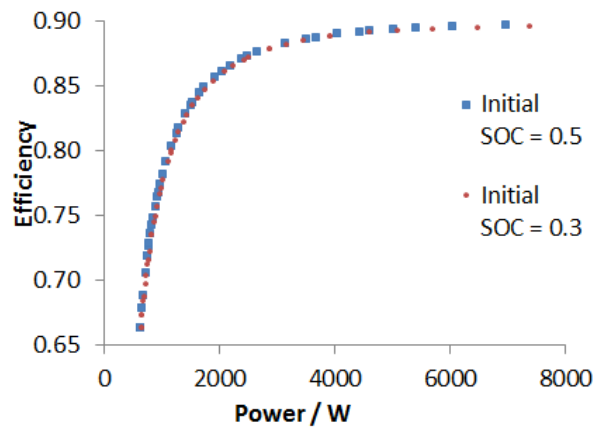
(b)
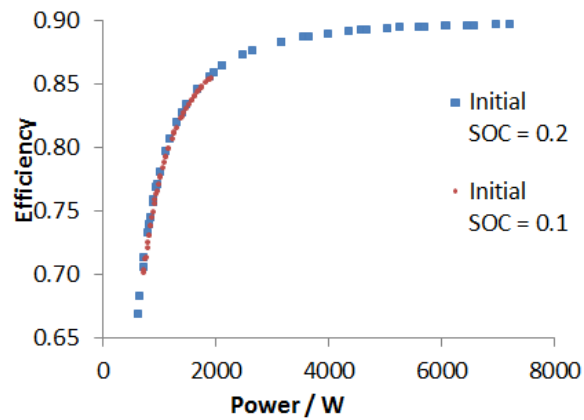
(c)

Fig. 13 Pareto fronts for different initial *SOC* values for Approach 2.
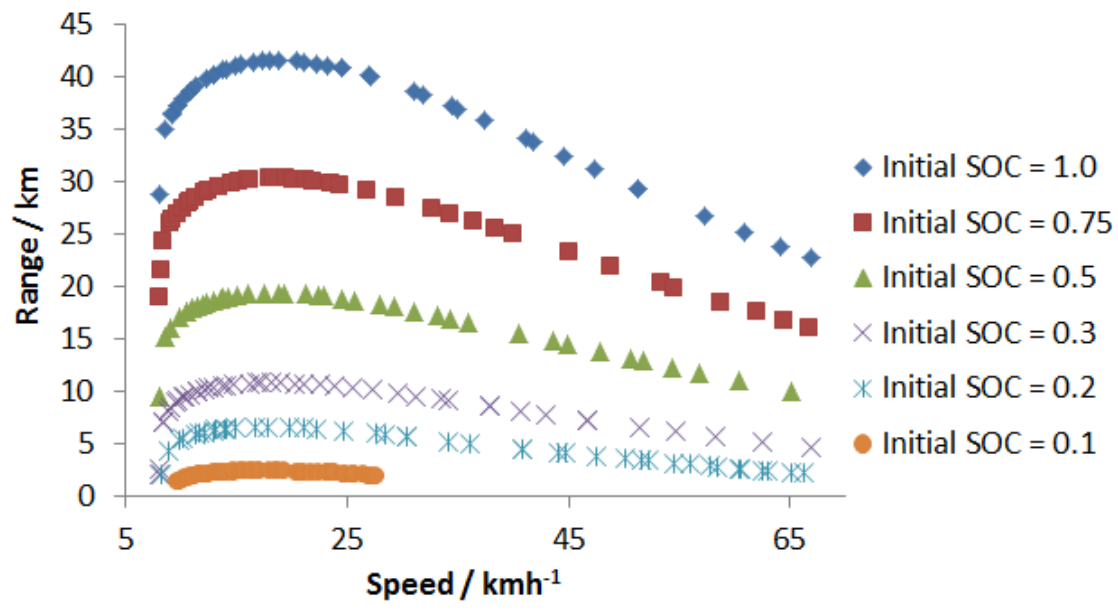
Fig. 14 Range versus speed for different initial *SOC* values for Approach 2.
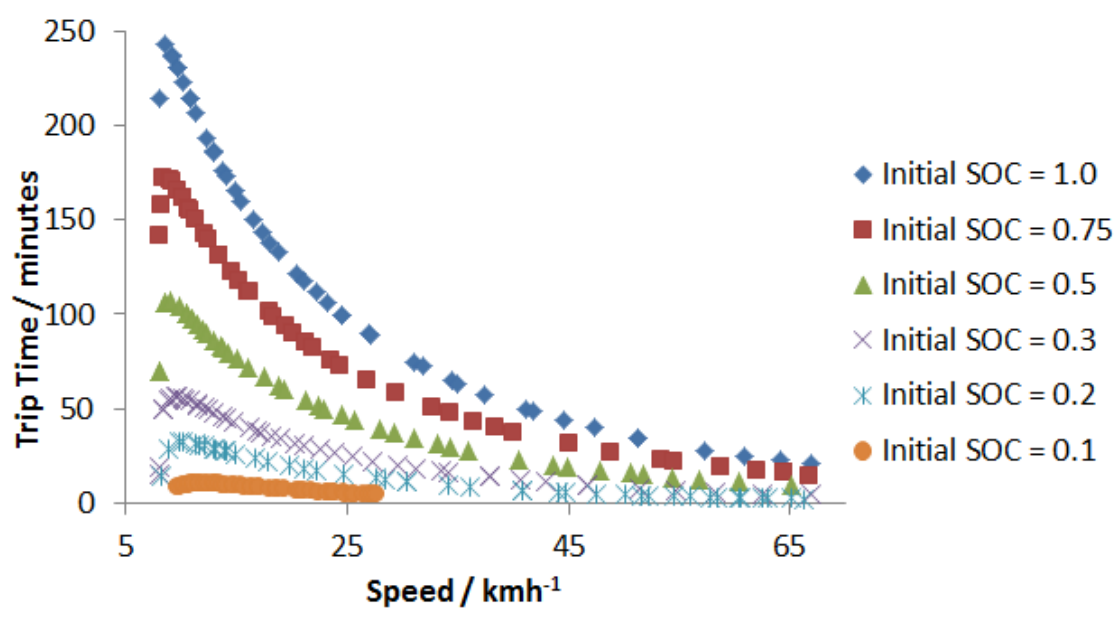
Fig. 15 Trip time versus speed for different initial *SOC* values for Approach 2.

III A Multi-Objective Approach to Find Optimal Electric Vehicle Acceleration:

Simultaneous Minimization of Acceleration Duration and Energy Consumption

Warren Vaz[1], Arup K. Nandi[2], Umit O. Koylu[3]

Department of Mechanical & Aerospace Engineering,

Missouri University of Science and Technology, Rolla, Missouri, USA

E-mail[1] (corresponding author): wsvvf9@mst.edu; E-mail[2]:

nandi@cmeri.res.in/nandia@mst.edu;

E-mail[3]: koyluu@mst.edu

Abstract –The high-energy consumption associated with acceleration requires electric vehicles (EVs) to accelerate to a chosen speed optimally, especially in urban driving cycles. Existing methods deal with the minimization of acceleration energy without considering the acceleration duration. This study focuses on solving a multi-objective optimization problem with two conflicting objectives: minimization of acceleration duration and minimization of energy consumption. Two approaches were used to reach a desired speed: using a single acceleration value and using multiple acceleration values. For each approach, demonstrative speed changes were chosen and the problem was solved using multi-objective genetic algorithms (MOGAs). The results (Pareto-optimal fronts) obtained by these two approaches were compared using suitable performance metrics. To validate the reliability of MOGA results, statistical analysis was carried out. Furthermore, a non-parametric study, the Wilcoxon signed-rank test, was conducted to compare the effectiveness of both approaches. It was found that the multiple accelerations were more effective in minimizing the duration and energy consumption than a single acceleration. For the same duration, multiple accelerations reduced the

energy consumption by up to 2%. Sensitivity analysis for both approaches with the electric motor model parameters was conducted. The simulation results of EV acceleration using the preferred optimal solution based on driving comfort and the Pareto front's knee suggested a strong implication towards driving assistance.

Highlights:

- A multi-objective approach was formulated to find optimal electric vehicle acceleration.

- Entire speed range of the electric vehicle was mapped.

- To accelerate to a selected speed, using multiple acceleration values was found to minimize the duration and energy consumption by up to 2% compared to a single acceleration value.

- Proposed method can be easily adopted and requires no modifications to the existing design.

Keywords: driving strategy, electric vehicle, optimal acceleration, acceleration duration, acceleration energy, multi-objective optimization, genetic algorithm, driving comfort

List of Symbols

a	Acceleration (ms^{-2})
a_{ref}	Reference acceleration (ms^{-2})
A_f	Frontal area (m^2)
B	Battery energy consumption (J)
C	Coverage of two fronts
Cap	Battery capacity (A·h)
cd_i	Crowding distance of the ith solution

C_D	Drag coefficient
$C_{Transient\_L}$	Battery long transient capacitance (MF)
$C_{Transient\_S}$	Battery short transient capacitance (MF)
D	Acceleration duration (s)
e	Acceleration error (ms^{-1})
f	Function
F	Non-dominated front
F_D	Aerodynamic drag force (N)
F_r	Friction force (N)
F_t	Traction force (N)
g	Gravitational acceleration (ms^{-2})
G	Overall gear ratio
H_0	Null hypothesis
i	Counter variable
I	Pareto-optimal front
I_a	Armature current (A)
I_{cell}	Current flowing through an individual battery cell (A)
I_f	Field current (A)
I_P	Battery pack current (A)
I_s	Solution on the Pareto-optimal front, I
J	Pareto-optimal front
J_s	Solution on the Pareto-optimal front, J

k	Optimal number of acceleration values out of 10
K	Geometric constant $(VA^{-1}(rads^{-1})^{-1})$
K_I	Integral grain
K_P	Proportional gain
L_a	Armature inductance (H)
m	Mass of the electric vehicle (kg)
min	Minimization
n	Number (e.g. number of iterations)
N	Number of Pareto-optimal solutions
N_P	Number cells in parallel
N_S	Number cells in series
P_t	Parent population
Q_t	Offspring population
R	Tire radius (m)
R_a	Armature resistance (Ω)
R_t	Combined population
$R_{Transient\_L}$	Battery long transient resistance (mΩ)
$R_{Transient\_S}$	Battery short transient resistance (mΩ)
R_{Series}	Battery series resistance (mΩ)
S_d	Size of the dominated space
SF	Switching function
SOC	State-of-charge
SOC_{init}	Initial state-of-charge

t	Time (s)
T	Critical value
v	Real vehicle speed (km/h)
V_{C_L}	Battery long transient capacitor voltage (V)
V_{C_S}	Battery short transient capacitor voltage (V)
V_{cell}	Voltage of an individual battery cell (V)
V_{OC}	Open-circuit battery voltage (V)
V_P	Battery pack voltage (V)
v_{ref}	Reference speed (km/h)
V_T	Terminal voltage (V)
δt	Time step (s)
μ	Rolling friction coefficient
ρ_{air}	Air density (kgm^{-3})
τ	Electric motor torque (Nm)
ω	Rotational speed (rads^{-1})

I. INTRODUCTION

Electric vehicles (EVs) are free of the widespread emissions suffered by internal

combustion (IC) engine vehicles, in addition to being more energy efficient [1]. They are

especially effective in reducing urban pollution [2]. Due to improvements in battery and

charging technology bolstered by government fiscal incentives, Evs are penetrating the

automotive market more than ever before. In order to improve various aspects (such as

performance, driving assistance, etc.) of Evs, several optimization studies on areas such

as wireless power transmission [3], real-time control for energy management [4], switched reluctance motor drives [5], and in-wheel motors [6] have been conducted. These improvements vary in complexity and some require significant changes to the EV in order to implement. As a result, these technologies have not yet permeated the market.

However, formulation of an assisted driving strategy is one of the essential improvements that immediately benefit the driver. It was found by [7] that driving parameters, such as harshness of acceleration, have an impact on the fuel economy. This was also confirmed by [8] for conventional vehicles and [9] for electric vehicles. Furthermore, changes to the driving behavior can significantly influence the vehicle energy consumption [10]. However, there is limited work on quantifying these effects, especially for Evs. Acceleration and deceleration comprise a small portion of a highway trip, but a much larger portion of urban trips. Due to their limited range, Evs have yet to see extended highway deployment. Additionally, the power associated with accelerating an EV to a constant speed is generally much higher than the power associated with maintaining that constant speed [11]. Consequently, it is crucial to quantify acceleration effects on current Evs, especially under urban driving conditions.

There are only a few studies that have considered acceleration effects on EV fuel economy and range. Once the driver choses a trip speed, s/he accelerates the vehicle from rest to the desired speed. Typically, the driver does not choose a particular value of acceleration. Additionally, the exact value of acceleration is not constant during a speed change [12]. The reason is that, for a constant acceleration, the applied torque is constant but as the vehicle speed increases, so does the air resistance, which causes the acceleration to reduce. The exact value of acceleration also depends on how aggressive

the driver is. EV data presented by [13] confirms the notion that acceleration value greatly influences energy consumption of EV. They reported a strong correlation coefficient (0.746) between acceleration and energy consumption. Therefore, a logical method to select an acceleration value for a given speed change is to adopt an optimization scheme that minimizes the amount of energy consumption.

Donoghue and Burghart [12] considered EV acceleration by maintaining a constant power. Using a parameter optimization method, they calculated the time to switch from the initial maximum acceleration to a constant power acceleration value along with finding the constant power to use. This method was found to mainly reduce the energy consumption. Imanishi et al. [14] developed another acceleration control technique for Evs based on the objective of reducing the energy consumption while maintaining drivability for a given load. Using this control methodology, the energy consumption was reduced by 1.9%. Lu and Ouyang [15] presented another study of acceleration control with minimum energy consumption for Evs, adopting analytical and dynamic programming methods to minimize energy while considering time as a constraint. The same control technique was previously presented for IC engines in [16]. Yao et al. [13] showed that, for a given speed change, the energy consumption was dependent on the chosen acceleration value. Thus, it is clear that acceleration of an EV consumes substantial battery energy and studies so far have focused on accelerating the EV with minimum energy consumption without necessarily focusing on the actual value of optimal acceleration.

By carefully analyzing the above studies, it was observed that the actual acceleration experienced by the vehicle was not a constant in any of these methods. Instead, the

acceleration to a chosen speed was executed via multiple acceleration values. The results of [14] and [15] implied the same phenomenon that one constant acceleration value might not guarantee minimum energy consumption for a chosen speed.

While the minimization of energy consumption is desirable, once a vehicle speed is chosen, the driver would like to accelerate to that speed in a reasonable amount of time. For example, the optimal acceleration method reported in [15] took 19.3 seconds to achieve a speed of 48 km/h from rest that might be too long for some drivers. Minimization of overall trip time is very important in several applications, including vehicle travel [17]. Consumer data clearly suggest that new vehicles sold in the United States have increasingly better acceleration times [18]. This is further illustrated by the fact that drivers drive at or around the speed limit and not significantly below it. The same can be said for acceleration: the driver would like to minimize the amount of time spent in accelerating to the desired speed. Therefore, time has not been considered as a constraint but as an objective to be minimized.

From previous studies in the literature, it has been observed that both the acceleration duration and the acceleration energy have not been considered simultaneously to find optimal (EV) acceleration(s). The main goal of this study was therefore to investigate the differences in finding optimal results by varying the number of accelerations to achieve a chosen speed for an EV by minimizing both these objectives. Two approaches were proposed here to find the optimal acceleration(s) for a speed change. Approach 1 considers a single acceleration, whereas Approach 2 uses multiple acceleration values. It must be noted that, in this study, each speed change was always from rest to a certain (chosen) speed. Optimality of acceleration was considered in the context of two

objectives: minimization of acceleration duration and minimization battery energy consumption. The two objectives are conflicting in nature: an improvement in one leads to deterioration in the other. Consequently, the problem of finding optimal acceleration values for chosen speeds becomes a multi-objective optimization problem (MOOP) with conflicting objectives and acceleration is the common decision variable in this optimization problem. The solution to this kind of problem results in a Pareto-optimal front consisting of many optimal solutions. The driver can choose a solution according to his/her preference based on trade-offs between the two objectives.

II. PROBLEM DEFINITION

Once a speed is chosen, the driver would like to accelerate the EV to this speed in the shortest duration while expending the least amount of stored battery energy possible. Therefore, the minimization of acceleration duration is one objective and the minimization of battery energy consumption is the other. These objectives are conflicting in nature, i.e. as one picks acceleration value(s) to minimize the duration, the energy consumption increases and vice versa. Because the acceleration value ultimately dictates the acceleration duration and the energy consumption, it was used as the common decision variable in the present study. Accordingly, the objectives were formulated as follows.

$$\text{min of } D = f_D(a) \tag{1}$$

$$\text{min of } B = f_D(a) \tag{2}$$

subject to

$$0.1 \le a \le 3.0 \tag{3}$$

where B is the battery energy consumption, D is the acceleration duration, and a is the acceleration value (decision variable). The objective of this study was to find acceleration values for different chosen speeds such that the EV accelerated to the chosen speed with minimum duration and energy. The range of acceleration considered in this study was presented by constraint Equation 3. The calculation of the two objectives is explained below in the next section. The genetic algorithm (GA) and its variants have recently become popular mainly because of its intuitiveness, ease of implementation, and the ability to effectively solve highly nonlinear, mixed integer optimization problems that are typical for complex systems. Moreover, compared to other evolutionary algorithms, although a GA is more computationally intensive, its performance exhibits superiority particularly when the problem deals with constrained nonlinear types with continuous or discrete decision variables [19]. Recently, GAs have been successfully applied to solve various single-objective and multi-objective optimization problems (MOOPs) for vehicles, such as powertrain component sizing and control strategy design for a fuel cell hybrid electric bus [20], plug-in hybrid vehicle powertrain design [21], optimal drivetrain component sizing for a plug-in hybrid electric transit bus [22], design of a hybrid electric vehicle battery [23] and hybridization of a plug-in hybrid electric vehicle [24]. Since, the present MOOP deals with constrained nonlinear types with continuous decision variables, it is expected that a multi-objective genetic algorithm (MOGA) is the most suitable approach. The MOGA using an elitist non-dominated sorting genetic algorithm (NSGA-II) [25] was adopted to solve the present problem.

III. FORMULATION OF OBJECTIVES: DURATION AND ENERGY

The EV model is described in this section, following the topology in [26]. The

components modeled included the battery, the electric motor, and the vehicle dynamics.

The electric motor was controlled using a proportional-integral (PI) controller. The model

was programmed in C++ with the reference acceleration, a_{ref}, and the chosen speed, v_{ref},

as the inputs. The simulation was terminated when the vehicle speed, v, reached within

1% of v_{ref}, corresponding to n loop iterations. It should be noted that the acceleration and

speed mentioned in Section 2 are actually the reference acceleration, a_{ref}, and the chosen

speed, v_{ref}. The vehicle model (described in Section 3.3) and parameters (shown in Table

I) were similar to [27] and [28]. For the sake of reducing complexity, a simplified model

was used, by ignoring certain minor effects, such as mechanical and power converter

losses. The entire EV model is summarized below for completeness.

A) Electric Motor Model

With the relevant electric motor parameters given in Table I, the model's inputs are the

battery voltage, V_P, the reference acceleration, a_{ref}, the vehicle acceleration, a, and the

rotational speed, ω, and the model's outputs are the battery current, I_P, and the electric

motor torque, τ. The motor was controlled using speed control. The inner current control

loop, which is a consideration in practical applications for protection of the motor from

overcurrent damage, was not included. The acceleration error is

$$e(i) = a_{ref} - a(i) \qquad (4)$$

A PI controller was used for acceleration control. The switching function of the electric

motor is

$$SF(i) = K_P e(i) + K_I \big(e(i-1) + e(i)\delta t \big), \ -1 < SF < 1 \qquad (5)$$

where K_P was taken to be 0.1 and K_I was taken to be 1. The terminal voltage applied to

the electric motor is

$$V_T(i) = V_P(i)SF(i) \tag{6}$$

The armature current is [29]

$$I_a(i) = I_a(i-1) + \frac{1}{L_a}\left(V_T(i) - KI_f\omega(i) - I_a(i)R_a\right)\delta t \tag{7}$$

The battery current is

$$I_P(i) = I_a(i)|SF(i)| \tag{8}$$

The torque generated is

$$\tau(i) = KI_a(i)I_f \tag{9}$$

Fig. 1 shows the maximum motor current and torque as a function of the motor speed.

B) Battery Model

The lithium-ion battery model used was similar to the one proposed in [30] with the

relevant battery parameters shown in Table I. The model's input is the battery current, I_P,

and the model's outputs are the battery voltage, V_P, and the state-of-charge, SOC. The

model is briefly described as follows.

$$I_{cell}(i) = \frac{I_P(i)}{N_P} \tag{10}$$

$$SOC(i) = SOC(i) - \frac{I_P(i)}{Cap}\delta t \tag{11}$$

$$V_P(i) = N_S V_{cell}(i) \tag{12}$$

$$V_{C\_L}(i) = V_{C\_L}(i-1) + \left(\frac{I_{cell}(i)}{C_{Transient\_L}} - \frac{V_{C\_L}(i-1)}{C_{Transient\_L}R_{Transient\_L}}\right)\delta t \tag{13}$$

$$V_{C\_S}(i) = V_{C\_S}(i-1) + \left(\frac{I_{cell}(i)}{C_{Transient\_S}} - \frac{V_{C\_S}(i-1)}{C_{Transient\_S} R_{Transient\_S}} \right) \delta t \quad (14)$$

$$V_{OC}(i) = -1.031e^{(-35SOC(i))} + 3.685 + 0.2156SOC(i)$$
$$- 0.1178SOC(i)^2 + 0.3201SOC(i)^3 \quad (15)$$

$$V_{cell}(i) = V_{OC}(i) - V_{C\_S}(i) - V_{C\_L}(i) - I_{cell}(i)R_{Series} \quad (16)$$

Note SOC_{init} is the same as $SOC(0)$ that in Equation 11.

C) Vehicle Model

The relevant vehicle parameters are given in Table I. The model's inputs are the electric

motor torque, τ, and the model's outputs are the vehicle acceleration, a, the vehicle speed,

v, the distance traveled, x, and the rotational speed, ω. The aerodynamic drag force acting

on the EV is

$$F_D(i) = \frac{1}{2} \rho_{air} A_f C_D v(i)^2 \quad (17)$$

The force due to friction between the road and wheel is

$$F_{rr}(i) = \mu mg \quad (18)$$

The traction force provided by the electric motor is

$$F_t(i) = \frac{\tau(i)G}{R} \quad (19)$$

Assuming the road has no gradient, neglecting the force due to the inertia of rotating

wheels, and having all the braking force come from the electric motor, the acceleration is

$$a(i) = \frac{\frac{\tau(i)G}{R} - \frac{1}{2}\rho_{air} A_f C_D v(i)^2 - \mu mg}{m} \quad (20)$$

The EV speed can be calculated using

$$v(i) = v(i-1) + a(i)\delta t \quad (21)$$

The rotational speed is given by

$$\omega(i) = \frac{v(i)G}{R} \tag{22}$$

The objective functions, acceleration duration and battery energy, are defined as follows:

$$f_D(a) = n \cdot \delta t \tag{23}$$

$$f_B(a) = \sum_{i=1}^{n} I_P(i)V_P(i)\delta t \tag{24}$$

IV. MULTI-OBJECTIVE OPTIMIZATION USING NSGA-II

Evolutionary algorithms (EAs) such as genetic algorithms (GAs) are search and optimization strategies that mimic the working principles of natural evolution and genetics [31]. Multi-objective genetic algorithms (MOGAs) are a class of tools based on GAs to solve multi-objective optimization problems (MOOPs) having conflicting objectives. Unlike a single-objective problem, to find a unique solution, the task of an optimizer in a MOOP is to obtain a set of solutions based on the concept of domination by comparing two solutions on the basis of whether one dominates the other solution or not. The plot of the objective functions using these non-dominated solutions is called a non-dominated front and the corresponding solutions are non-dominated solutions. If the non-dominated solutions are optimal, then the non-dominated front is called the Pareto-optimal front and the solutions lying on the Pareto-optimal front are called Pareto-optimal solutions. Thus, the primary goal in a MOOP is to obtain a set of solutions as close as possible to the Pareto-optimal front in addition to being spread out as diversely as possible throughout the Pareto front. The advantage of MOGAs over other optimization methods like dynamic programming or optimal control is the availability of multiple solutions after a single run of MOGA, offering flexibility. In the present work, a non-

dominated sorting GA, NSGA-II [25] was adopted because it is one of the most popular and widely used MOGA for such kinds of problems. The basic working of MOGA using NSGA-II is described lucidly in [32] and can be summarized in the flow diagram illustrated in Fig. 2.

For a given set of GA parameters, such as population size (six in Fig. 2), a maximum number of generations (set as the termination criterion of the MOGA), a reproduction scheme (crowded tournament selection with a chosen tournament size), a mutation scheme (with a mutation probability), and a crossover scheme (with a crossover probability), a maximum of six non-dominated solutions can be obtained after a complete MOGA generation. In the crowded tournament selection procedure, the solution having a lower rank value than other solutions is allowed to win a tournament. If more than one solution in a tournament has the same rank, then the solution that had a larger crowding distance value is permitted to win. After each generation, both the parent (P_t) and offspring (Q_t) populations are mixed up to form a combined population, R_t. Then, non-dominated sorting is carried out on the combined population in order to classify the solutions based on their rank. The solutions in a class having the same rank create a front. Fig. 2 shows that there are three fronts (F_1, F_2, and F_3) obtained after the non-dominated sorting of R_t corresponding to rank values. Since the population size of the GA is constant throughout the generations, solution(s) of different non-dominated fronts, one at a time, are used to fill the new population (P_{t+1}). The filling starts with the best non-dominated front having a lower rank value and so on. Since the overall population size of R_t is double the size of population (twelve in Fig. 2), not all fronts may be accommodated in N slots available in the new population, P_{t+1}. All fronts, which could not be

accommodated, are simply deleted. When the last allowed front is considered, there might be more solutions in the last front than the remaining slots in the new population. In Fig. 1, such a situation happens with F_2. Instead of arbitrarily discarding some members from the last front, it is better to use a niche-preserving strategy to choose the members of the last front, which is decided by the least crowded region in that front. That means that the solution having higher crowding distance (cd_i) will be preferred compared to others. A random selection is taken among the solutions having same crowding distance value. Based on this new population, P_{t+1} (now considered as the parent population, P_t) another offspring population Q_t is created using genetic operators like crowded tournament selection, crossover, and mutation in the next generation. This cycle is continued until a specified number of generations have been reached or other specified termination criteria have been fulfilled.

V. PROPOSED APPROACHES TO FIND OPTIMAL ACCELERATION(S) USING MOGA

The main purpose of this study is to investigate the efficacy of using Approach 1 and Approach 2 described in the Section 1 for different speeds. For demonstrative purposes, the entire speed range of a typical EV (8-112 km/h) was divided into three zones, as proposed in [33]: neighborhood (<40 km/h), urban (40-72 km/h), and highway (>72 km/h). One speed from each of these zones (say, 40 km/h, 72 km/h, and 104 km/h) was selected to compare the effectiveness of two approaches. This section presents the methodology using MOGA (summarized in Section 4) to solve the present multi-objective problem (stated in Section 2) and the corresponding optimization results.

A) Single Acceleration Approach

In this approach, the number of decision variables associated with the objective functions (Equations 1 and 2) is one (acceleration, *a*) subject to the constraint equation (Equation 3). The GA selected a value of acceleration from this search space and calculated the duration and energy based on Equations 1 and 2. The NSGA-II algorithm was run to solve the MOOP based on the EV simulation parameters given in Table II for computing the objective functions.

B) Multiple Acceleration Approach

This approach uses multiple accelerations to reach the chosen speed. Keeping in mind practical driving situations and for the sake of reducing the computational complexity, the maximum number of accelerations (that can be adopted by the driver to reach the chosen speed) was limited to 10. The role of MOGA is not only finding the Pareto-optimal front but also determining the optimal number of acceleration(s) out of 10 (denoted as *k*) along with optimal values of those accelerations and their duration(s). The sum of these durations is equal to the total acceleration duration (Equation 27). Thus, the objective functions given in Equations 1 and 2 comprised 10 different acceleration values instead of a single acceleration value. The associated time duration of the ith acceleration is t_i. Since Equation 27 is an equality constraint, the number of time (decision) variables associated with *k* accelerations becomes *k*-1. Thus, in Approach 2, each of the objective functions consisted of 19 decision variables (ten accelerations and nine durations). The modified equations of the objectives may be rewritten as follows.

$$\min \text{of } D = f_D\left(a_1,...,a_k,t_1,...,t_{k-1}\right) \tag{25}$$

$$\min \text{of } B = f_B\left(a_1,...,a_k,t_1,...,t_{k-1}\right) \tag{26}$$

$$D = \sum_{i=1}^{k} t_i \qquad (27)$$

The maximum and minimum limits of each acceleration value (Equation 3) were the same as in Approach 1. However, it was important to carefully constrain the selection of time decision variables in order to have realistic and appropriate search spaces for each time (decision) variable. A large, unconstrained search space resulted in a longer time for the GA to converge. On the other hand, an arbitrarily created short search space does guarantee a global minimum to be reached by GA. Therefore, appropriate values for the maximum and minimum limits of each time duration (decision) variable corresponding to each accelerations value were set carefully as follows.

To achieve a particular speed when multiple accelerations are used, there is a possibility that the first few accelerations may have a positive time duration whereas the rest may have a zero time duration. Based on this consideration, the lower limit of each time duration decision variable was kept as zero. On the other hand, if one can use a single acceleration, a, to achieve a chosen speed, v, it will take a theoretical value of $\frac{v}{a}$ seconds. It is easy to see that the time duration (decision) variable cannot be significantly more than this value (allowing some time for the controller build up to a). Thus, the maximum value of ith time duration (decision) variable corresponding to i^{th} acceleration (a_i) was set to $\frac{v}{a_i}$.

C) Performance metrics Used to Compare Pareto Fronts Obtained by Approach 1 and

Approach 2

In order to compare the results of the two approaches to find optimal accelerations to reach a chosen speed, MOEA outputs (Pareto fronts) were measured with the help of three performance metrics [34]:

1. Number of non-dominated solutions in the Pareto front, N

2. Size of the dominated space, $S_d(I)$

3. Coverage of two Pareto fronts, $C(I, J)$

Using the same population size, one approach is said to be better than another if it contains a higher number of non-dominated solutions. The size of the dominated space, $S_d(I)$, of a Pareto front, I, indicates a measure of how much of the objective space is weakly dominated by the Pareto front, I. A higher value of $S_d(I)$ indicates better performance. The size of the dominated space, $S_d(I)$, is measured by normalizing the objectives taking maximum and minimum values of duration and energy obtained in the corresponding Pareto-front. Coverage of two Pareto fronts, I and J, $(C(I, J))$, provides the fraction of J weakly dominated by I and is calculated as follows.

$$C(I,J) = \frac{\left|\left\{J_s \in J \mid \exists I_s \in I : I_s \succ J_s\right\}\right|}{|J|} \qquad (28)$$

where $|J|$ is the cardinality of the Pareto optimal set J and $I_s \succ J_s$ means that solution I_s dominates the solution J_s. If, $C(I, J) > C(J, I)$, it means that the Pareto front, I, has better solutions than the Pareto front, J. The measurements, size of the dominated space and coverage of two Pareto fronts suggest the degree of convergence of a Pareto front. The

following results demonstrate the superiority between the two approaches from different perspectives.

D) Comparison of Approach 1 and Approach 2

The elapsed time at the termination of the EV simulation was recorded as the acceleration duration. The total energy consumption of the EV until the termination of the simulation was considered as the acceleration energy. For Approach 2, the simulation was followed according to the GA-selected values of accelerations (and corresponding duration) one by one until its termination. After the simulation termination, the rest of the acceleration values (out of ten) were assigned a zero duration.

1) Comparison of Proposed Approaches

Fig. 3 shows the Pareto fronts obtained for the demonstrative speeds considered. Each plot has two fronts that are typical for conflicting objectives: one obtained by Approach 1 (single acceleration value) and one obtained by Approach 2 (multiple acceleration values). From Fig. 3, it could be seen that the fronts differed more and more as the speed increased, the greatest difference appearing when the desired speed was 104 km/h. Additionally, it appeared that the front with multiple acceleration values consistently dominated the front with single acceleration values.

These observations point to the idea that multiple acceleration values to reach a chosen speed can optimize the two conflicting objectives in a better way than a single acceleration value, similar to the observations in [14] and [15]. An explanation for this has been proposed in the follwing.

Fig. 4 shows a map of the electric motor efficiency as a function of the rotational speed and the torque. One solution for each approach (reference speed = 104 km/h) has

been plotted in Fig. 4. Both solutions had the same duration of 37.6 s. However,

Approach 1 solution's energy was 1.200E6 J and Approach 2 solution's energy was

1.177E6 J; a 2% reduction. The reason for the lower energy consumption in Approach 2

is that Approach 2 follows a higher efficiency path in Fig. 4 than Approach 1. However,

when the rotational speed reached 97 rads^{-1}, Approach 2 moved to a lower efficiency but

with a higher torque. This is necessary to ensure the duration does not suffer. However,

the net result was lower energy consumption than Approach 1, which followed an

efficiency path that was in between. The 2% reduction is significant for EVs because the

driver is able to reach the desired speed with lower energy without the duration suffering.

When one considers that acceleration can constitute up to 50% of the total non-idle time

for urban driving cycles [35], a reduction of 2% without sacrificing drivability is

noteworthy.

2) Statistical Analysis

The results of a GA are stochastic in nature because it depends on the chosen initial

solutions as well as randomness. Accordingly, there is a need to compare the results of

both approaches statistically for confidence of acceptance. Therefore, a detailed statistical

study was conducted independently for each of the three speeds to confirm the results

obtained by both the approaches were statistically reliable. Twenty independent MOGA

runs were performed with 20 different values of random seed (in the range of 0.1 to 1.0).

The mean and standard deviation (SD) of N, S_d, and C obtained in Approach 1 and

Approach 2 in twenty different runs are listed in Table III. The significance of these

metrics is that a Pareto front having higher values of N, S_d, and C is better than the other.

It was observed that N obtained in each case was 100. However, a higher mean value for

the size of the dominated space in Approach 2 was found, suggesting that Approach 2 was superior to Approach 1 regardless of the stochastic nature of GA. This phenomenon was more pronounced with increasing speed. Moreover, a very low value of standard deviation of S_d was observed, which indicated that the results were statistically fairly stable. The same result of superiority of Approach 2 was observed in case of coverage of two Pareto fronts. For the coverage metric, the mean values differed slightly more when twenty runs were compared to one run. That was the reason a relatively high standard deviation value was calculated for this metric. Thus, it seems that while the Approach 2 fronts may be superior to the Approach 1 fronts in general, the exact difference between the two approaches varies somewhat. Certain Approach 1 fronts (resulting from particular random seeds) may be better than certain other Approach 2 fronts.

3) Wilcoxon signed-rank test

Considering the stochastic nature of GAs, a further investigation was carried out using a statistical test, namely the Wilcoxon signed-rank test (a non-parametric statistical test for testing hypothesis on median [36]) in order to determine whether the optimization results of Approach 1 and Approach 2 were equivalent or not. The Wilcoxon signed-rank test was performed on the values of two metrics, S_d and C (as defined in Section 5.3) that were calculated based on the results obtained by Approach 1 and Approach 2 for 20 random seed values. The outcome of the test is illustrated in Table IV.

From Table IV, it was obvious that Approach 2 was superior over Approach 1 in the case of coverage of two Pareto fronts for all the three speeds. In the case of size of the dominated space, Approach 2 was found to be better than Approach 1 for all the three

speeds with the exception of a significance level lower than 0.1 where both the

approaches were found to be equivalent according to Wilcoxon signed-rank test.

4) Sensitivity Analysis

The most important component of the EV model that dictates the nature of the results in

Sections 5.4.2 and 5.4.3 is the electric motor. In order to investigate the dependence of

the number of acceleration values picked by MOGA on the electric motor model,

sensitivity analysis was performed. The parameters used to define the model were varied

to assess whether or not the observation from optimization results, i.e., multiple

accelerations performing better than a single acceleration in terms of minimizing duration

and energy, would still hold. For this investigation, two speeds were chosen, 40 km/h and

72 km/h. Using different electric motor model parameters, three metrics were formulated

as follows: gear ratio (G), ratio of motor geometric constant to field current (K/I_f), and

ratio of armature resistance to armature inductance (R_a/L_a). The reason for creating these

metrics is that certain motor parameters are interdependent: changing one typically

causes the other to also change. Ranges for parameter variation were selected according

to typical motor parameter values found in the literature [37] while ensuring that the EV

would still achieve the selected speed. It was found that in 75% of the cases, Pareto fronts

produced by Approach 2 were better than those produced by Approach 1 (in terms of

Pareto-optimality).

In Section 3, it was mentioned that minor losses were ignored. The most

important loss is in the electric motor and that was considered for both approaches.

However, to examine the effects that the losses have on both approaches, the mechanical

efficiency (taken to be 0.95 [28]) was added to Equation 19 while the power converter

efficiency (taken to be 0.96 [28]) was added to Equation 8. Equation 29a shows the battery current calculation in the case of motoring and Equation 29b shows the battery current calculation in the case of regeneration. Similarly, Equation 30a shows the traction force calculation in the case of motoring and Equation 30b shows the traction force calculation in the case of regeneration.

$$I_P(i) = \frac{I_a(i)|SF(i)|}{0.96} \tag{29a}$$

$$I_P(i) = 0.96 \times I_a(i)|SF(i)| \tag{29b}$$

$$F_t(i) = \frac{0.95 \times \tau(i)G}{R} \tag{30a}$$

$$F_t(i) = \frac{\tau(i)G}{0.95 \times R} \tag{30b}$$

After repeating the optimization process, it was found that the multiple acceleration front continued to dominate the single acceleration front. The energy savings without losses were reported as being up to 2% in Section 5.4.1. After including losses, the energy savings were found to be up to 1.84%. This corresponds to a difference of 8% with losses compared to without losses. It must be noted that the solutions with the same duration were used when comparing energy savings. This difference is quite low because adding losses to the EV model affects both approaches as the same EV model is used for both approaches.

From the above discussion in Section 5.4, Approach 2 is clearly the better approach for the majority of the conditions considered here and was used to further study each of the three speed zones in greater detail.

VI. EFFECTIVENESS OF THE APPROACHES FOR DIFFERENT SPEED ZONES

In this section, a statistical investigation was reported to determine the effectiveness of both approaches within three separate speed zones (neighborhood, urban, and highway), as suggested by [33]. To do so, 20 speeds from each zone (uniformly distributed throughout the speed zone) were considered. Based on these speeds, the MOGA was independently run for a random seed value of 0.4, keeping the other parameters the same as in Table II. Additionally, the Wilcoxon signed-rank test was also applied to the results.

Table V shows the statistical results of number of solutions, dominated size, and coverage of Pareto fronts obtained by both approaches for each speed zone. According to Table V, the results were as seen previously: even for different speed zones, multiple acceleration values gave better results compared to a single acceleration value. The only exception was for S_d metric in the neighborhood speed zone as the mean value of S_d was slightly greater for Approach 1 than it was for Approach 2. However, Approach 2 fronts dominated more solutions (mean difference value = 24.9) of Approach 1 fronts. Also, a low value of standard deviation (SD) for S_d was observed, suggesting the statistical reliability of MOGA results. For the same reason as mentioned in Section 5.4.2, a high value of SD for C in Table V was found.

The statistical results of the distribution of optimal number of accelerations (out of 100 solutions) found by MOGA in Approach 2 for three speed zones are presented in Table VI. The mean value of the distribution of the number of acceleration was averaged for 20 random speeds in each zone. Once again, only one acceleration value was never picked by MOGA at all in any speed zone. Two acceleration values were picked 90.2%

of the time followed by three (8.8%), four, and five acceleration values. Also, the chances of fewer accelerations being picked were higher as the speed increased. Solutions with six acceleration values or higher were never picked in any of the runs. Therefore, limiting the number of acceleration decision variables to 10 did not affect the results in any way. Finally, the high standard deviations relative to the mean values for three, four, and five acceleration values indicated that, within a particular speed zone, certain speeds could be optimally reached with a greater number of different acceleration values whereas certain other speeds could be optimally reached with a fewer number of different acceleration values. If there are two similar speeds (e.g. 72 km/h and 75 km/h), a driver may choose one with fewer acceleration values because it may be easier to drive or more comfortable. Such considerations are discussed in the next section. It is interestingly noticed that solutions with only one acceleration were never chosen by MOGA for any of the three speeds indicating the suboptimality of these solutions.

The Wilcoxon signed-rank test was repeated for investigating the equivalence of Approach 1 and Approach 2 in three speed zones. By analyzing the results of S_d, both approaches were found to be equivalent in the neighborhood and urban speed zones for a high significance value (0.1). But, for the highway speed zone, Approach 2 prominently showed better results than Approach 1 even for a low significance level (0.01). On the other hand, a comparison of test results of C indicated that Approach 2 maintained its superiority of obtaining better solutions than Approach 1 for any speed zone.

VII.   IMPLEMENTATION OF OPTIMAL RESULTS

There are several different ways to consider implementation of the results obtained. One way to pick a solution for a chosen speed out of a set of Pareto-optimal solutions is to use

the concept of knee [38]. Sometimes, the shape of Pareto-optimal front is such that there may be solutions where a small improvement in one objective would lead to a large deterioration in any of the other objectives, which makes moving in either direction unattractive. A solution point having such characteristics is called a knee point. For a problem of minimization of $f_1(i)$ and minimization of $f_2(i)$, a knee-value of a solution point (i) is defined by Equation 31.

$$\text{Knee Value}_i = \frac{\dfrac{f_1^{(i+1)} - f_1^{(i)}}{f_2^{(i+1)} - f_2^{(i)}} + \dfrac{f_2^{(i-1)} - f_2^{(i)}}{f_1^{(i-1)} - f_1^{(i)}}}{2} \tag{31}$$

It must be noted that the objective function values in Equation 31 are normalized (between 0 and 1).

A solution point having a higher knee value is said to be a stronger knee point compared to the others. Without any knowledge about the user's preferences, it may be argued that the region comprising the knee points is most likely to be interesting for the decision maker.

Another way to pick a solution is on the basis of driving comfort. The metric used to define comfort (modified for use in this study) was presented in [39] as follows.

$$d = \sum |\Delta a| \tag{32}$$

where d is the level of discomfort associated with a particular solution and Δa is the difference between consecutive acceleration values (e.g. a_1-a_2, a_2-a_3, so on, where a_1, a_2, a_3, etc. are the consecutive acceleration values). The driver would like to pick a solution with minimal discomfort, i.e., a solution that not only as fewer different acceleration values but acceleration values that are quite similar to each other in magnitude.

Based on the above decision-making criteria, the method of selecting an optimal solution for real implementation is presented here. Fig. 5 shows the level of discomfort for the top five knee values (calculated using Equation 31), considering the optimization results obtained using Approach 2 for different speeds. The top five knee values represented the best trade-off between duration and energy. The trade-off was defined above as the loss in either the duration or energy per unit gain in either the energy or duration, respectively. However, as seen in the figure, the best knee value did not always correspond to the most comfortable acceleration situation. The figure also showed that the discomfort generally increased with the chosen speed. This is because for higher speeds, a solution comprising multiple acceleration values is more likely to have acceleration values that are significantly different in order to optimize both the objectives.

The significance of the discomfort decision-making criterion is that even though all the Pareto solutions having multiple accelerations are optimal, it is necessary to include discomfort to choose one solution before implementation. An example of this is as follows.   Fig. 6 demonstrates the simulation of EV after implementing an optimal solution obtained by Approach 2 for a chosen speed of 48 km/h. The driver selects the first knee solution (marked by a circle in Fig. 5) consisting of two accelerations that also happens to have the lowest jerk value. As seen in the Fig. 6, the EV experienced a smooth transition from rest to the desired speed. The acceleration durations are definitely long enough for the driver to be able to change from the first acceleration value to the second. The overall acceleration duration of 16.9 s was shorter than the 19.3 s duration reported in [15] to achieve for the same chosen speed (48 km/h). Based on these observations,

such kinds of solutions are intuitively preferred for real implementation. The EV model

used in [15] was of a significantly smaller EV than the one used in the present study, so

the energy consumption for both methods was expected to be different and could be

compared.

The driver has several optimal solutions from which to choose. For example, for 48

km/h, MOGA picked two solutions whose duration was similar to the duration reported

in [15]. The energy consumption was lower but the discomfort was higher. The driver

could choose whether s/he preferred a faster, more comfortable acceleration experience

as shown in Fig. 6 or one that consumed less energy.

The other advantage of the proposed method is that it can immediately benefit

drivers without any modifications to the EV design. It is a marked improvement over

previous methods because acceleration duration is considered here as an objective of the

optimization problem along with energy consumption, leading to multiple solutions being

presented to the driver.

VIII.   SUMMARY AND CONCLUSIONS

The aim of this study was to investigate the optimum utilization of the stored battery

energy in EVs by considering the efficacy of using multiple acceleration values instead of

a single acceleration value to get to a chosen speed using an EV vehicle. To minimize

acceleration duration and energy consumption, two approaches were used: achieving a

chosen speed using a single acceleration value (Approach 1) and using multiple

acceleration values (Approach 2). The problem was solved using a MOGA to find the

optimal acceleration values. In addition, particularly in multiple acceleration approach,

the algorithm decided what the optimal number of accelerations was and for how long they would be maintained.

For each approach, initially, three speeds were chosen and a separate Pareto front was obtained in each case. It was observed that difference between the two approaches increased as the reference speed increased. To test the reliability of optimization results, MOGA was independently run 20 times with different random seeds for the three selected speeds. The resulting Pareto fronts were compared using metrics such as number of Pareto-optimal solutions, size of the dominated spaces, and coverage of the two fronts. The mean and standard deviation values of the runs were used. It was found that multiple accelerations gave better optimization results than a single acceleration. For the same acceleration duration, up to 2% reduction in energy consumption was observed. Furthermore, a non-parametric statistical study was conducted to compare the performances of the two approaches. It was confirmed that multiple accelerations were better than a single acceleration with a significance level of 0.1. Finally, sensitivity analysis on the electric motor model showed that, in 75% of the cases considered, the multiple acceleration approach was superior over the single acceleration approach.

In order to examine the effect of Approach 2 for different speed values, the entire speed range of the EV was divided into three zones. In each zone, the two approaches were applied to 20 randomly chosen speeds. The Pareto fronts obtained were compared using the same metrics mentioned above. It was found that multiple accelerations gave better results in all metrics except for size of the dominated space in the neighborhood zone by 0.1%. These results led to the conclusion that multiple accelerations to reach a chosen speed were indeed better than a single acceleration value. This was confirmed

again by the Wilcoxon signed-rank test. It was found that solutions with two

accelerations (out of a possible 10 accelerations) were chosen 90.2% of the time and that

with three accelerations were chosen about 8.8% of the time. Finally, a method using the

knee concept and driving comfort was presented to choose a preferred solution from

Pareto optimal front for implementation. EV simulation results using the optimum

solution demonstrated that the multiple acceleration approach definitely provided better

assistance to the EV driver that could be easily implemented without any extra cost.

ACKNOWLEDGMENTS

REFERENCES

[1] Faria R, Moura P, Delgado J, De Almeida AT. A sustainability assessment of electric vehicles as a personal mobility system. Energy Conversion and Management 2012;61:19-30.

[2] Wang B, Xu M, Yang L. Study on the economic and environmental benefits of different EV powertrain topologies. Energy Conversion and Management 2014;86:916-926.

[3] Ko YD, Jang YJ. The optimal system design of the online electric vehicle utilizing wireless power transmission technology. IEEE Transactions on Intelligent Transportation Systems 2013;14(3):1255-1265.

[4] Wang L, Collins Jr. EG, Li H. Optimal design and real-time control for energy management in electric vehicles. IEEE Transactions on Vehicular Technology 2011;60(4):1419-1429.

[5] Xue XD, Cheng KWE, Lin JK, Zhang Z, Luk KF, Ng TW, Cheung NC. Optimal control method of motoring operation for SRM drives in electric vehicles. IEEE Transactions on Vehicular Technology 2010;59(3):1191-1204.

[6] Xue XD, Cheng KWE, Ng TW, Cheung NC. Multi-objective optimization design of in-wheel switched reluctance motors in electric vehicles. IEEE Transactions on Industrial Electronics 2010;57(9):2980-2987.

[7] Cheng C, McGordon A, Poxon J, Jones R, Jennings P. A model to investigate the effects of driver behaviour on hybrid vehicle control. 25th World Battery, Hybrid, and Fuel Cell Electric Vehicle Symposium and Exhibition 2010; November 5-9, Shenzhen, China.

[8] Knowles M, Scott H, Baglee D. The effect of driving style on electric vehicle performance, economy, and perception. Int. J. of Hybrid Vehicles 2012;4(3):228-247.

[9] Bingham C, Walsh C, Carroll S. Impact of driving characteristics on electric vehicle energy consumption and range. IET Intell. Transp. Syst. 2012;6(1):29-35.

[10] Fiat Eco: Drive 2010. Eco-driving uncovered: the benefits and challenges of eco-driving based on the first study using real journey data. Available at http://www.lowcvp.org.uk/assets/reports/Fiat_Eco-Driving%20Uncovered.pdf.

[11] Gao DW, Mi C, Emadi A. Modeling and simulation of electric and hybrid vehicles. Proceedings of the IEEE 2007;95(4):729-745.

[12] Donoghue JF, Burghart JH. Constant power acceleration profiles for electric vehicles. IEEE Transactions on Industrial Electronics and Control Instrumentation 1987;34(2):188-191.

[13] Yao EJ, Wang MY, Song YY, Zuo T. Estimating the cruising range of electric vehicle based on instantaneous speed and acceleration. Applied Mechanics and Materials 2013;361-363:2104-2108.

[14] Imanishi H, Takada Y, Wakisaka T. An acceleration control algorithm for an electric motor driven vehicle in consideration of the reduction of energy consumption. Nippon Kikai Gakkai Ronbunshu, C Hen/Transactions of the Japan Society of Mechanical Engineers, Part C 2002;68(5):1512-1517.

[15] Lu D, Ouyang M. Torque-based optimal acceleration control for electric vehicle. Chinese Journal of Mechanical Engineering (English Edition) 2014;27(2):319-330.

[16] Saerens B, Diehl M, Van Den Bulck E. Optimal control using pontryagin's maximum principle and dynamic programming. Lecture Notes in Control and Information Sciences 2010;402:119-138.

[17] Lipp T, Boyd S. Minimum-time speed optimisation over a fixed path. International Journal of Control 2014;87(6):1297-1311.

[18] Mackenzie D, Heywood J. Acceleration performance trends and evolving relationship between power, weight, and acceleration in U.S. light-duty vehicles. Transportation Research Record 2012;2287:122-131.

[19] Eberhart, R.C., Shi, Y. Comparison between genetic algorithms and particle swarm optimization. Evolutionary Programming VII, Lecture Notes in Computer Science 1998; 1447:611-616.

[20] Jain M, Desai C, Williamson SS. Genetic algorithm based optimal powertrain component sizing and control strategy design for a fuel cell hybrid electric bus. 5th IEEE Vehicle Power and Propulsion Conference, VPPC 2009;5289740:980-985.

[21] Ribau JP, Sousa JMC, Silva CM. Plug-in hybrid vehicle powertrain design optimization: energy consumption and cost. Lecture Notes in Electrical Engineering 2013;191(3):595-613.

[22] Desai C, Berthold F, Williamson SS. Optimal drivetrain component sizing for a plug-in hybrid electric transit bus using multi-objective genetic algorithm. EPEC 2010 - IEEE Electrical Power and Energy Conference: "Sustainable Energy for an Intelligent Grid" 2010; Halifax, NS, August 25-27:1-5.

[23] Dandurand B, Guarneri P, Fadel G, Wiecek MM. Equitable multi-objective optimization applied to the design of a hybrid electric vehicle battery. Journal of Mechanical Design, Transactions of the ASME 2013; 135(4):041004.

[24] Shahi SK, Wang GG, An L, Bibeau E, Pirmoradi Z. Using the Pareto set pursuing multiobjective optimization approach for hybridization of a plug-in hybrid electric vehicle. Journal of Mechanical Design, Transactions of the ASME 2012;134(9):094503.

[25] Deb K, Pratap A, Agarwal S, Meyarivan T. A fast elitist non-dominated sorting genetic algorithm for multi-objective optimisation: NSGA-II. IEEE Transactions on Evolutionary Computation 2002;6(2):182-197.

[26] Xu G, Li W, Xu K, Song Z. An intelligent regenerative braking strategy for electric vehicles. Energies 2011;4:1461-1477.

[27] Gantt LR, Alley RJ, Nelson DJ. Battery sizing as a function of powertrain component efficiencies for various drive cycles. Proceedings of the ASME International Design Engineering Technical Conferences & Computers and Information in Engineering Conference (IDETC/CIE 2011) 2011; August 28-31, Washington, DC.

[28] Larminie J, Lowry J. Electric vehicle technology explained. 2nd Edition, John Wiley & Sons, Ltd., 2012; Chichester, West Sussex, UK.

[29] Leonhard, W. Control of electrical drives. Springer-Verlag 1985.

[30] Chen M, Rincón-Mora GA. Accurate electrical battery model capable of predicting runtime and I-V performance. IEEE Transactions on Energy Conversion 2006;21(2):504-511.

[31] Holland JH. Adaptation in natural and artificial systems. Ann Arbor, MI: MIT Press 1975.

[32] Nandi AK. GA-Fuzzy approaches: application to modeling of manufacturing process. Statistical and Computational Techniques in Manufacturing 2012; Springer-Verlag, Berlin, Heidelberg, ISBN: 978-3-642-25858-9, DOI 10.1007/978-3-642-25859-6):145-185.

[33] Berry MI 2010. The effects of driving style and vehicle performance on the real-world fuel consumption of US light-duty vehicles. M.S. Thesis, Massachusetts Institute of Technology, available at http://web.mit.edu/sloan-auto-lab/research/beforeh2/files/IreneBerry_Thesis_February2010.pdf.

[34] Nandi AK, Datta S, Deb K. Design of particle-reinforced polyurethane mould materials for soft tooling process using evolutionary multi-objective optimization algorithms. Soft Computing 2012;16(6):989-1008.

[35] Barlow TJ, Latham S, McCrae IS, Boulter PG. A reference book of driving cycles for use in the measurement of road vehicle emissions. TRL PPR354 2009.

[36] Siegel S. Non-parametric statistics for the behavioral sciences. New York: McGraw-Hill 1956:75-83.

[37] Krause P, Wasynczuk O, Sudhoff S. Analysis of electric machinery. IEEE Press 1995.

[38] Branke J, Deb K, Dierolf H, Osswald M. Finding knees in multi-objective optimization. Yao, X., et al. (eds.) PPSN 2004, LNCS 3242, Springer, Heidelberg 2004:722–731.

[39] Dovgan E, Tušar T, Javorski M, Filipič B. Discovering comfortable driving strategies using simulation-based multiobjective optimization. Informatica (Slovenia) 2012;36(3):319-326.

List of Tables

TABLE I EV model parameters.

Electric Motor	
Armature inductance, L_a (H)	0.1
Armature resistance, R_a (Ω)	0.5
Field current, I_f (A)	1.0
Geometric constant, K (VA^{-1}(rads^{-1})$^{-1}$)	1.5
Maximum efficiency	88%
Maximum Power (kW)	56
Type	DC brushed
Battery	
Capacity, Cap (A·h)	80
Initial state-of-charge, SOC_{init}	1.0
Number of cells in parallel, NP	1
Number of cells in series, NS	96
Type	Lithium-Ion
Voltage, V_P (V)	394
$C_{Transient\_L}$ (MF)	0.22375
$R_{Transient\_L}$ (mΩ)	0.9968
$C_{Transient\_S}$ (MF)	0.03518
$R_{Transient\_S}$ (mΩ)	0.9338
R_{Series} (mΩ)	1.4932
Vehicle	
Air density, ρ_{air} (kgm-3)	1.225
Drag coefficient, CD	0.35
Frontal area, Af (m2)	2.5
Gravitational acceleration, g (ms-2)	9.81
Mass, m (kg)	1350
Overall gear ratio, G	2.1:1
Rolling friction coefficient, μ	0.014
Tire radius, R (m)	0.3429
Transmission	Single speed

TABLE II GA parameters used for solving MOOP.

Type of GA	Binary-coded GA
Population size	100
Recombination type	Standard tournament selection (size=2)
Crossover probability	0.985
Mutation probability	0.01
Random seed	0.4
Number of generations	100
Time step, δt (s)	0.001

TABLE III Statistical information of the solutions obtained by 20 independent runs with

different random seeds for two approaches.

Speed (km/h)	Approach	Number of Pareto-optimal solutions obtained		Size of the dominated space, S_d			Coverage of two Pareto fronts, C		
		Mean	SD	Mean	SD	Absolute Mean difference	Mean	SD	Absolute Mean difference
40	Single acceleration	100	0	0.850	0.0012	0.004	10.9	2.58	18.0
	Multiple accelerations	100	0	0.854	0.0046		28.9	3.91	
72	Single acceleration	100	0	0.812	0.0013	0.013	8.7	3.22	22.5
	Multiple accelerations	100	0	0.825	0.0095		31.2	2.54	
104	Single acceleration	100	0	0.794	0.0020	0.034	22.7	19.43	33.8
	Multiple accelerations	100	0	0.828	0.0069		56.5	18.29	

TABLE IV Wilcoxon signed-rank test on the results obtained by both approaches for 20 independent runs with different random seeds.

Speed (km/h)	Perfor-mance metric	Number of non-zero difference of paired data ($A_{Approach\ 1}$ - $A_{Approach\ 2}$)	Sum of the positive ranks (S_{PR})	Sum of the negative ranks (S_{NR})	Value of Test statistics, T (minimum of S_{PR} and S_{NR})	Critical value of Wilcoxon Test for a two tailed significance level (SL)	Remark (based on two tailed significance level)
40	S_d	20	5	205	5	37 for SL=0.01	$T<37$, reject H_0 (i.e., Approach 2 is better than Approach 1)
	C	20	0	210	0	37 for SL=0.01	$T<37$, Reject H_0 (i.e., Approach 2 is better than Approach 1)
72	S_d	20	56	154	56	60 for SL=0.1; 52 for SL=0.05	$T>37$ for SL of 0.05, cant reject H_0; But for 0.1 SL, reject H_0
	C	20	0	210	0	37 for SL=0.01	$T<37$, reject H_0 (i.e., Approach 2 is better than Approach 1)
104	S_d	20	0	210	0	37 for SL=0.01	$T<37$, reject H_0 (i.e., Approach 2 is better than Approach 1)
	C	20	0	210	0	37 for SL=0.01	$T<37$, reject H_0 (i.e., Approach 2 is better than Approach 1)

TABLE V Statistical information of the solutions obtained by 20 independent runs with different speeds for two approaches.

Speed Zone	Approach	Number of Pareto-optimal solutions obtained		Size of the dominated space			Coverage of two Pareto-fronts		
		Mean	SD	Mean	SD	Absolute Mean difference	Mean	SD	Absolute Mean difference
Neighborhood	Single acceleration	100	0	0.869	0.0124	0.001	9.6	1.93036	24.9
	Multiple accelerations	100	0	0.868	0.0126		34.5	8.28124	
Urban	Single acceleration	100	0	0.829	0.0113	0.004	10.75	3.53739	18.05
	Multiple accelerations	100	0	0.833	0.0200		28.8	3.9416	
Highway	Single acceleration	100	0	0.803	0.0060	0.022	27.4	11.8650	33.4
	Multiple accelerations	100	0	0.825	0.0101		60.8	18.1415	

TABLE VI Distribution of optimal number of accelerations found by MOGA in Approach 2 in three speed zones.

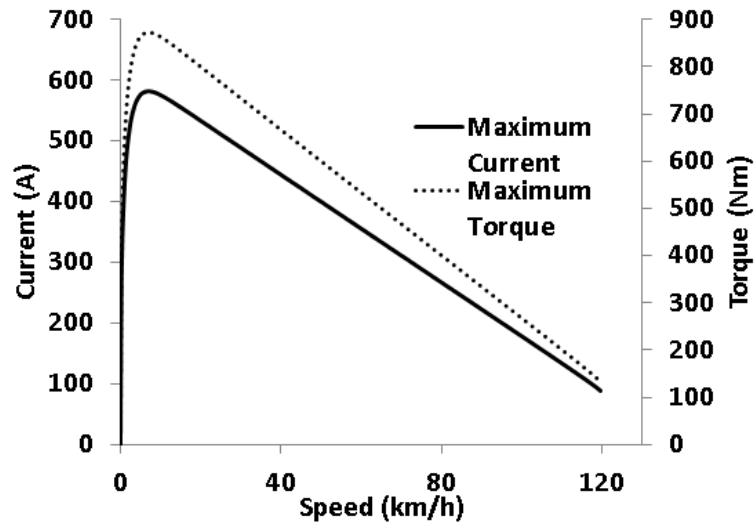| Speed Zone	One Acceleration	Two Accelerations		Three Accelerations		Four Accelerations		Five Accelerations	
	Mean	Mean	SD	Mean	SD	Mean	SD	Mean	SD
Neighborhood	0	85.8	8.5997	11.7	8.1520	1.9	1.8529	0.6	1.2649
Urban	0	92.2	4.2895	7.4	4.2478	0.4	0.69292	0	0
Highway	0	92.6	7.4714	7.4	7.4714	0	0	0	0

List of Figures

Fig. 1: Electric motor characteristics: maximum current and torque for different speeds.
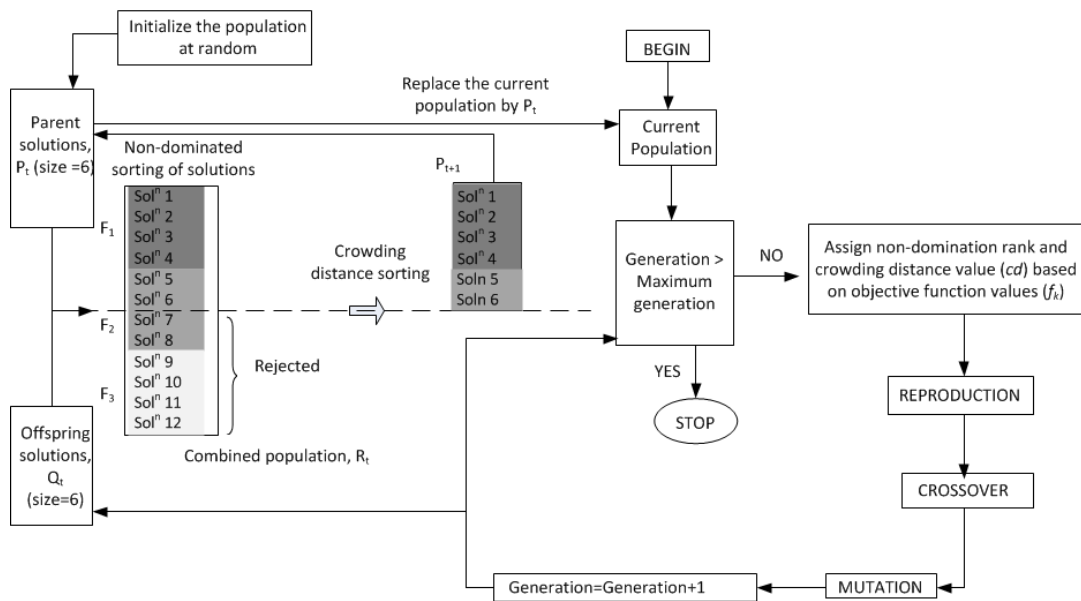
For a maximization problem, any two solutions (*a* and *b*) with M objectives, a dominates b is represented by the expressions:
$$\begin{cases} f_j(a) < f_j(b), \text{ for all } j = 1, 2, \ldots, M \\ f_j(b) < f_j(a), \text{ for at least one } j\ (j = 1, 2, \ldots, M) \end{cases}$$

Rank of ith solution: $R_i = 1 + n_i$, n_i is the number of solutions dominates i

Crowding distance value of ith solution: $cd_i = \sum_{k=1}^{M} \frac{f_k^{i+1} - f_k^{i-1}}{f_k^{max} - f_k^{min}}$

Fig. 2: Schematic representation of the working of MOGA using NSGA-II.
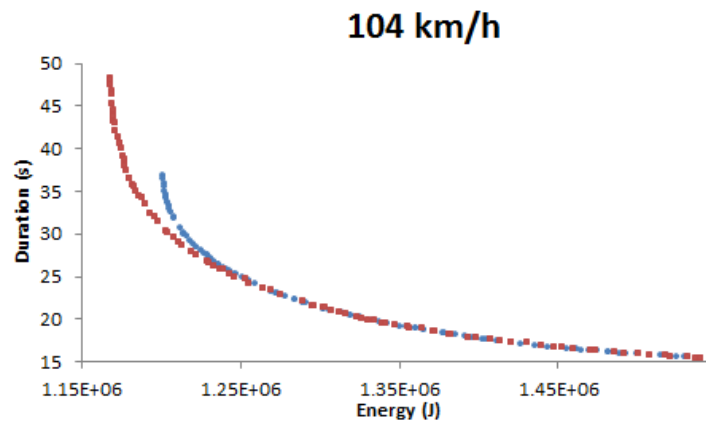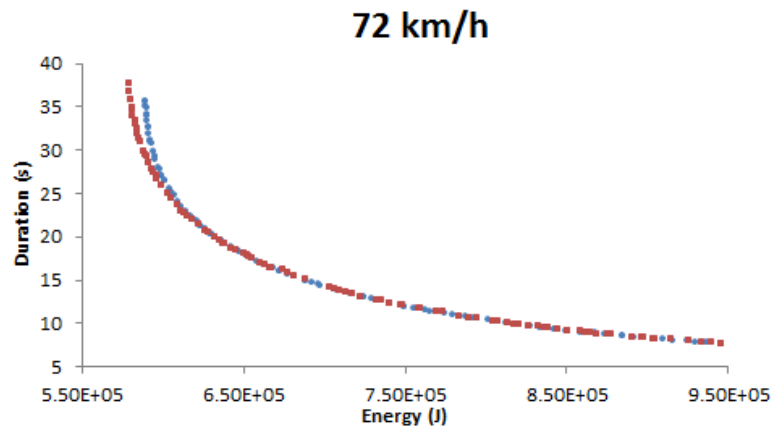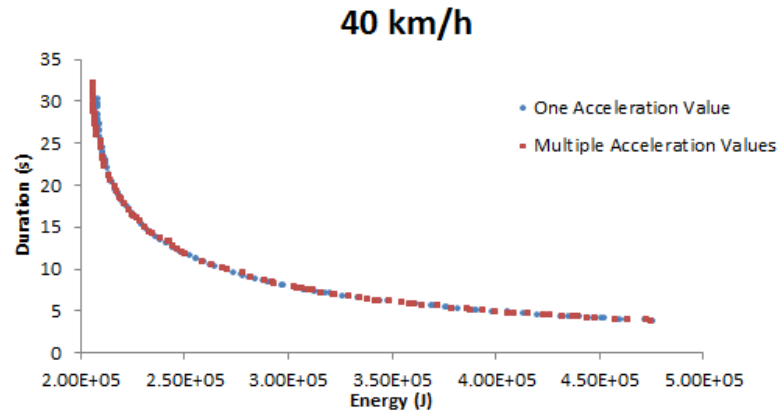
Fig. 3: Comparison of Pareto-optimal fronts obtained in two approaches for chosen speed

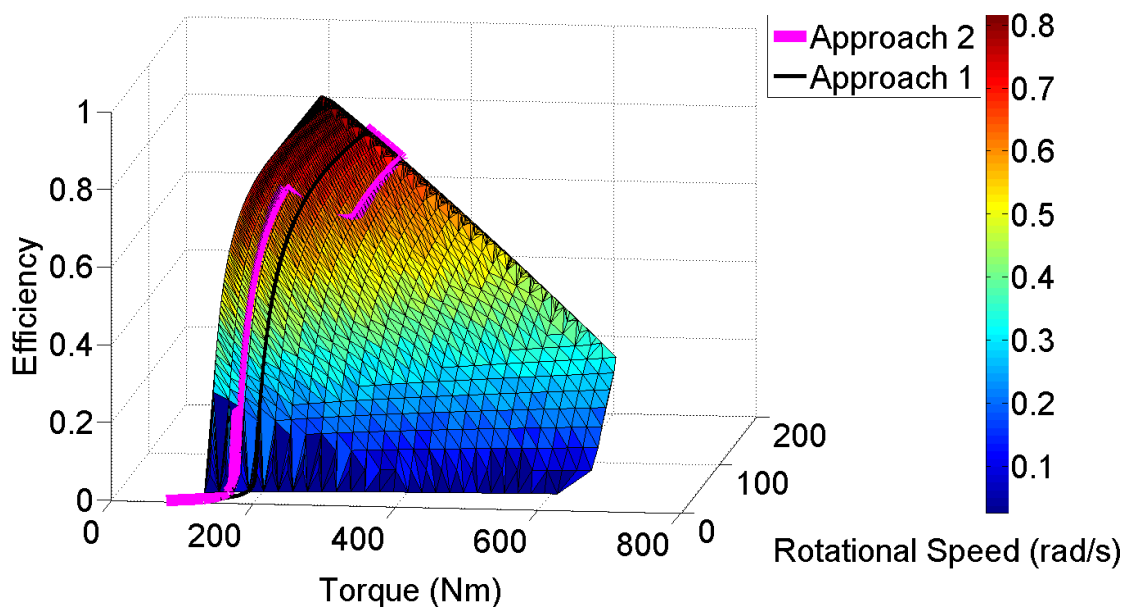of a) 40 km/h b) 72 km/h and c) 104 km/h.

Fig. 4: Comparison of Approach 1 and Approach 2 using electric motor efficiency as a function of rotational speed and torque.
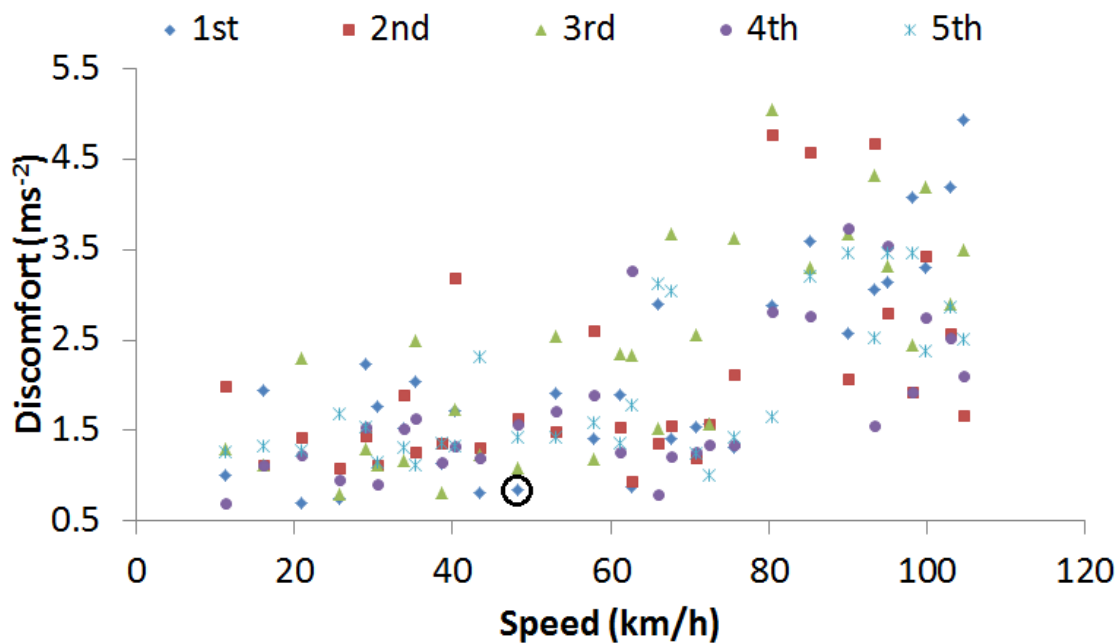

Fig. 5: Level of discomfort for top five knee values for different speeds.
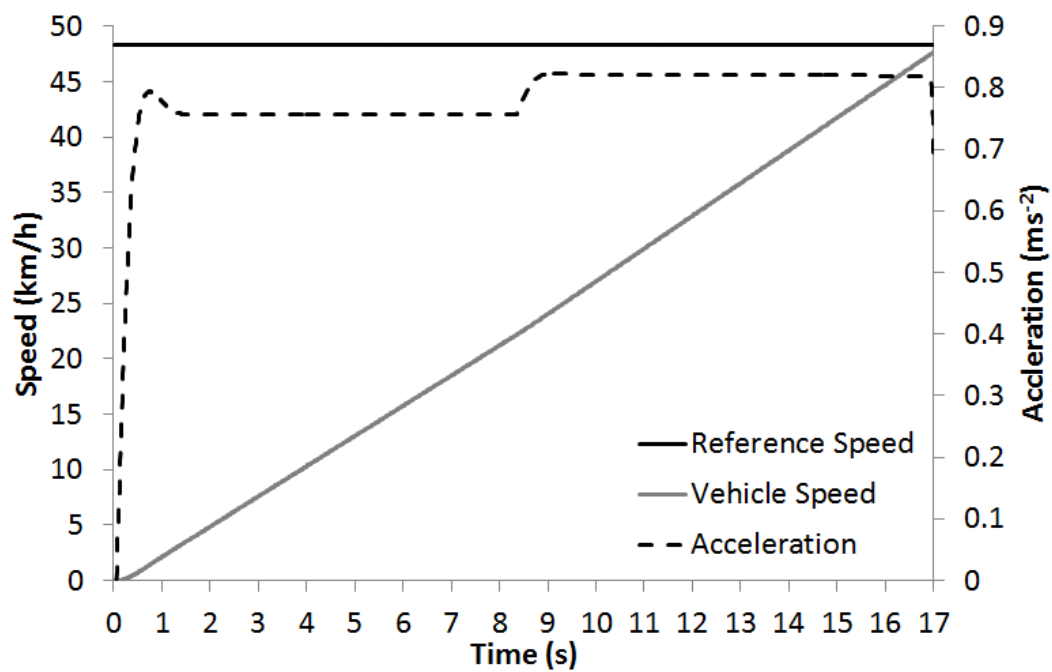
Fig. 6: Demonstration of a single solution selected from Fig. 5.

IV FINDING AN OPTIMAL DRIVING STRATEGY FOR AN ELECTRIC BUS BASED ON OPERATIONAL DATA

Warren Vaz

Department of Mechanical and Aerospace Engineering, Missouri University of Science and Technology, Rolla, MO, USA

Arup K. Nandi

Department of Mechanical and Aerospace Engineering, Missouri University of Science and Technology, Rolla, MO, USA

Umit O. Koylu

Department of Mechanical and Aerospace Engineering, Missouri University of Science and Technology, Rolla, MO, USA

ABSTRACT

One of the clean energy initiatives at Missouri S&T is an electric shuttle bus service, the Ebus. It provides valuable operational data for a fleet-type electric vehicle (EV) operating over a fixed route. The primary aim of this study is to use the daily operational data obtained from the Ebus in order to formulate an optimal driving strategy. Existing research efforts to improve EVs focus on improvements to the architecture and the energy management strategy. However, they fail to provide the driver with an optimal driving strategy leading to suboptimal use of the stored battery energy. This shortcoming was addressed here by implementing a multi-objective approach to find an optimal driving strategy for an electric bus. The driving strategy was taken to comprise two parts: a constant trip speed and an acceleration value to achieve that speed. From the operational data, the efficiency and power consumption of the electric motor were

computed for different speeds. By assuming the entire trip was executed at a constant speed, the range for each speed was calculated. The speeds were ranked based on their corresponding ranges. Then, to achieve the optimal speed, the acceleration duration and energy consumption for different acceleration values were computed. The values were ranked based on the trade-off between duration and energy. The choice of driving strategy (exact speed and acceleration values) is left to the driver since different strategies would be needed for different road conditions. This multi-objective approach gives flexibility to the driver and promotes optimal use of the stored battery energy, thereby enhancing the energy efficiency and range of the Ebus. It can be easily implemented in other electric vehicles as well.

INTRODUCTION

Electric vehicles (EVs) have recently received a lot of attention due to being classified as zero emissions vehicles and being more energy efficient. Electric buses are of great interest for urban mobility applications since the route is generally fixed and they can be deployed as a fleet. Reference [1] details the many advantages, including being locally emission-free, suffering no energy losses during idle operation, more energy efficient than conventional buses, quiet, able to recover braking energy, etc. Electric buses provide additional advantages such as being able to have a low floor to comply with regulations [2]. Lajunen's study [3] on city buses concluded that electric buses have tremendous potential to improve energy efficiency when replacing conventional buses as well as to reduce emissions and life-cycle costs. However, operation route planning and scheduling were found to be important in managing the life cycle costs.

Existing research efforts on EVs can broadly be divided into two categories. The first category is improvements to the hardware of the vehicle, such as the energy storage (namely, the battery) [4], the charging device [5], electric motor improvements [6], etc. The second category is improvements to the energy management strategy (EMS) of the vehicle, examples of which can be found in [7-9]. In this study, a third category is proposed: improvements to the driving strategy adopted by the driver. A driving strategy refers to the combination of acceleration and speed values chosen by the driver to traverse a given distance. The importance of this category of research is as follows. The need for an EMS came about when researchers realized that it was simply not enough to improve the hardware of the EV; it was also important to use the stored energy of the battery in the most optimal manner. The goal of the EMS is to properly manage the energy of the EV while fulfilling the driver's demand. However, the driver does not typically plan a trip based on acceleration and speed values. The driver typically follows the flow of traffic, which means the chosen driving strategy may be suboptimal. This means that, no matter how much the hardware and the EMS are improved, the EV will not perform to the best extent possible because the driver's demands cause the EMS to waste energy by operating the hardware in a suboptimal regime. Therefore, it is essential to adopt a driving strategy that optimally operates the EV hardware and allows the EMS to properly manage the stored energy. This is termed optimal driving or adopting an optimal driving strategy.

Optimal driving is a new concept and there are few existing studies that can be stated as belonging to this category. There are several studies [10-14] to support the notion that driving parameters, such as the harshness of acceleration or braking, the

average trip speed, the number of starts or stops, all influence the vehicle energy

consumption and, consequently, the range. Reference [15] is a study specifically for

electric buses, which concluded that the main reason for differences in the energy

consumption of electric buses operating on the same bus line was the difference in the

way the acceleration pedal was used. Yao et al. [16] showed that the energy consumption

was dependent on the chosen acceleration value for a given speed change. Vaz et al. [17]

showed that a certain zone of speeds in the speed range of an EV could optimize the

objectives of range and trip time.

The Missouri University of Science and Technology (Missouri S&T) has

developed and promoted energy sustainability initiatives on its campus through various

projects, such as the Solar Village, the E^3 Commons, and the renewable energy

microgrids. One of the latest clean energy initiatives at Missouri S&T is the Ebus, which

is the first fully electric shuttle in Rolla, MO. In addition to providing free public

transportation to the university students and raising awareness about electric vehicle (EV)

technology, the Ebus also provides valuable operational data for a fleet-type EV

operating over a fixed route.

The Ebus, which is an electric bus servicing the Missouri S&T campus is depicted

in Fig. 1. It can accommodate 20 seated passengers and 10 standing passengers. Its range

is between 120-150 miles. This study finds an optimal driving strategy for the Ebus by

analyzing the operational data. The study by Ye et al. [18] is a typical example of the

design of a hybrid electric bus based on modeling. He et al. [19] used parameter matching

to design and simulate the performance of an electric city bus. Chymera et al. [20]

proposed an alternative modeling approach by using the movement data of a tram system

to calculate the energy required. This study uses a similar approach. Operational data of the Ebus was analyzed to find the optimal zone for trip speed selection. Additionally, it was used to find a suitable acceleration strategy to achieve the optimal speeds. A bus simulation was developed using the parameters provided by the manufacturer and the findings were compared with the simulation predictions.

Fig. 1: Photograph of the Ebus [21].

OPTIMAL DRIVING APPROACH

A driver typically drives the bus based on experience and based on real-time traffic conditions. This results in a random, suboptimal driving strategy, meaning the accelerations and speeds chosen by the driver to negotiate a particular distance may not guarantee optimal use of the battery energy. However, since the strategy is random, the optimal accelerations and speeds may be adopted by the driver some of the time, without

the driver realizing that these are optimal values. Therefore, it is necessary to find and extract the optimal driving strategy from all the operational data.

The aim of this study is to find an optimal driving strategy for the Ebus. A multi-objective approach was used to find optimal speeds, as proposed by Vaz et al. [17], who showed that it was possible to find a trip speed that gave the maximum range by maximizing the electric motor efficiency and minimizing the power consumption. In other words, the energy per unit distance (taken as miles) would be the lowest at this optimal speed. The first aim of this study is to identify the optimal speed or optimal speed zone specifically for the Ebus. It is important to present the driver with a range of solutions since the optimal speed may be too slow or unfeasible for various reasons.

Once the optimal speed is chosen, the driver would like to accelerate the bus to that speed in the shortest time duration while using the least energy possible. These objectives are conflicting, meaning if the driver chooses acceleration values that minimize the acceleration duration, the energy expended will increase. From a driving standpoint, the driver does not typically choose a particular acceleration value. Rather, the driver maintains a pedal position.

Based on these observations and the literature review, the second aim is to identify an acceleration strategy that will result in non-dominated objective function values with the objectives being the energy consumption and time duration. Two solutions, A and B, each corresponding to the same two objective functions, f_1 and f_2, which have to be minimized, are said to be non-dominated with respect to one another if either $f_1(A) < f_1(B)$ and $f_2(B) < f_2(A)$ or $f_1(B) < f_1(A)$ and $f_2(A) < f_2(B)$. A is said to dominate B if $f_1(A) < f_1(B)$ and $f_2(A) < f_2(B)$. Correspondingly, A is said to be dominated by B. Non-

dominated solutions represent a trade-off between the different objectives that are being optimized. In the absence of any higher-level information, any non-dominated solution may be suitable for implementation.

In general, acceleration consumes more power than constant speed operation. However, it usually comprises a much shorter portion of the trip. For a campus electric bus with stop-and-go driving, it is important to focus on both aspects. Due to the complexities involved with daily driving, including auxiliary effects from the different onboard systems, gradient effects, etc., and due to the randomness associated with daily driving, it may be difficult to extract a comprehensive driving strategy from the operational data. Therefore, a bus simulation was developed using the parameters provided by the manufacturer. Since it was convenient to control the conditions of simulations, it was relatively straightforward to extract the optimal driving strategy and to compare it with the strategy that was extracted from the operational data of the Ebus.

DATA ACQUISITION SYSTEM (DAQ)

The DAQ onboard the Ebus comprised several instruments and sensors to measure various operational parameters, data processing (filtering and signal conversion) circuits, and a vehicle computer that recorded all the data. The measured data were filtered and output to an Excel file. Eight samples were averaged each second and recorded in the vehicle computer.

For this study, only seven different data elements from the DAQ were used: battery current, battery voltage, battery state of charge (SOC), time, road gradient, vehicle speed, and the distance traveled. Fig. 2 shows a schematic of the data acquisition system.

As seen in the figure, the current and voltage were directly measured from the bus circuitry and fed to the contactor board. The current was integrated each second and this integrated value was treated as a fraction of the total capacity to obtain the *SOC*. A magnetic pick-up on the chain drive was used to read pulses to obtain the speed. The vehicle speed pulses were integrated in order to determine the distance traveled. The gradient data was measured using an accelerator on board the bus. The time was obtained directly from the vehicle computer recordings.
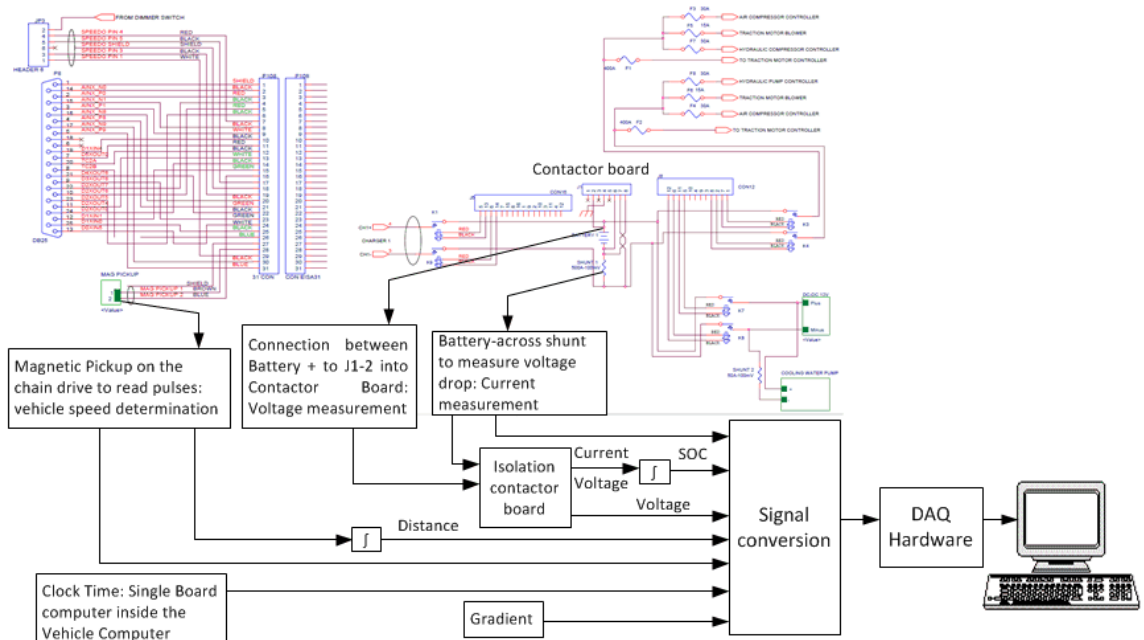

Fig. 2: Data acquisition system of the Ebus.

ELECTRIC VEHICLE (EV) MODEL

To confirm the trends found from the experimental data, a MATLAB model of the Ebus was created using the parameters provided by the manufacturer. Only the critical components were modeled. The models required for the battery, the electric motor, and the vehicle dynamics can be found in [22-25]. The relevant bus model

parameters are listed in Table 1. Certain parameters, such as the air density and the gravitational acceleration were typical local values. The most important equations are summarized below. For a given reference speed, v, the tractive power needed is

$$Pte = \left(\frac{1}{2} \rho_{air} C_D A_f v^2 + \mu mg + mg\sin\theta + Ima \right) v \tag{1}$$

Where a is the acceleration and θ is the gradient. The electric motor efficiency is

$$\eta = \frac{\tau\omega}{\tau\omega + k_c \tau^2 + k_i \omega + k_w \omega^3 + C} \tag{2}$$

Where τ and ω are the electric motor torque and rotational speed, respectively. If the tractive power is positive, the battery current is

$$I_P = \frac{Pte}{B_{eff} C_{eff} G_{eff} \eta} \frac{1}{V_P} \tag{3}$$

Finally, the state-of-charge of the battery is

$$SOC = SOC_{init} - \int \frac{I_P}{Cap} dt \tag{4}$$

The model was validated by benchmarking with the operational data. Fig. 3 shows the measured and simulated vehicle speed and battery current for a short trip (108 s). The simulated speed closely matched the measured speed. The resulting battery current was a little more complex. It could be seen that the simulated current generally followed the measured battery current, especially during acceleration and deceleration. The deviations were to be expected because the operational data contained real world conditions that were not simulated, such as auxiliary systems. On the other hand, the large variations in the simulation current were due to the fact the simulation followed the measured data, implying that the controller had to compensate for the sudden, unexpected changes in the

speed. Even though the two current plots looked vastly dissimilar, when considering the total energy consumed during the trip, the difference was only 3%. Constant-speed operation is expected to be a lot closer. For example, at 30 mph, the power consumption at zero gradient was measured to be 13 kW, whereas was the simulation produced a power of 13.5 kW, that is, a difference of about 4%. All this confirmed that the simulation was able to capture the operational characteristics of the Ebus.

Table 1: Relevant bus model parameters.

|	
Air density, ρ_{air} (kg m^{-3})	1.17
Drag coefficient, C_D	0.6
Frontal area, A_f (m^2)	6.11
Gravitational acceleration, g (ms^{-2})	9.81
Inertia coefficient	1.05
Mass, m (kg)	6740
Maximum speed (mph)	45
Overall gear ratio, G	10.07:1
Rolling friction coefficient, μ	0.0082
Tire radius, R (m)	0.39
Battery	
Auxiliary power (W)	25
Capacity, Cap (A·h)	400
Initial state-of-charge, SOC_{init}	1.0
Number of cells in parallel, N_P	1
Number of cells in series, N_S	96
Type	Lithium-Ion
Motor	
Critical rotational speed (rads^{-1})	250
Maximum rotational speed (rads^{-1})	513
Maximum torque (Nm)	406
Power (kW)	75.4
Losses	
Battery efficiency, B_{eff}	0.99
Converter efficiency, C_{eff}	0.96
Transmission efficiency, G_{eff}	0.99
Electronic losses, C (W)	100
Copper losses, k_c	0.3
Iron losses, k_i	0.01
Windage losses, k_w	0.000005

The model was validated by benchmarking with the operational data. Fig. 3 shows the measured and simulated vehicle speed and battery current for a short trip (108 s). The simulated speed closely matched the measured speed. It can be seen that the simulated current generally followed the measured battery current, especially during acceleration and deceleration. The deviations were to be expected because the operational data contained real world conditions that were not simulated, such as auxiliary systems. Even though the two current plots look dissimilar, when considering the total energy consumed during the trip, the difference was only 3%. Constant-speed operation is expected to be a lot closer. For example, at 30 mph, the power consumption at zero gradient was measured to be 13 kW, whereas was the simulation produced a power of 13.5 kW, that is, a difference of about 4%. All this confirmed that the simulation was able to capture the operational characteristics of the Ebus.

RESULTS AND DISCUSSION

Optimal Speed Zone: The first aim of this research was to identify the optimal speed zone. The bus operational data was obtained in an Excel spreadsheet for several days. The different columns contained different data elements (e.g., speed, current). The different rows contained different time steps, starting from the beginning of a day and stopping at the end. The time step was 1 s when the Ebus was moving and 30 s when parked. Therefore, there were about 24,000 rows in a spreadsheet for any given day with about 6 hours of moving data.
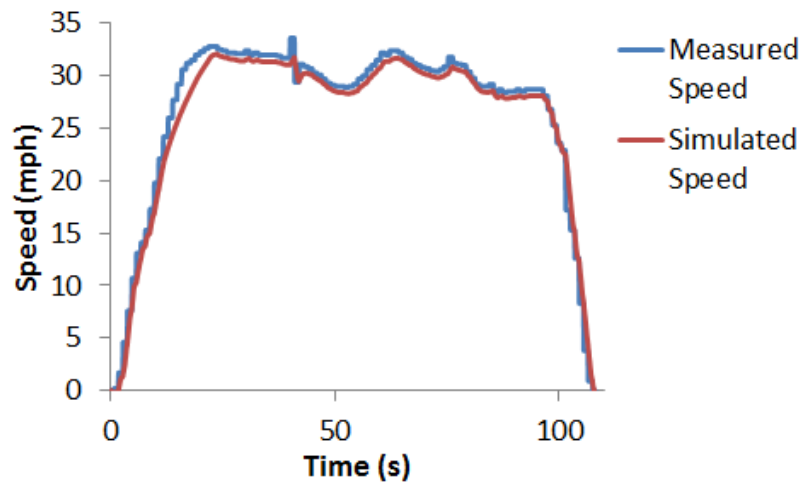
(a)
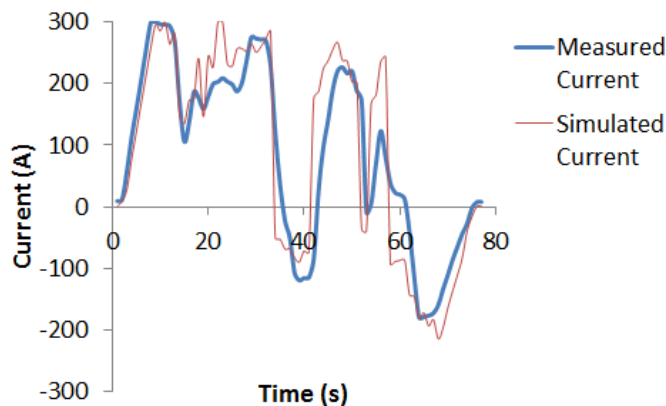
(b)

Fig. 3: Comparisons of measured and simulated data for: (a) vehicle speed (b) battery current.

A MATLAB script file was written to extract the six data elements required from a typical day's operational data. This script file only extracted the battery current and voltage (to calculate the power consumption) when the bus' speed was constant. Fig. 4 shows the measured power for different speeds, v, as well as the gradient at the time step that the power was extracted. Only positive gradients were considered. In general, the

power consumption increases with the speed and the gradient. However, the power at 40 mph in Fig. 4 was lower than the power at 3 mph because the gradient was significantly lower: 1.5° instead of almost 4°. This implies that gradient effects contribute significantly to power consumption. The predicted power in Fig. 4 was calculated by running the Ebus simulation with the same operational data (gradient and speed) as the measured power. It could be seen that the predicted power matched the measured power quite well with the average deviation being only 10.2%. It was observed that the operational data lacked any instances of zero gradient operation which was to be expected for the topography of Rolla. As such, the simulation was used to calculate the power consumption of the bus at zero gradients. This was displayed in Fig. 3, for which the power curve followed a quadratic rise in accordance with the v^2 nature of the drag force. This agrees with the quadratic trend found in [17] using a different model for a passenger EV.
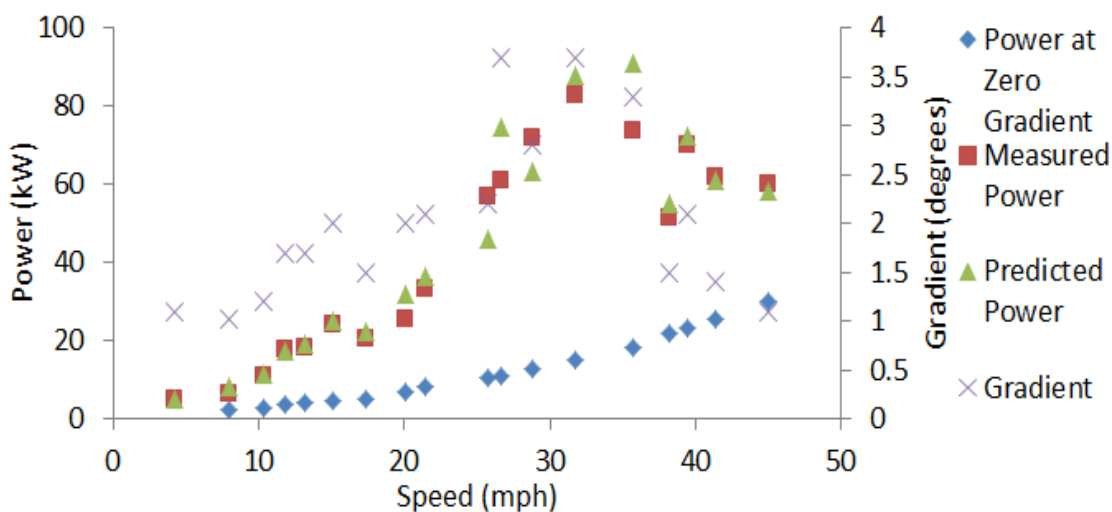

Fig. 4: Measured and predicted power along with power at zero gradient for different bus speeds; gradient values correspond to measured power values.

The simulation was used to obtain the electric motor torque for each of the speeds in Fig. 3. The rotational speed was calculated using the bus' linear speed, and using this and the electric motor torque, the output power of the electric motor was calculated. The efficiency of the electric motor at each speed was calculated by dividing the output power by the measured power consumption values in Fig. 4. Fig. 5 shows the efficiency as a function of speed, v. It was seen that the efficiency curve followed the expected trend, barring experimental outliers, of increasing as the speed increased, reaching a maximum value before finally starting to decline.
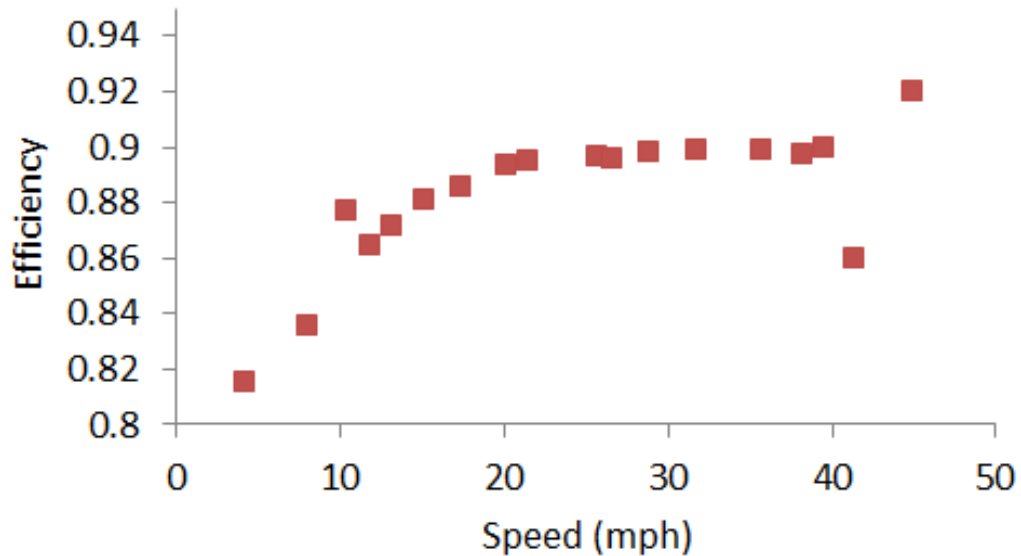

Fig. 5: Electric motor efficiency versus Ebus speed.

From an optimality standpoint, it is desirable to operate the bus with maximum efficiency and minimum power consumption, thereby getting maximum range. From Figs. 4 and 5, it is clear that these are conflicting objectives: no unique speed optimizes both objectives. Using data from Figs. 4 and 5, the range of the bus was calculated along with the total trip time for the associated speeds. The initial SOC was 1.0 and the final

SOC was 0.5. The results are illustrated in Fig. 6. The trip time followed a $1/v$ trend, as

expected, implying that, the trip time will decrease as the driver chooses a higher speed.

The range, however, has a more complex relationship with the speed. For both the

experimental and simulation data, the range increased as the speed increased, up to about

8 mph, after which it decreased. The initial increase was due to the increase in efficiency

and the subsequent decrease was due to the increase in power consumption. Therefore,

for zero gradient, the trip speed that gave the maximum range was 8 mph. However, if

the driver desires a shorter trip time, a higher speed can be chosen from Fig. 6. For

example, at 20 mph, the range decreased by only about 16% but the trip time decreased
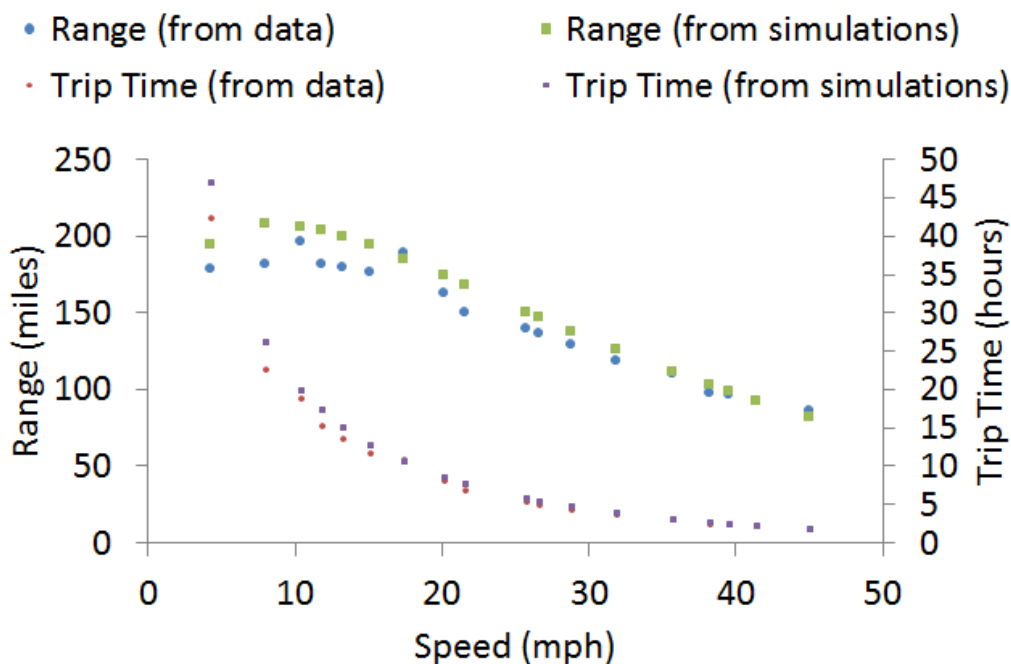
by about 69%.

Fig. 6: Range and trip time for different speeds using measured and simulated bus data.

From Fig. 4, it is clear that the gradient significantly changes the power

consumption. Therefore, the Ebus simulation was run at the same trip speeds as Fig. 6 but

with gradient values between 0º and 5º. The resulting Fig. 7 shows the optimal speed also increases as the gradient increases.

Instead of only looking at how many miles can be traveled with a certain number of kilowatt-hours, as in Fig. 5, it may be instructive to also consider the energy per mile. A second MATLAB script file was written to process several days' operational data so as to group the data into nine speed zones, 0-4.99 mph, 5-9.99 mph, and so on up to 45 mph. For each speed zone, the energy per mile was calculated whenever the bus speed was constant, taken to be within 2.5 mph of the preceeding speed and the following speed. The gradient was also recorded. Finally, the energy and gradient values were averaged so that each speed zone had a representative energy per mile and gradient. The results can be seen in Fig. 8. The general trend was that the energy per mile decreased as the speed increased up to a certain value and then increased with the speed. As expected, this was the opposite of Fig. 6 and confirmed the idea that a medium speed would give the maximum range. The gradients for all these zones were not zero but fairly low. Due to this gradient effect, the optimal speed zone was not 5-9.99 mph, as would be expected from Fig. 6, but 15-19.99 mph. Considering the speed limits within the city of Rolla, MO, this is definitely feasible.
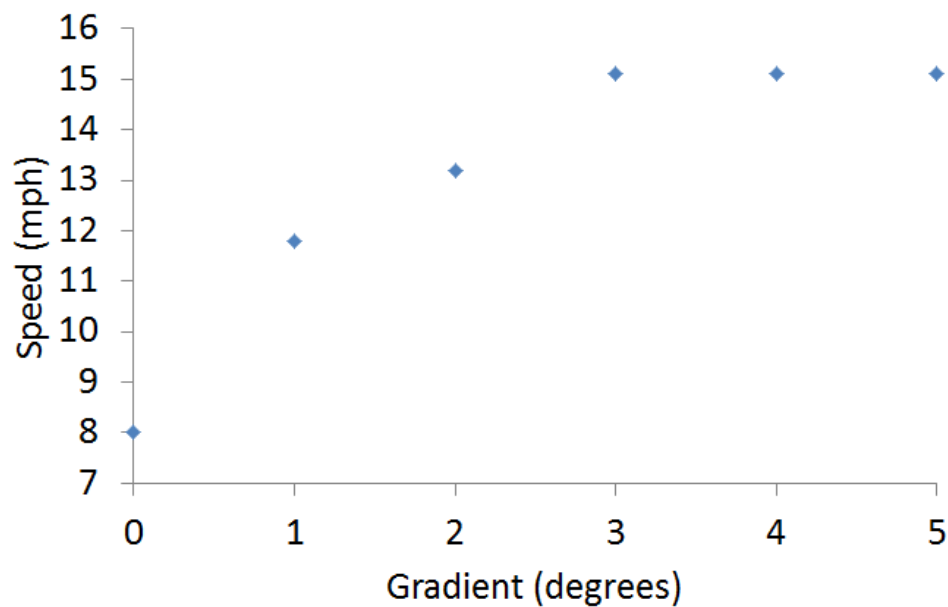
Fig. 7: Optimal speeds in terms of range for different gradients.

Based on prior experience, the Ebus was billed as having an energy consumption around 1 kWh/mi. This, of course, includes acceleration and deceleration periods as well so the constant speed energy consumption is expected to be much lower.
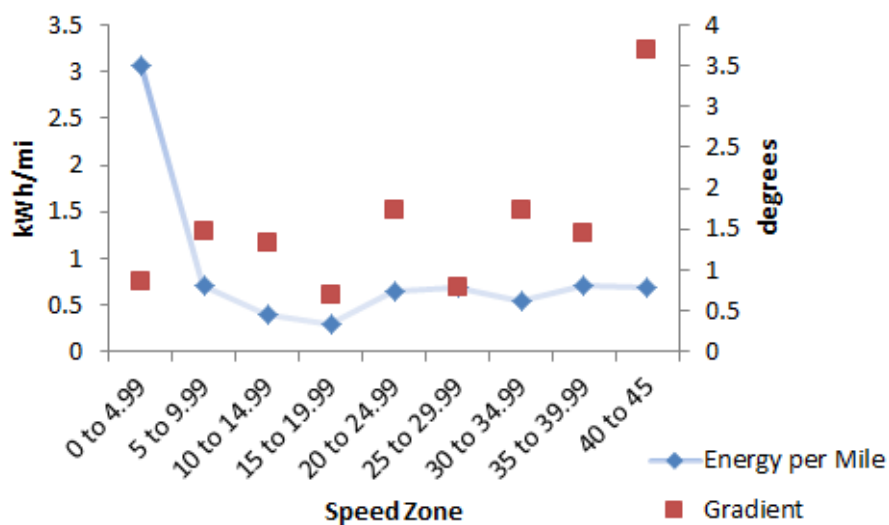

Fig. 8: Energy per mile and gradient from operational data for nine speeds zones.

As seen in Fig. 8, the energy consumption was between 0.6-0.7 kWh/mi for most speed zones. Finally, the energy consumption for the lowest speed zone was quite high, about 3.1 kWh/mi, even though the gradient was fairly low. This was due to the fact that the bus was usually accelerating in this speed zone so that even the constant speed data were not really constant. Upon adjusting the tolerance of the script file to 0.1 mph, the energy consumption was found to be about 2.4 kWh/mi.

Acceleration Strategy: The second aim was to identify an acceleration strategy that would result in non-dominated objective function values. A third MATLAB script file was written to compute the acceleration for different time steps for the operational data of several days. It was observed that the acceleration values drastically varied when accelerating from rest to a chosen speed, implying that it would be impossible to select an optimal acceleration value from the operational data. Therefore, the MATLAB script file was modified to identify all the speed changes from 0 mph up until the bus speed reached a constant value. Then, the acceleration values during each speed change were computed, and the maximum, mean, and standard deviation of each speed change were calculated. After analyzing these statistical parameters for different speed changes, a trend was noticed that the mean acceleration value was primarily responsible for dictating the acceleration duration, as expected. If a low duration is desired, a high mean acceleration value can be adopted but at the cost of consuming more energy. If energy savings is the prime concern, a low mean acceleration can be adopted at the cost of having a longer duration. However, the maximum and standard deviation were responsible for deciding non-domination of solutions. Fig. 9 shows the acceleration duration and energy for dominated and non-dominated solutions with a reference speed of $v_{ref} = 25$ mph. It could

be seen that the solutions with a low standard deviation (0.8-1.2 ms^{-2}) dominated the solutions with a high standard deviation (1.3-1.5 ms^{-2}). This trend was also noticed for other reference speeds and confirmed by the simulation. The solutions with a high standard deviation also had a higher maximum acceleration value (3.5-4.6 ms^{-2}) than those with a low standard deviation (2.7-3.5 ms^{-2}).
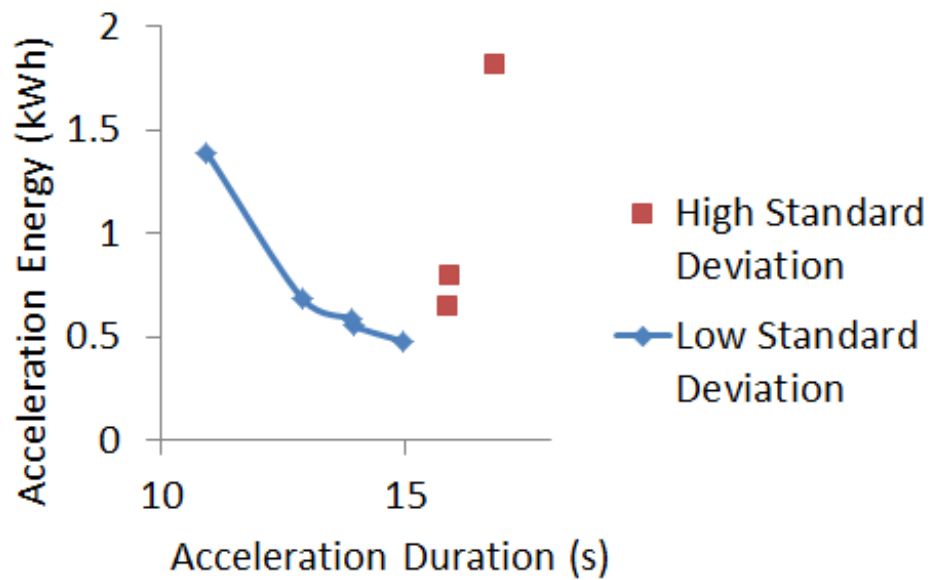

Fig. 9: Acceleration duration and energy for dominated and non-dominated solutions with v_{ref} = 25 mph.

Finally, it is important to consider the effect of the gradient on the acceleration strategy. After carefully analyzing the acceleration values, a trend was found that, for a certain speed change with comparable gradient values, the solution with a higher mean acceleration had a lower energy consumption than a solution with a lower mean acceleration. This can be seen in Fig. 10 for different speed changes. In each case, gradient values are comparable. However, it was also noticed that it was necessary to

keep the maximum and standard deviation of the acceleration as low as possible, even on graded roaded. Once again, these findings were confirmed with the present Ebus simulations.
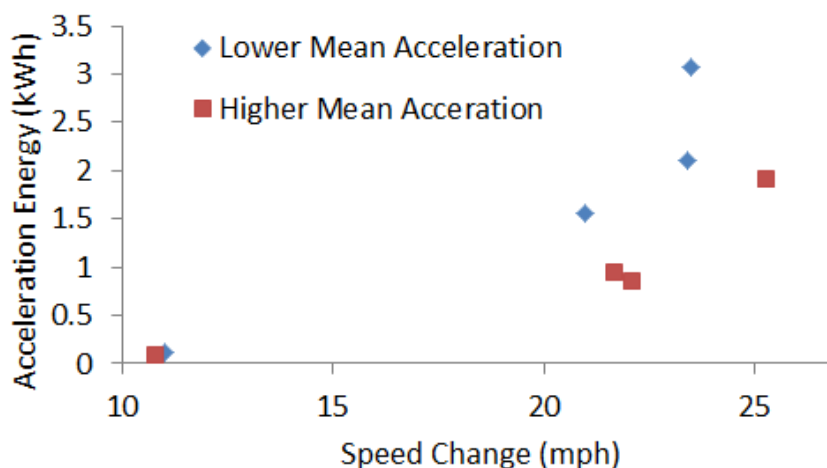

Fig. 10: Energy consumption for different speed changes for solutions with comparable gradient.

SUMMARY AND CONCLUSIONS

The main aim of this study was to find an optimal driving strategy for the Ebus servicing the Missouri S&T campus. The operational data was used to find an optimal speed. A simulation of the bus was created in order to confirm the experimental findings. By considering maximization of electric motor efficiency and minimization of power consumption, the optimal trip speed was found to be 8 mph. When adding gradient effects, it was found that the optimal speed increased as the gradient value increased and leveled off at 15 mph. These findings were further validated by measuring the energy per mile during the daily bus operation. It was found that the 15-19.99 mph speed zone had the least constant speed energy consumption out of the entire bus speed range (0-45

mph). The recommendation to the driver would be to maintain the Ebus speed as close to 15 mph as possible, especially on graded roads.

The operational data was further analyzed to find an appropriate acceleration strategy. It was found that the mean acceleration dictated the acceleration duration, but the maximum and standard deviation decided non-domination. High maximum and standard deviation values produced solutions that were dominated by those with low maximum and standard deviation values. Additionally, it was found that a higher mean acceleration value resulted in lower energy consumption for graded roads. The recommendation to the driver would be to vary the mean acceleration based on whether duration or energy consumption is of prime concern. In general, a higher mean acceleration value should be adopted on graded roads. However, in all cases, the maximum and standard deviation values should be as low as possible, implying a constant pedal position for the speed change.

With the efficiency of diesel buses being 6-10 kWh per mile, the Ebus is already an improvement in terms of energy efficiency and sustainability. The Ebus consumes 40-60 kWh and covers 40-60 miles per day. Optimal driving would significantly lower this, although more work is needed to quantify how much of a reduction is possible under daily driving conditions. The gradient's effect on the energy consumption is unavoidable, but the driver has control over the acceleration and speed. By careful route planning, unnecessary stops could be avoided in the future thereby allowing more constant-speed operation. While most of the passengers who use the bus would otherwise walk, the Ebus is seeing additional deployment to transport people into downtown Rolla and also to the Hy Point campus located about 5 miles away from the main campus. Future work on

usage will need to estimate not only the energy reduction but also the emissions reduction. It is necessary to take into account the emissions generated from producing the electricity used to charge the battery. The present optimal driving strategy could also be adopted for other electric vehicles.

ACKNOWLEDGMENTS

REFERENCES

[1] Kühne, R. (2010). Electric buses - An energy efficient urban transportation means. Energy 35 (12), pp. 4510-4513.

[2] King, Robert D., Haefner, Kenneth B., Salasoo, Lembit, Koegl, Rudolph A. (1995). Hybrid electric transit bus pollutes less, conserves fuel. IEEE Spectrum 32 (7), pp. 26-31.

[3] Lajunen, A. (2014). Energy consumption and cost-benefit analysis of hybrid and electric city buses. Transportation Research Part C: Emerging Technologies 8, pp. 1-15.

[4] Ma, Z., Jiang, J., Shi, W., Zhang, W., Mi, C.C. (2015). Investigation of path dependence in commercial lithium-ion cells for pure electric bus applications: Aging mechanism identification. Journal of Power Sources 274, pp. 29-40.

[5] Yong, J.Y., Ramachandaramurthy, V.K., Tan, K.M., Mithulananthan, N. (2015). Bi-directional electric vehicle fast charging station with novel reactive power compensation for voltage regulation. International Journal of Electrical Power and Energy Systems 64, pp. 300-310.

[6] Han, G.W., Zhang, C.N., Zhang, S., Wu, X.H. (2014). Control strategy of the dual motors coupling propulsion for battery electric buses. Applied Mechanics and Materials 528, pp. 364-370.

[7] Jinrui, N., Fengchun, S., Qinglian, R. (2006). A study of energy management system of electric vehicles. 2006 IEEE Vehicle Power and Propulsion Conference, VPPC 2006 (4211329).

[8] Vulturescu, B., Trigui, R., Lallemand, R., Coquery, G. (2013). Implementation and test of a hybrid storage system on an electric urban bus. Transportation Research Part C: Emerging Technologies 30, pp. 55-66.

[9] Kong, Z., Zhu, C., Yang, S., Cheng, S. (2006). Study of bidirectional DC-DC converter for power management in electric bus with supercapacitors. 2006 IEEE Vehicle Power and Propulsion Conference, VPPC 2006 (4211286).

[10] Bingham, C., Walsh, C., Carroll, S. (2012). Impact of driving characteristics on electric vehicle energy consumption and range. IET Intelligent Transport Systems 6 (1), pp. 29-35.

[11] Cheng, C., McGordon, A., Poxon, J., Jones, R., Jennings, P. (2010). A model to investigate the effects of driver behaviour on hybrid vehicle control. 25th World Battery, Hybrid, and Fuel Cell Electric Vehicle Symposium and Exhibition, November 5-9, Shenzhen, China.

[12] Fiat Eco: Drive ((2010). Eco-driving Uncovered: the Benefits and Challenges of Ecodriving Based on the First Study Using Real Journey Data. Available at: http://www.lowcvp.org.uk/assets/reports/Fiat_Eco-Driving%20Uncovered.pdf.

[13] Knowles, M., Scott, H., Baglee, D. (2012). The effect of driving style on electric vehicle performance, economy, and perception. International Journal of Hybrid Vehicles 4 (3), pp. 228-247.

[14] Van Mierlo, J., Maggetto, G., Van De Burgwal, E., Gense, R. (2004). Driving style and traffic measures – influence on vehicle emissions and fuel consumption. Proceedings of Institute of Mechanical Engineers Part D: Journal of Automobile Engineering 218 (1), pp. 43-50.

[15] Yan, Y., Zhuang, J., Xie, H. (2014). Influence of the driver behavior difference on the energy consumption of the pure electric buses. Tianjin Daxue Xuebao (Ziran Kexue yu Gongcheng Jishu Ban)/Journal of Tianjin University Science and Technology 47 (3), pp. 231-236.

[16] Yao E.J., Wang M.Y., Song Y.Y., Zuo T. (2013). Estimating the cruising range of electric vehicle based on instantaneous speed and acceleration. Applied Mechanics and Materials 361-363, pp. 2104-2108.

[17] Vaz, W., Nandi, A.K.R., Landers, R.G., Koylu, U.O. (2015). Electric vehicle range prediction for constant speed trip using multiobjective optimization. Journal of Power Sources 275, pp. 435-446.

[18] Ye, X., Jin, Z., Hu, X., Li, Y., Lu, Q. (2013). Modeling and control strategy development of a parallel hybrid electric bus. International Journal of Automotive Technology 14 (6), pp. 971-985.

[19] He, F., Wu, H.B., Li, H., Li, Y.M. (2014). Parameter matching and simulation for powertrain system of pure electric city bus. Advanced Materials Research 977, pp. 218-221.

[20] Chymera, M.Z., Renfrew, A.C., Barnes, M., Holden, J. (2010). Modeling electrified transit systems. IEEE Transactions on Vehicular Technology 59 (6), 5464260, pp. 2748-275.

[21] Office of Sustainable Energy and Environmental Engagement (2014). Available at: http://ose3.mst.edu.

[22] Gantt, L.R., Alley, R.J., Nelson D.J. (2011). Battery sizing as a function of powertrain component efficiencies for various drive cycles. ASME International Design Engineering Technical Conferences & Computers and Information in Engineering Conference (IDETC/CIE 2011), August 28-31, Washington, DC.

[23] Larminie, J., Lowry, J. (2012). Electric Vehicle Technology Explained, second ed., John Wiley & Sons, Ltd., Chichester, West Sussex, UK.

[24] Chen, M., Rincon-Mora, G.A. (2006). Accurate electrical battery model capable of predicting runtime and I-V performance, IEEE Trans. Energy Convers. 21 (2), pp. 504-511.

[25] Xu, G., Li, W., Xu, K., Song, Z. (2011). An intelligent regenerative braking strategy for electric vehicles, Energies 4 (2011), pp. 1461-1477.

SECTION

2. MULTI-OBJECTIVE DRIVING STRATEGY FOR EBUS

2.1. INTRODUCTION

A driver typically drives based on experience and traffic conditions. In the absence of a scientific driving strategy, the chosen accelerations and speeds tend to have randomness associated with them, which a vehicle driven by the same driver over the same route would experience varying energy consumption and trip duration values from trip to trip. The purpose of the research presented in this dissertation is to formulate an optimal driving strategy that will help the driver to drive more efficiently and more consistently. This chapter focuses on demonstrating the methods for optimal driving developed so far.

During any given trip, the vehicle has different modes: acceleration, constant speed, and deceleration. The previous papers presented constant speed and optimal acceleration approaches aimed at optimizing certain trip objectives. The objective here is to combine the constant speed approach with the optimal acceleration approach in order to account for all vehicle modes during a trip. It may be noted that the deceleration portion of the trip was not optimized. Instead, a constant deceleration value was used. The optimization objectives are energy consumption and trip time, both of which are to be minimized. These objectives are conflicting, meaning an improvement in one leads to deterioration in the other. Therefore, the problem becomes a multi-objective optimization

problem, which can be solved using multi-objective genetic algorithms (MOGAs). The goal of MOGA is to search for acceleration values, acceleration duration values, and constant trip speed values that, when adopted by the driver, will optimize both the objectives in question, thereby leading to efficient and consistent driving.

2.2. PROBLEM DEFINITION

The electric vehicle (EV) studied is the Ebus. The trip for which the optimal driving strategy was created was from the Havener Center located on the main Missouri S&T campus to the Hy Point Industrial Park located on the auxiliary Missouri S&T campus about 7 km away and back to the Emerson Electric Company Hall, located on the main Missouri S&T campus. The entire trip was divided into smaller micro-trips. A micro-trip may be defined as an excursion between two locations at which the vehicle is at rest [7]. While traveling between two locations, a vehicle may need to stop for many reasons: the preceding vehicle has stopped, the vehicle is at a stop sign or traffic light, etc. Therefore, most real-world trips comprise several smaller micro-trips. The recorded bus data for the trip studied in this chapter (referred to henceforth as the trip) was analyzed. The trip comprised 13 micro-trips of varying size. Table 1 shows the micro-trip characteristics.

Table 2.1: Micro-trip characteristics for Ebus round trip.

Micro-Trip	Speed Limit(s) (mph)	Start (GPS)	End (GPS)	Cause	Time (s)	Distance (m)
1	15	37.9546034 - 91.7754615	37.9533365 - 91.7768928	Stop sign	69	227.1406
2	35	37.9533381 - 91.776912	37.9550085 - 91.7769718	Traffic light	37	192.8527
3	35	37.9550028 - 91.776985	37.9592967 - 91.7709043	Traffic light	77	778.0178
4	35	37.9592937 - 91.7708945	37.9622737 - 91.7655583	Traffic light	69	649.861
5	45	37.9622757 - 91.7655532	37.9780511 - 91.7252101	Turn	348	4869.017
6	35	37.978248 - 91.7251765	37.9826565 - 91.7246826	Turn	47	559.8273
7	25	37.9826652 - 91.7246232	37.9815497 - 91.7222004	Destination	45	298.5575
8	15	37.9815547 - 91.7221994	37.9815489 - 91.7221508	Turn	53	156.5979
9	25	37.981561 - 91.7221527	37.9820979 - 91.7221348	Turn	18	62.9878
10	25	37.9821134 - 91.7221386	37.9826996 - 91.7245381	Turn	33	233.8909
11	35	37.9827073 - 91.7245451	37.9777485 - 91.725295	Turn	56	568.6339
12	45	37.9777394 - 91.7252969	37.9709235 - 91.7606587	Stop sign	269	3782.22
13	45/35/25	37.9709948 - 91.7610715	37.9564367 - 91.7726944	Destination	205	2262.242
				Total	1326	14641.85

A model of the bus was created in MATLAB. The battery model used is described in [8]. The energy consumption and vehicles dynamics were modeled using the model proposed in [9]. Some of the bus parameters were obtained from the manufacturer, Ebus, Inc. (Downey, CA). The unknown parameters were estimated by using model optimization. The battery model was fine-tuned by using regression analysis. The input was the measured battery current and the output was the simulated battery voltage. A regression coefficient (R^2) between the measured battery voltage and the simulated battery voltage was computed, and the battery parameters were optimized such that R^2 was maximized. Using this approach, the best R^2 value was found to be 0.95. A similar

approach was used for the energy consumption and vehicle dynamics model. The

unknown parameters were optimized by minimizing the difference between the measured

and the simulated battery currents. Table 2 shows the known bus parameters listed by

component. Table 3 shows the unknown parameters that were determined via the model

optimization.

Table 2.2: Ebus model parameters.

Vehicle	
Air density, ρ_{air} (kg m^{-3})	1.1
Drag coefficient, C_D	0.6
Frontal area, A_f (m^2)	6.11
Gravitational acceleration, g (ms^{-2})	9.81
Inertia coefficient	1.05
Mass, m (kg)	6740
Maximum speed (km/h)	72
Overall gear ratio, G	10.07:1
Rolling resistance coefficient, c_{rr}	0.0082
Tire radius, R (m)	0.39
Battery	
Capacity, Cap (A·h)	400
Number of cells in parallel, N_P	1
Number of cells in series, N_S	96
Type	Lithium-Ion
Voltage (V)	300
Motor	
Maximum torque (Nm)	406
Power (kW)	75.6

Table 2.3: EBus parameters from model optimization.

Vehicle	
Auxiliary power (W)	249.9
Converter electronic losses (W)	499.9
Transmission efficiency, G_{eff}	0.99
Battery	
$C_{Transient\_L}$ (MF)	0.22375
$R_{Transient\_L}$ (mΩ)	0.9968
$C_{Transient\_S}$ (MF)	0.03518
$R_{Transient\_S}$ (mΩ)	0.9338
R_{Series} (mΩ)	1.4932
Open-circuit voltage coefficients	
Exponential multiplier	-0.8669
Exponential power	-13.7926
Constant coefficient	4.23
Linear coefficient	0.1265
Quadratic coefficient	0.1453
Cubic coefficient	0.1014
Motor	
Regenerative fraction	0.4
Copper losses, k_c	0.1
Iron losses, k_i	0.01
Windage losses, k_w	0.00005

In order to minimize the trip energy and time, suitable decision variables must be selected by the MOGA. Each micro-trip requires four decision variables: two acceleration values, the duration for the first acceleration value, and the constant speed. This is because the number of optimal accelerations was fixed at two based on previous studies. Also, the deceleration mode for each micro-trip was executed at a constant deceleration value of 1 m/s^2. Since 13 micro-trips comprised the trip being optimized, a total of 52 decision variables comprised each solution. The goal of MOGA is to find different sets of solutions that will minimize the trip energy and time. After that, using higher-level

information, one solution will be presented to the driver as the optimal driving strategy for implementation.

2.3. RESULTS

After obtaining the bus model, it was made to follow the same speed profile as the one followed by the Ebus during the trip. The time durations for both expectedly matched 100%. The measured energy consumption of the Ebus was about 94% the energy consumption of the simulation. It must be noted that the Ebus makes the trip several times a day during weekdays. However, one particular dataset pertaining to a trip on 10/14/2014 was used for model optimization and comparison. The MOGA was run with different settings in terms of number of generations, number of solutions, crossover fraction, mutation probability, etc. There are certain important considerations that guide the choice of parameters. It is important to search the solution space exhaustively, but in a reasonable amount of time. It is necessary to allow sufficient diversity within the population, but also necessary to allow the solutions to converge. The upper and lower limits of the decision variables were determined based on the performance capability of the bus. For the speeds, however, the lower limits were taken to be 5 km/h, thereby guaranteeing that the trip would definitely be completed. The upper limits were based on the speed limits of the individual micro-trips.

Based on the above considerations, several MOGA runs were conducted to search for optimum driving strategies. Figure 1 shows the results of some of the MOGA runs.

Two things are obvious. An increase in the number of generations tends to produce better solutions in terms of the objectives. The second and third Pareto fronts were obtained by using different MOGA parameter settings. The mutation probability was 0.3 instead of 0.2 and the crossover fraction was 0.8 instead of 1.0. A crossover fraction of 1.0 means all the offspring other than elite ones are as a result of crossover. A crossover fraction of 0.8 means 80% of the offspring other than elite ones are from crossover and the rest are purely from mutation. A higher mutation probability gives better diversity within the population, but if it is too high, the search becomes a random search.

Figure 1 showed that MOGA's results were satisfactory: there were plenty of solutions from which to choose and these solutions spanned a broad range for both objectives. However, it is necessary to compare the performance of the proposed approach with the measured objective values. Figure 2 shows the energy consumption and trip time for different trips of the Ebus along the same route. These are plotted along with the best results from Figure 1. It must be noted that the energy consumption values have been reduced by about 6% to account for the discrepancy between the actual bus and the bus model. It can be seen that the random driving produces some non-dominated solutions and some dominated solutions. Additionally, some of the bus solutions are dominated by other bus solutions, implying the random driving of the bus is not necessarily optimal in any sense.
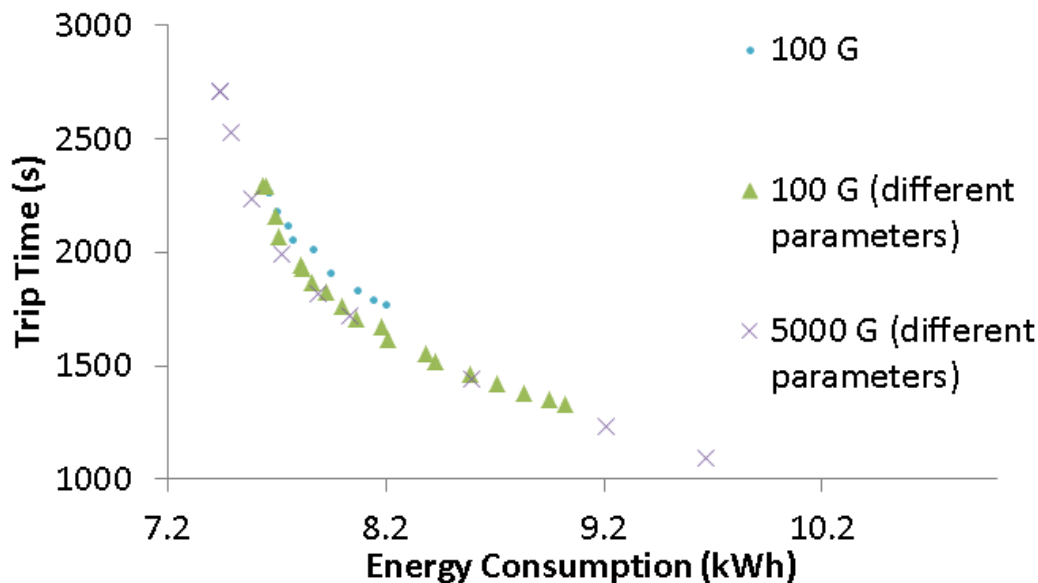
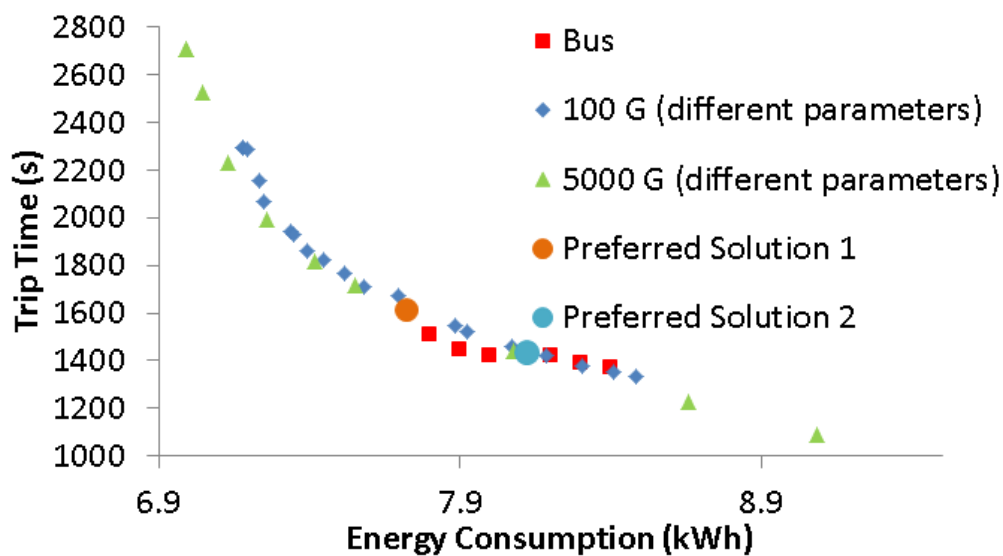Fig. 2.1: MOGA results obtained for different settings.

Fig. 2.2: Adjusted MOGA results and measured bus data.

To make a recommendation about the optimal driving strategy to the driver, it is necessary to choose one solution for implementation. Usually, the choice is left up to the driver who can decide which of the two objectives is more important. Indeed, this may

change from day to day or even from trip to trip. For the sake of demonstration, two different decision-making techniques have been shown in Figure 2. The first preferred solution is based on the reference point technique. In this method, the solution that is close to the ideal point (the origin in this case) is selected. The second preferred solution is based on choosing a solution with a very similar trip time as a bus solution, but with a lower energy. Table 4 summarizes the energy savings that can be obtained by adopting either of the preferred solutions.

Table 2.4: Energy savings for two preferred solutions compared to measured bus objectives.

Solution	Energy Savings (%)	Trip Time Increase (%)
Preferred Solution 1	1.0	0.9
Preferred Solution 2	5.9	13.9

Of course, the energy savings will be more if one of the solutions with lower energy consumption is chosen. The trip time, however, will definitely be higher. It must be noted that these values are based on the model that was used by the MOGA. Besides the overestimation of energy consumption, the model is dependent on the bus data, which is noisy and prone to measurement errors. There may also be a delay between actual parameter readings and the values that are recorded. Additionally, unforeseen driving circumstances, such as a green light instead of a red light, may cause the number of micro-trips to increase or decrease. As such, it is necessary to properly test these solutions in order to see how much energy can actually be saved.

2.4. SUMMARY AND CONCLUSIONS

The constant speed approach was combined with the optimal acceleration approach into one simulation in order to obtain an optimal driving strategy that accounts for all phases of a trip. A demonstrative trip of the Ebus was selected for optimization. The trip was divided into smaller micro-trips. The objectives to be minimized were the trip energy and time, which depended on 52 decision variables. A model of the bus was created in MATLAB, and a MOGA was used to obtain Pareto fronts.

The trip was successfully optimized using the proposed approach. Several non-dominated solutions that spanned a broad range of both the objectives were obtained. It was found that some of the measured objective values were dominated by the optimization fronts whereas others were non-dominated. Two preferred solutions for implementation were selected. It was found that energy savings of up to 5.6% could be obtained for an increase of about 13.9% in the trip time. Proper testing of these solutions would enable one to determine how much energy can actually be saved under real-world driving conditions.

3. SUMMARY AND CONCLUSIONS

In the present study, an optimal driving strategy was developed using a multi-objective approach. In the first part, a neural network strategy to classify the driving situation was developed. Two neural networks were successfully trained to classify the driving behavior as aggressive or defensive and the driving cycle as highway or urban using the acceleration and brake pedal positions. This helps the driver to know whether or not he/she is driving aggressively or defensively. The driver can then modify the driving behavior accordingly. It also gives the drive an idea about what the approximate average trip speed should be: high for highway driving and low for urban driving.

The next part helped the driver to choose an exact optimal trip speed based on trade-offs between maximum range and minimum trip time. By maximizing the electric motor efficiency and minimizing the power consumption, a Pareto-optimal front of optimal trip speeds was obtained. It helps the driver to avoid driving at suboptimal speeds, which results in wasting the stored battery energy. Additionally, the multi-objective approach allows the driver to choose how much range would be sacrificed for a reduction in the overall trip time and vice versa.

The third part helped the driver to choose an appropriate acceleration strategy. The conflicting objectives of minimization acceleration duration and minimization of acceleration energy were considered. To optimize the two objectives, two approaches were considered: using a single acceleration and using multiple accelerations to achieve a reference speed. It was found that using multiple acceleration values optimized the objectives more effectively than using a single acceleration value throughout the speed range of the EV. For the same duration and reference speed, up to 2% energy savings

were observed when using multiple acceleration values. Multi-criterion decision-making techniques such as comfort and "knee" were used to demonstrate the implementation of a single solution for a practical driving situation.

The proposed approach was investigated for the Ebus, an electric bus that operates on the campus of the Missouri University of Science and Technology. By analyzing the operational data, it was found that the bus consumed the least energy per mile when operating between 15-19.99 mph. Due to the complexity involved with the acceleration data, it was not possible to find constant acceleration values. Instead, the maximum, mean, and standard deviation were used to develop an appropriate acceleration strategy. It was found that the mean acceleration dictated the acceleration duration, but the maximum and standard deviation decided non-domination. High maximum and standard deviation values produced solutions that were dominated by those with low maximum and standard deviation values. Additionally, it was found that a higher mean acceleration value resulted in lower energy consumption for graded roads. Finally, the constant speed approach was combined with the optimal acceleration approach into one simulation. A demonstrative trip of the Ebus, from the Havener Center to the Hy Point Industrial Park and back to the Emerson Electric Company Hall, was selected. The trip was divided into 13 micro-trips that needed four decision variables each to fully describe the optimal driving strategy. After optimization, the Pareto fronts that were obtained for different search parameter settings were compared. Two preferred solutions for implementation were selected. It was found that energy savings of up to 5.6% could be obtained for an increase of about 13.9% in the trip time.

The proposed strategy has the following benefits. The multi-objective approach results in several non-dominated solutions being available. The driver ultimately can choose which solution to implement based on trade-offs between the objectives so there is inherent flexibility. Besides using the stored battery energy in an optimal manner, the proposed strategy assists the driver in trip planning. The strategy is easy to implement with minimal changes to existing EV designs. In fact, as pointed out in the second part, the optimal driving strategy gives EV designers some insight into how EV designs can be improved so that optimal operating points are closer to normal driving conditions.

In the future, the scenarios and simulations used in the study can be improved with more conditions and constraints, thereby giving high-fidelity results. This is essential before the strategy can be implemented in a practical driving situation. Adopting the constant speed and optimal acceleration strategies in everyday driving may be especially beneficial to existing advanced driver assistance or automated driving systems. The implementation of the optimal driving strategy in real traffic situations involving multiple vehicles needs to be carried out. Additionally, this study also needs to be carried out for IC engine vehicles as well as hybrid vehicles. Finally, a trip planning system can be developed, one that imbibes the basic tenets of the proposed strategy and incorporates GPS and other satellite data regarding the route and traffic characteristics.

Widespread adoption of the optimal driving approach could have major impacts. Besides patently improving the energy efficiency and range of EVs, a reduction in the associated greenhouse gas emissions would also occur. A detailed study on this is needed, especially for a larger scale. Revisiting the design of existing EVs and EV transmissions and also the design of roads and speed limits are also possible outcomes.

APPENDIX A.

CHOOSING THE NUMBER OF NEURONS

The neural network must be designed with the right number of neurons for the best possible classification results. This becomes evident when regression analysis is performed. The MATLAB training function "train" performs regression analysis to give an idea of how close the output values after training are to the target values. In other words, the R-value gives an idea of how close the simulated output values are to the desired target values (ones and zeroes). An R-value of 1.0 implies that after training, the neural network produces exactly ones and zeroes. Figure A.1 shows a plot of the R-value versus the number of neurons in the neural network. The neural network had two layers for every datum point except for the first one where it had one layer. When the number of neurons is lesser than 4, the neural network is not able to generate exactly ones and zeroes after training, which makes it necessary to introduce the rule where any number greater than 0.5 was taken as a "1" and any number lesser than 0.5 was taken as a "0". When the number of neurons is more than 10, the neural network also has trouble generating exactly ones and zeroes. When such neural networks are presented with fresh data, misclassification of data occurs. Too few neurons are not enough to recognize a pattern but too many neurons cause inputs to be misclassified by the neural network.
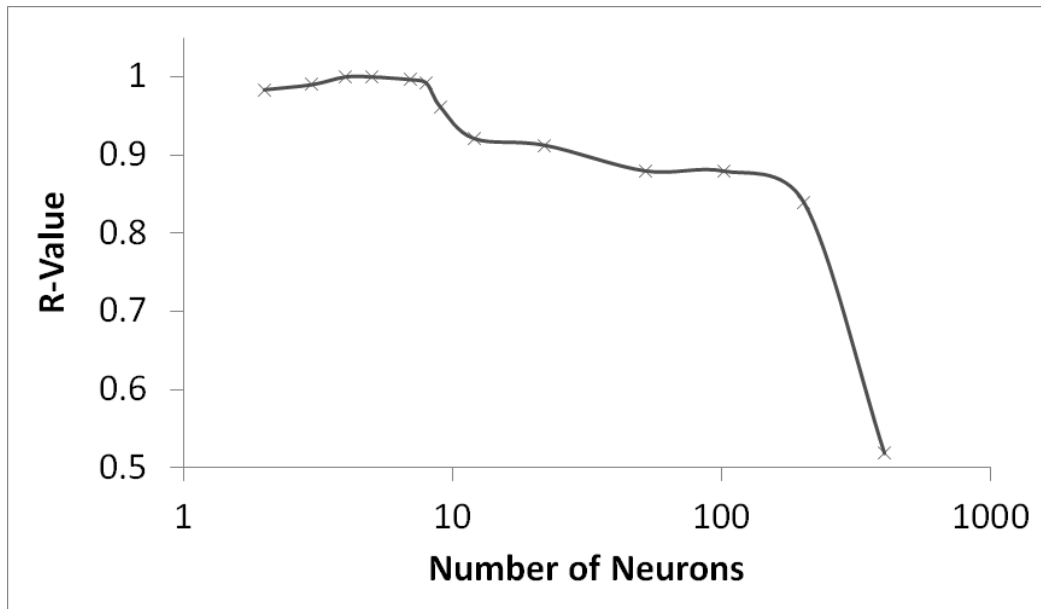
Figure A.1: R-Value versus number of neurons in a neural network trained with 22 input

vectors with 10 rows and target vectors with 2 rows.

APPENDIX B.

ELECTRIC MOTOR SENSITIVITY ANALYSIS

Figure B.1 shows the results of sensitivity analysis. Figures B.1a and B.1b suggest that the main thesis is fairly immune to changes in the gear ratio. For a chosen speed of 45 mph, certain gear ratios lead to Approach 1 fronts with greater dominated space than Approach 2 (Figure B.1b) but they also dominate fewer solutions (Figure B.1a). For K/I_f, in Figure B.1c, extreme values suggest Approach 2 is better for 25 mph whereas in-between values suggest that Approach 1 is better. For 45 mph, Approach 2 is clearly better. In Figure B.1d, the difference between the approaches for both speeds is very small. However, more K/I_f ratios point to Approach 2 being better than Approach 1. Finally, Figures B.1e and B.1f show R_a/L_a results. Figures B.1e indicates that Approach 2 is clearly superior to Approach 1 considering the former's fronts dominate more solutions than the latter's fronts. Figure B.1f shows interesting results. More R_a/L_a ratios suggest that Approach 1 is better than Approach 2. For 25 mph, lower R_a/L_a ratios favor multiple accelerations and higher ratios favor a single acceleration. For 45 mph, Approach 1 results are fairly constant regardless of the R_a/L_a ratio. Approach 2 is favored by higher R_a/L_a ratios. These results need to be confirmed using different electric motor models.
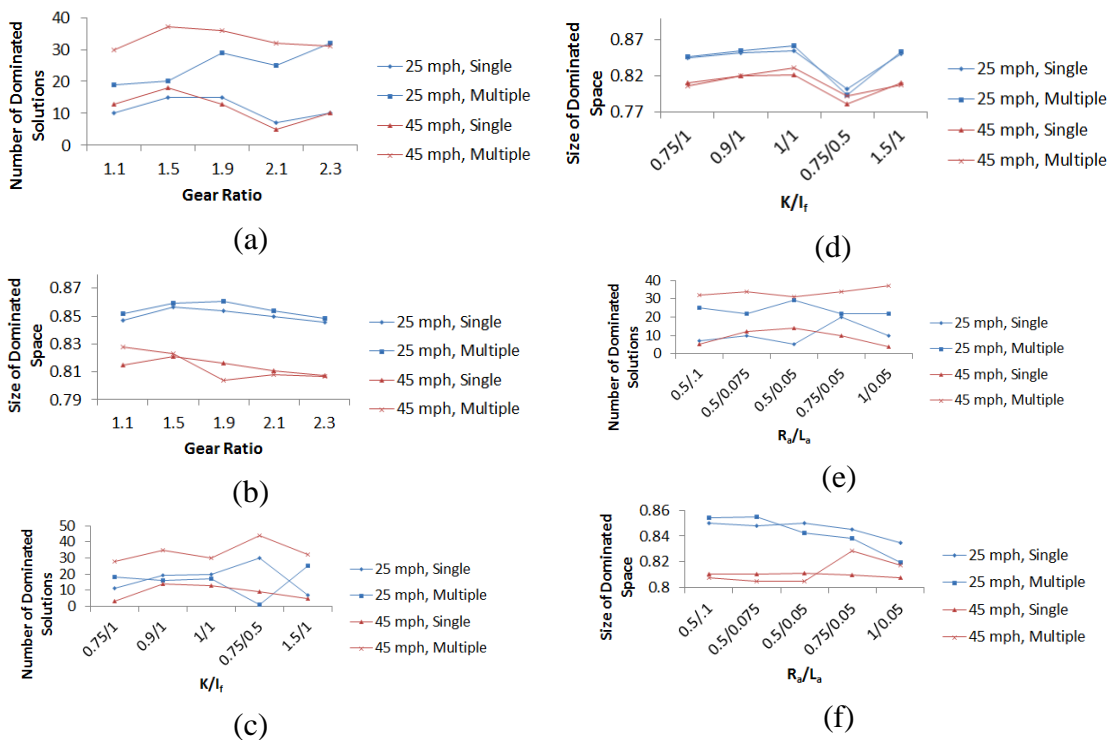
Figure B.1: Results of sensitivity analysis for two chosen speeds.
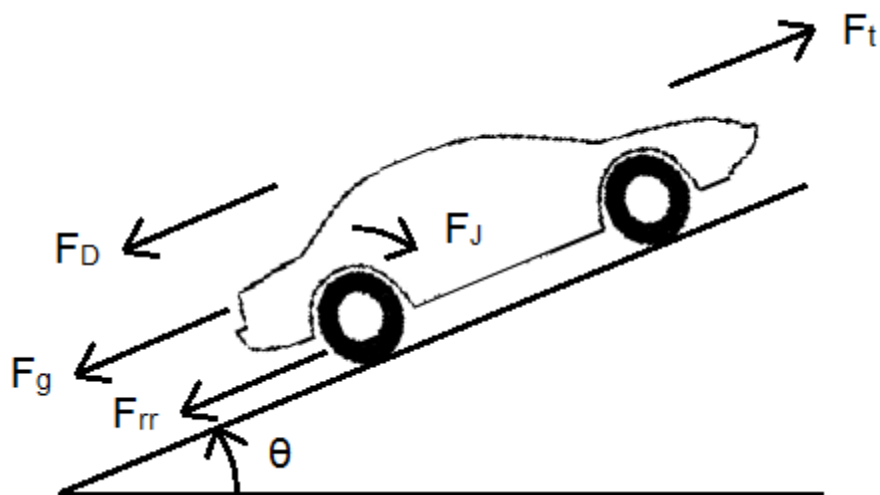
APPENDIX C.

ADDITIONAL FIGURES
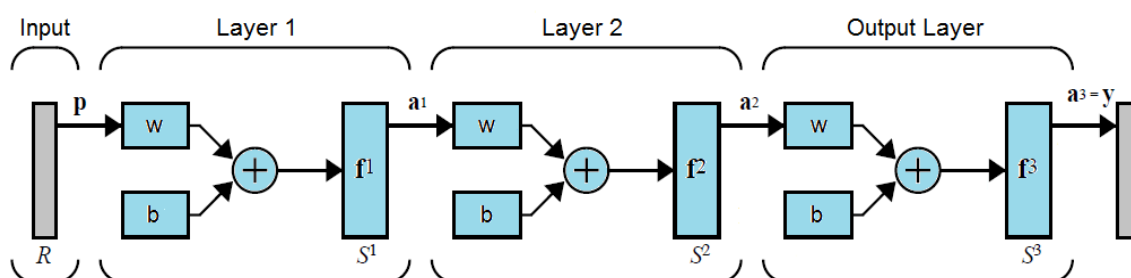
Figure C.1: EV free body diagram.

Figure C.2: Multi-layer neural network with an input layer, an output layer, and two

hidden layers.

BIBLIOGRAPHY

[1]   AllianceBernstein. "The emergence of hybrid vehicles," 2006.

[2]   R. Faria, P. Moura, J. Delgado, A.T. De Almeida. "A sustainability assessment of electric vehicles as a personal mobility system," *Energy Conversion and Management*, 61, pp. 19-30, 2012.

[3]   B. Wang, M. Xu, L. Yang. "Study on the economic and environmental benefits of different EV powertrain topologies," *Energy Conversion and Management*, 4 (86), pp. 916-926, 2014.

[4]   Electric Drive Transportation Association. "Electric car sales," 2013.

[5]   Navigant Research. "Electric vehicle geographic forecasts," 2013.

[6]   D. Mable. "The spark is gone: what's going on with electric cars," *Car and Driver Magazine*, February 2013.

[7]   P.D. Haan, M. Keller. ''Real-world driving cycles for emission measurement: ARTEMIS and Swiss cycles," Final Report, 2001.

[8]   M. Chen, G.A. Rincón-Mora. "Accurate electrical battery model capable of predicting runtime and I-V performance," IEEE Transactions on Energy Conversion 21(2), pp. 504-511, 2006.

[9]   J. Larminie, J. Lowry. "Electric vehicle technology explained," 2nd Edition, John Wiley & Sons, Ltd., Chichester, West Sussex, UK, 2012.

RELATED PUBLICATIONS

[1]   Vaz, W., Landers, R.G., Koylu, U.O. Neural network strategy for driving behavior and driving cycle classification. **International Journal of Electric and Hybrid Vehicles** 6 (3), 255-275, 2014.

[2]   Vaz, W., Nandi, A.K., Landers, R.G., Koylu, U.O. Electric vehicle range prediction for constant speed trip using multi-objective optimization. **Journal of Power Sources** 275, 435-446, 2015.

[3]   Vaz, W., Nandi, A.K., Koylu, U.O. A multi-objective approach to find optimal electric vehicle acceleration. **IEEE Transactions on Vehicular Technology** (under review).

[4]   Vaz, W., Nandi, A.K., Koylu, U.O. Finding an optimal driving strategy for an electric bus based on driving data. Proceedings of the 9th International Conference on Sustainable Energy, ES2015, June 28-July 2, San Diego, California, USA (accepted – #2015-49089), 2015.

VITA

Warren Santiago Vaz was born on the 17th of May, 1987 in Bombay, India. He earned his bachelor's degree in nuclear engineering from the Missouri University of Science and Technology in Rolla, Missouri in the United States (formerly the University of Missouri-Rolla) in May 2009. He earned his master's degree in nuclear engineering from the same university in July 2010.

During the course of his doctoral studies, he was involved with several different research projects related to the U.S. Air Force, the industry, and the field of transportation. He was also involved with teaching in different capacities including being a teaching assistant for ME 280 (ME 4480) Control Systems Laboratory and being the instructor for ME 227 (ME 2527) Thermal Analysis. He graduated with a doctorate in mechanical engineering under the guidance of Dr. Umit O. Koylu in August 2015.